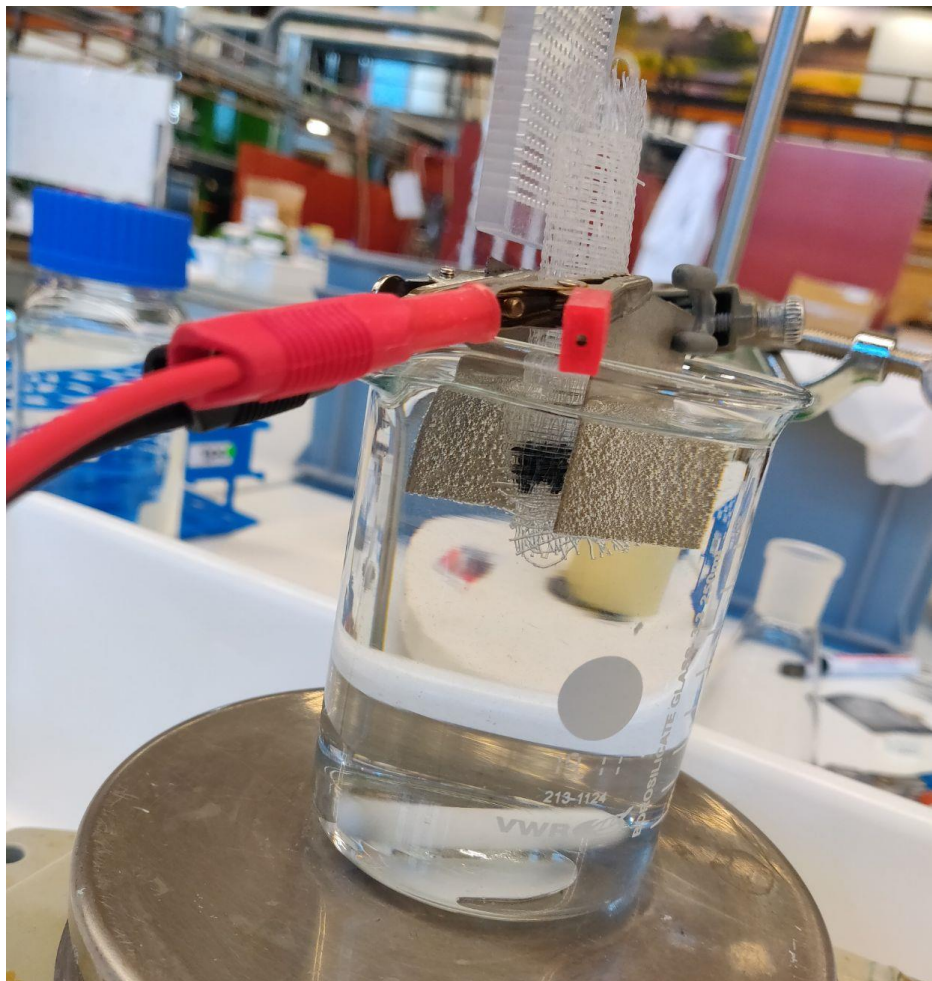


Evaluating the Adsorption and Regeneration Properties of a Novel Carbon-Iron Composite Material

Hong Ting Au (Connie)
August 2022



Evaluating the Adsorption and Regeneration Properties of a Novel Carbon-Iron Composite Material

By

Hong Ting Au (Connie)

to obtain the degree of
Master of Science in Civil Engineering (Track of Water Management)
at the Delft University of Technology.

Student number:	4942817	
Project duration:	November, 2021 – August, 2022	
Assessment Committee:	Prof.dr.ir. L.C. (Luuk) Rietveld, Dr. Ing. K.M. (Kim Maren) Lompe, Dr. Atul Bansode,	TU Delft, chairman TU Delft TU Delft



PREFACE

This is the research report of the master thesis project in the Sanitary Engineering Department at the Delft University of Technology. The novel material used within this study was provided by BASF.

Readers who are interested in the background and motivation of this study can read chapter 1. The results and analysis of the research are discussed in chapter 4. The adsorption properties for a range of micropollutants on this material are listed and discussed in sections 4.1 and 4.2. Readers who are interested in the regeneration properties can find this in sections 4.4 - 4.9. PFAS regeneration results are presented in section 4.10.

This study and report were designed and written by Hong Ting Au (Connie) under the supervision of Dr. Ing. K.M. (Kim Maren) Lompe. The author is very grateful for the provision of the material given by BASF, and the valuable advice given by Prof.dr.ir. L.C. (Luuk) Rietveld and Dr. Atul Bansode.

TABLE OF CONTENT

ABSTRACT	iv
LIST OF ABBREVIATIONS.....	v
LIST OF FIGURES.....	vi
LIST OF TABLES	vii
1 INTRODUCTION	1
1.1 Background and problem statement	1
1.2 Purpose of project and report	3
1.3 Research questions and approaches.....	4
2 LITERATURE REVIEW.....	5
2.1 Theory of electrochemical regeneration.....	5
2.1.1 Definition of electrochemical regeneration.....	5
2.1.2 Electrodesorption	6
2.1.3 Change in pH	7
2.1.4 Ionized species	8
2.1.5 Degradation of contaminant species.....	8
2.2 Reactor configuration	9
2.2.1 Fixed bed versus fluidized bed.....	10
2.2.2 Cathodic versus anodic regeneration	11
2.2.3 Undivided versus divided cell.....	12
2.3 Operating parameters of the electrochemical process	13
2.3.1 Effect of applied current	13
2.3.2 Effect of treatment time.....	13
2.4 PFAS background information.....	15
3 MATERIALS AND METHODS	16
3.1 Adsorbent materials.....	16
3.2 Micropollutants, PFAS and water matrices	17
3.2.1 Choice of pollutants and preparation of solutions	17
3.2.2 Analytical method	19
3.2.3 Water matrices	20
3.3 Adsorption experiments.....	21
3.4 Electrochemical regeneration experiments	23
3.5 Adsorption isotherm and kinetic models	25
4 RESULTS AND DISCUSSIONS	26
4.1 OMP adsorption capacity in different water matrices.....	26

4.2	OMP adsorption kinetics in different water matrices	30
4.3	Adsorption performance comparison between the novel adsorbent and regular GAC.....	33
4.4	OMP regeneration efficiency profile in multiple cycles of adsorption and regeneration.....	34
4.5	Effect of cell configuration	36
4.6	Effect of surface chemistry modifications.....	37
4.7	Effect of operating parameters: current applied and treatment time	38
4.8	OMP concentration profile	41
4.9	Impact of regeneration on adsorbent durability.....	43
4.10	PFAS regeneration efficiency profile in multiple cycles of adsorption and regeneration	44
5	CONCLUSIONS	46
6	LIMITATIONS AND FURTHER RECOMMENDATIONS	47
	BIBLIOGRAPHY.....	48
	APPENDIX A – OMP PROPERTIES AND INITIAL SPIKED CONCENTRATION.....	55
	APPENDIX B – CHEMICAL STRUCTURES OF OMP MOLECULES.....	56
	APPENDIX C – OMP ADSORPTION ISOTHERM PLOTS.....	57
	APPENDIX D – OMP ADSORPTION KINETIC PLOTS.....	59
	APPENDIX E - PROTOCOL OF MAKING OMP STOCK SOLUTION	61
	APPENDIX F – Overview of all performed experiments	68

ABSTRACT

A novel activated carbon-iron composite material has been developed as an adsorbent for water treatment. Due to its activated carbon (AC) content, the material could be used to remove pollutants such as organic micropollutants (OMP). Fast AC bed exhaustion makes adsorption a cost-intensive solution. Regeneration of AC is done off-site and requires transport and high energy consumption for heat treatment. Due to the iron and graphite content of the novel adsorbent, catalytic regeneration could allow for in-situ regeneration.

This property would present a major advantage over common AC. Regeneration could potentially be realized by applying an electric current across an exhausted bed of this adsorbent. Such a setup is called a “particle electrode”, where electrically conductive particles are placed between an anode and cathode. Upon application of an electric current across an exhausted bed of adsorbent, two mechanisms are hypothesized to result in the restoration of adsorption capacity: (1) desorption and (2) degradation of the pollutant.

This study evaluated the adsorption capacity and rate constants for 17 OMP on two different versions of this partly graphitized carbon (with and without iron content) as an alternative to conventional AC for drinking water treatment. By batch adsorption experiments, the adsorption properties of this novel carbon were investigated.

Oxidation of zero-valent iron on the iron containing version of carbon resulted in yellowish water. This version was therefore considered not appropriate for general drinking water treatment, and the remaining experiments were conducted only with the version without iron.

The material adsorbed a great variety of OMP, including different charges and hydrophobicity. Its graphite content probably promoted the adsorption of neutral compounds. A negatively charged layer formed by NOM accumulation on adsorbent surfaces assisted positively charged compounds adsorption.

Investigation of regeneration efficiency was conducted with alternative cycles of adsorption and regeneration with high OMP concentration solutions. This material could be electrochemically regenerated. Reverse adsorption could be achieved on neutral, positively and negatively charged compounds in multiple cycles of regeneration. Electrodesorption is probably the major mechanism responsible for regeneration. Permanent and partial loss of adsorption capacity was recorded, probably due to poor NOM desorption and change in surface chemistry.

Regeneration efficiency was not positively correlated with elevating applied current. Increasing cell voltage is not always beneficial to the electrochemical process. Prolonged treatment time improved the regeneration efficiency, but the marginal benefit was considered to be uneconomical. Poor NOM regeneration was responsible and more concerning for the loss of adsorption capacity.

Long-chain PFAS regeneration was achieved over cycles of regeneration. Short-chain PFAS regeneration was unfavorable due to blockage of micropores.

LIST OF ABBREVIATIONS

2D	Two-dimensional.
3D	Three-dimensional.
AC	Activated carbon.
ATC	Acid treatment carbon bodies.
CECs	Contaminants of emerging concerns.
DWTP	Drinking water treatment plants.
FMC	Ferromagnetic carbon bodies.
GAC	Granular activated carbon.
MQ	Milli-Q water.
NOM	Natural organic matters.
OMP	Organic micropollutants.
PFAS	Per- and polyfluoroalkyl substances.
PSO	Pseudo Second Order model.
RE	Regeneration efficiency.
TW	Delft tap water.
WW	RWZI Harnaschpolder wastewater treatment plant effluent.
WWTP	Wastewater treatment plants.

LIST OF FIGURES

Fig. 1 Representative sources and routes of micropollutants in the environment.....	1
Fig. 2 Mechanism scheme of 3D electrode.....	5
Fig. 3 Electrochemical cell configuration schematic drawing	10
Fig. 4 Schematic drawing of (a) anodic regeneration and (b) cathodic regeneration	11
Fig. 5 Ion-exchange membrane is placed inside the electrochemical cell.....	12
Fig. 6 Flow charts of (A): adsorbents preparation and (B): adsorption isotherm and kinetic experiments	21
Fig. 7 Left: Zoom in of FMC after pre-test in Milli-Q water.....	22
Fig. 8 Electrochemical cell schematic.....	23
Fig. 9 A picture of electrochemical cell used in the regeneration experiment in all cases.	23
Fig. 10 Isotherms for carbamazepine (CBZ), sotalol (STL) and sulfamethoxazole (SMX) in three test solutions.....	27
Fig. 11 The n values obtained from isotherm data by fitting the Freundlich model.	27
Fig. 12 Freundlich constants K_F -values versus OMP properties in MQ water.	28
Fig. 13 Freundlich constants K_F -values versus OMP properties in TW and WW.....	29
Fig. 14 Adsorption kinetic profiles of CBZ, STL and SMX (adsorbent dose: 200 mg/L).	31
Fig. 15 PSO constants k_2 at GAC dose of 200 mg/L from three water matrice	31
Fig. 16 PSO constants k_2 as a function of the Freundlich model constants K_F in TW.	32
Fig. 17 k_2 values in TW as a function of OMP' K_F values and charge at pH 7.....	32
Fig. 18 Seven OMP regeneration profile over six adsorption cycles.	35
Fig. 19 Regeneration efficiency over six cycles of adsorption and electrochemical regeneration.....	36
Fig. 20 The effect of applied current on regeneration efficiency.....	38
Fig. 21 The effect of current applied on regeneration efficiency for GBP (zwitterion).....	39
Fig. 22 The effect of regeneration time on regeneration efficiency	39
Fig. 23 The effect of regeneration time on regeneration efficiency for GBP (zwitterion).....	40
Fig. 24 Profile of seven residual OMP concentrations as a function of regeneration time	42
Fig. 25 Regeneration efficiency of three tested PFAS	44
Fig. A: 1 Chemical structures of OMP molecules.	56
Fig. A: 2 OMP adsorption isotherm plots.	57
Fig. A: 3 OMP adsorption isotherm plots (cont.).	58
Fig. A: 4 OMP adsorption kinetic plots.....	59
Fig. A: 5 OMP adsorption kinetic plots (cont.).....	60

LIST OF TABLES

Table 1 Research approaches relevant to research sub-questions.....	4
Table 2 Regeneration efficiencies (RE) of adsorbents achieved for different cell configurations	9
Table 3 Structure, physical-chemical properties and regulation examples for PFAS.	15
Table 4 Abbreviations and adsorbent properties.	16
Table 5 Application and physical-chemical properties of the 17 studied OMP	17
Table 6 Studied OMP in multiple cycles of regeneration experiment.....	18
Table 7 Physical-chemical properties and structures of three studied FPAS.	18
Table 8 Characteristics of the three tested water matrices.	20
Table 9 Standard procedure of regeneration experiment.	24
Table 10 Adsorption isotherm parameters for ATC applying the Freundlich model.	26
Table 11 Kinetic parameters (PSO model) for OMP adsorption onto ATC (200 mg/L) for 312h.....	30
Table 12 Comparison of kinetic constants between F400 FAC and ATC.....	33
Table 13 Comparison of Freundlich model constants between F400 FAC and ATC.	33
Table 14 Characterization of surface area and pore volume of ATC before and after regeneration.	43
Table 15 Residual PFAS concentration profile by the end of regeneration.....	45
Table A: 1 OMP properties and initial spiked concentration.	55

1 INTRODUCTION

1.1 Background and problem statement

Conventional water treatment plants are designed to remove dominating pollutants, for instance, nutrients, suspended solids and heavy metals. With the rapid development of analytical methods, health issues arise as many other contaminants have entered the public's eye. In the past 20 years, several sources of drinking water have been found polluted by newly recognized contaminants of emerging concerns (CECs). One of the categories is organic micropollutants (OMP) which are found at very low/trace concentrations. Surface water and groundwater with OMP concentrations between ng/L to µg/L have been detected in Spain (Matamoros & Bayona, 2006).

OMP include pharmaceuticals, pesticides, personal care products, industrial compounds etc. They enter the drinking water treatment plants (DWTPs) via point and diffuse sources (Fig. 1). Sources and transportation of the OMP can be complex. But they are likely to eventually arrive at our drinking water source.

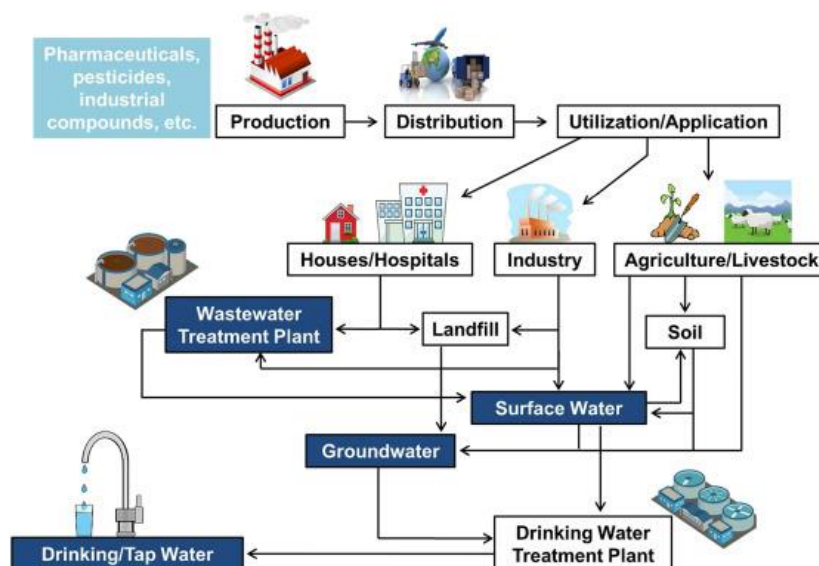


Fig. 1 Representative sources and routes of micropollutants in the environment (Barbosa et al., 2016).

According to Barbosa et al., 2016), OMP enter the water cycle and consequently DWTPs via different pathways. Pharmaceuticals consumed by domestic households and medical treatment enter landfills and the environment after disposal. Industrial compounds may enter the aquatic system by the improper discharge of wastewater. Those OMP incorporated in the products may enter landfills and eventually groundwater. Pesticides enter the soil from agricultural activities or water cycle directly through irrigation flow. Even for effluents from wastewater treatment plants (WWTPs), OMP are not completely removed. Tijani et al. (2013) reported that most WWTPs do not aim at removing organic compounds at low concentrations.

Despite the low concentrations, the presence of OMP in the drinking water supply system have aroused growing concern among the public, as they can cause endocrine disruption in humans (Gavrilescu et al., 2015). As a consequence, more DWTPs are designed or upgraded to eliminate OMP.

There are mainly three kinds of technologies for OMP removal: chemical oxidation (Katsoyiannis et al., 2011), membrane separation (Baresel et al., 2019) and adsorption by porous materials (Moreno-Castilla, 2004). All of these have their own drawbacks and obstacles. Chemical oxidation requires oxidant consumption and by-product formation, and membrane separation faces fouling and concentrate problems. They result in high operational costs and are not broadly chosen by DWTPs as means to remove OMP.

Adsorption by porous materials, especially by granular activated carbon (GAC), the main focus of this research, is generally considered most cost-effective way for OMP removal. GAC has a broad spectrum to remove effectively a wide range of OMP (Mohammad-Khah & Ansari, 2009). Their good adsorption properties are related to their large internal surface area, well-developed structure and high surface reactivity (Hornig et al., 2008; Moreno-Castilla, 2004; Mumford et al., 2014), making them the most preferable candidates for removing different OMP in DWTPs.

However, upon treatment in GAC reactors, OMP enter pores located on the adsorbent surface. Subsequently, they are attached to the adsorbents by physical and/or chemical adsorption. Upon reaching the maximum adsorption capacity, the filled adsorbents are regarded as exhausted or saturated. The adsorbents reach the state of saturation when the entire porous surface is accumulated with pollutants, when no further adsorption takes place. The spent GAC needs to be replaced with fresh GAC when the maximum acceptable effluent concentration is reached. The universal approach is to send the exhausted carbon to landfills for disposal or sent to off-site reactivation facilities. In the Netherlands, they are sent to incinerator. When disposed in landfills, leakage of these toxic contaminants into the soil is possible (L. Wang & Balasubramanian, 2009). Some of the OMP could be toxic and recalcitrant (Srivastava et al., 2021). This can create a heavy burden on the environment. In this context, different techniques aiming at reusing the exhausted GAC have been extensively studied and developed.

The process of restoring the initial adsorption capacity of the exhausted GAC is defined as regeneration. This is achieved by desorption and decomposition of contaminants accumulated on the surface areas and in the pores (VanVliet, 1991). Regeneration methods include thermal reactivation, chemical (Martin & Ng, 1984) and biological regenerations (ElGamal et al., 2018; Salvador et al., 2015).

However, these methods have encountered different limitations and shortcomings: carbon attrition, high energy consumption (Álvarez et al., 2004), as well as slow and incomplete regeneration performance (Aktaş & Çeçen, 2007; Oller et al., 2011). In addition, the above regeneration methods are mostly limited to off-site applications. Transport to central reactivation facilities accounts for about 75 % of total operating and maintenance costs required for running an activated carbon adsorption process (Leng & Pinto, 1997). In this context, electrochemical regeneration emerges as an environmentally friendly and cheaper alternatives (Zhang et al., 2013).

Electrochemical regeneration on GAC refers to placing the exhausted carbon in between two oppositely charged electrodes. By applying currents desorption and decomposition of accumulated contaminants on the carbon surfaces take place. The adsorption capacity is then restored for the next cycle of adsorption. The process can be operated at ambient pressure and temperature, making it a potential solution for in-situ regeneration (Berenguer et al., 2010). Other advantages include exclusive use of non-toxic additional reagents and materials, and ease of automation (Martínez-Huitle et al., 2015). This method is also known as the three-dimensional electrochemical process.

Previous studies have proven the possibility of regenerating commonly used and commercially available GAC via an electrochemical process, with over 80%, or even 100% regeneration efficiency at the lab-scale (McQuillan et al., 2018). However, large-scale implementation of electrochemical regeneration on GAC has not yet been seen. This is partly due to the poor conductivity of conventional GAC. As a result, the electrochemical process consumes high amounts of energy (Asghar et al., 2012). Gogate & Pandit (2004) reported that a charge of 1500 C g^{-1} is required for GAC regeneration at 95% regeneration efficiency. The general objective of this study is to investigate the feasibility of a novel, highly conductive carbon composite for electrochemical regeneration.

1.2 Purpose of project and report

In this MSc project, electrochemical regeneration of a highly conductive adsorbent material was tested. This novel material has been designed by BASF to overcome the weakness of conventional GAC. A commercial activated carbon was taken as the parent material to prepare graphitic carbon bodies with increased conductivity. The project partner BASF provided two graphitic materials for the project: ferromagnetic carbon bodies (FMC) and acid treated carbon bodies (ATC) (which do not contain iron). The conductivity of both materials is up to a factor 12 higher than non-graphitized carbon. This opens the possibility of applying electrochemical regeneration and pollutant oxidation to this material without the use of additional electrolytes.

The nature of this study was a feasibility exploration. To answer the main question: “Is this partly-graphitized activated carbon suitable for in-situ electrochemical regeneration of organic micropollutants?”. Further, the effect of operating parameters such as contact time and applied current on the regeneration efficiency were investigated in this study.

Chapter 2 reviews the recent development and discussions related to the field of electrochemical regeneration. Chapter 3 lists the methodology and summarizes the materials. Chapter 4 discusses and analyses the results of the experiments. Chapter 5 concludes the main findings of this study and answers the research questions. Chapter 6 gives the limitation and provides suggestions for future studies.

1.3 Research questions and approaches

The main objective of this project was to evaluate the novel graphitized carbon material as an adsorbent for OMP and PFAS removal and subsequent electrochemical regeneration.

The following sub-questions were formulated:

1. What are the adsorption capacity and kinetics of the selected OMP by the novel iron-graphitic activated carbon in different water matrices (tap water and wastewater treatment plant (WWTP) effluent)?
2. To which degree can the novel adsorbent be regenerated electrochemically?
3. How do the operating parameters (applied current, treatment time) affect regeneration efficiency?
4. How does the electrochemical regeneration affect the physical stability of the novel carbon?
5. To which degree can the PFAS-loaded novel adsorbent be regenerated electrochemically?

To answer the research questions, the research approaches were divided into five steps (Table 1):

Step I: Determine the adsorption isotherms and kinetics of the selected OMP by the novel composite in tap water and WWTP effluent in the batch experiment.

Step II: Design the regeneration setup and electrochemical cell reactor. Perform multiple cycles of adsorption and regeneration to determine the regeneration efficiency.

Step III: Determine the regeneration efficiency as a function of different operating parameters.

Step IV: Determine the initial pore size distribution of the pristine material and compare it with the pore size distribution after multiple regeneration cycles.

Step V: Determine the regeneration efficiency via alternating PFAS adsorption and regeneration cycles.

Table 1 Research approaches relevant to research sub-questions.

	STEP I	STEP II	STEP III	STEP IV	STEP V
RESEARCH QUESTION 1	✓				
RESEARCH QUESTION 2		✓	✓		
RESEARCH QUESTION 3		✓	✓		
RESEARCH QUESTION 4				✓	
RESEARCH QUESTION 5					✓

2 LITERATURE REVIEW

2.1 Theory of electrochemical regeneration

2.1.1 Definition of electrochemical regeneration

Electrochemical regeneration on activated carbon is recognized as an application of the three-dimensional (3D) electrochemical process, which is established based on the two-dimensional (2D) electrochemical process. The conventional (i.e. 2D) electrochemical process only involves the use of two electrode plates, anodes and cathodes. The addition of particle electrodes or bed electrodes turns the conventional process from 2D into 3D, from two to three (Fig. 2). Granular materials are generally used and, in this study, a saturated graphitized carbon was used.

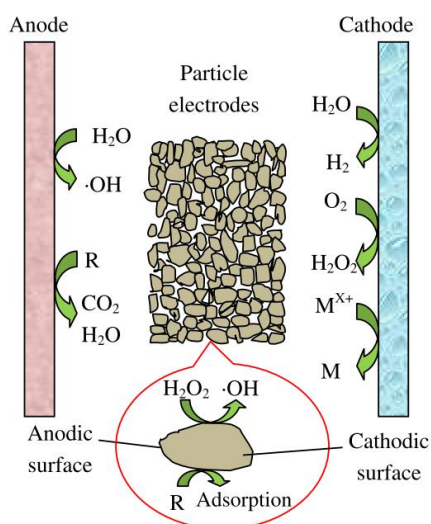


Fig. 2 Mechanism scheme of 3D electrode (Zhang et al., 2013).

In this basic setup, the particle electrodes are placed between anode and cathode. By applying an appropriate current, they are polarized to form microelectrodes which have an anodic surface on one side and a cathodic surface on the other side (Zhang et al., 2013). Reactions occur on the surface of all electrodes, including the charged surface of inserted particles.

For GAC regeneration, two mechanisms are expected during the electrochemical process: enhanced desorption and/or pollutants degradation.

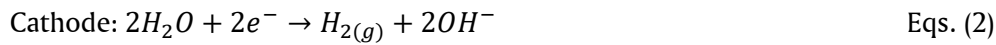
2.1.2 Electrodesorption

Upon current application, the GAC surface is charged on which electrodesorption takes place. GAC particles form microelectrodes with anodic and cathodic surfaces. Similarly charged contaminants species are forced to displace from the adsorbent surface due to enhanced electrostatic repulsion and return to the bulk solution, resulting in adsorption site liberation (Bán et al., 1998; Navalon et al., 2011; Z.Wu et al., 2005). Electrostatic forces have shown to have significant effects on adsorbent-solvent interaction: Bán et al., (1998) applied a cathodic potential to the carbon surface and yielded an increased number of cations adsorbed. Simultaneously, anions adsorption is discouraged due to electrostatic repulsion forces. On the contrary, desorption occurs when opposite potentials are imposed (Foo & Hameed, 2009). Charged ions shift to the opposite site of charged electrodes (C. C.Huang & Su, 2010). Bán et al., (1998) also revealed that electrodesorption is not only limited to charged species but also impacts uncharged molecules. Higher desorption rates were recorded when increased anodic and cathodic potentials were applied (REF). Bain et al., (2010) had similar findings with cationic arsenic removal. The anionic GAC surface was first used to adsorb oppositely charged arsenic. By reversing the applied current, they achieved the full restoration of the GAC adsorption capacity, and the initial arsenic concentration in the solution was recovered.

In this study, it is hypothesized that electrodesorption would be the dominating desorption mechanism since the other two are not significant due to the cell configuration. This will be further explained in section 3.4. On top of that, the novel graphitized material exhibits high conductivity. Therefore, it is expected that it can hold a stronger surface charge, which results in more effective electrostatic repulsion. Saturated GAC particles will be placed in the middle of two electrodes. The same amount of positively and negatively charged surface is expected to form. Similar regeneration efficiency is expected on positively and negatively charged OMP.

2.1.3 Change in pH

At an appropriate current, electron transportation takes place between electrodes through electrolytes. This creates a positively charged anode and a negatively charged cathode, in which oxidation and reduction reactions occur, respectively (Zhang et al., 2013). Most often, electrochemical systems employ aqueous solutions, and the principle electrolysis reactions of water into oxygen and hydrogen occur at the anode and cathode, respectively (Eqs. (1) and Eqs. (2)). Simultaneously with the electrolysis reaction, acidic protons (H^+) and basic hydroxyl ions (OH^-) are produced, resulting in the development of an acidic and cathodic front in the electrochemical system. The electrolyte close to electrodes is known as anolyte (acidic) and catholyte (basic).



In the case of GAC regeneration, a change in pH is relevant to the adsorptive equilibria between adsorbent and adsorbate. Semmens et al., (1986) argued that increasing pH raises the contaminant species solubility (depending on their properties) and shifts the adsorptive equilibria, which in return promotes desorption. They also indicated increasing pH encourages competitive adsorption with hydroxyl ions. On the contrary, a decreased pH environment could neutralize the carboxylic acid functional groups on the GAC surface and decrease the solubility of organic compounds (Semmens et al, 1986). Karimi-Jashni & Narbaitz (2005) demonstrated that by electrochemical treatment 30% higher regeneration efficiency of phenol loaded GAC was achieved in a pH 12 catholyte than in a pH 2 anolyte. At high pH, it is speculated anionic compounds experience greater electrostatic repulsion force with anionic functional groups on the GAC surface, which triggers enhanced desorption and achieves thus adsorptive capacity restoration.

In this study, however, the effect of pH during regeneration is expected to be inferior and not as important as electrodesorption. Loaded GAC is placed between electrodes at a distance of a half centimeter. Without direct contact with the cathode, the shift of adsorptive equilibria by a change in pH is expected to be less significant. Constant mixing and circulation of electrolytes also hinder the formation of a deep acidic or a basic front.

2.1.4 Ionized species

Various aqueous electrolyte solutions are employed in the electrochemical process, for instance, NaCl, NaHCO₃, Na₂SO₄, CH₃COONa (Xu et al., 2008), NaOH and Na₂CO₃ (Oriňáková et al., 2006). The addition of salt might change the ionic strength of the water, which results in a reduction or change in the solubility of some contaminants. (Zhang et al., 2013). Simultaneous with the gaseous generation by the principle reactions (Eqs. (1) and Eqs. (2)), dissociation of electrolytes into ionized species are demonstrated to enhance desorption and GAC regeneration. Neti & Misra, (2012); X.Wu et al., (2008) revealed increased sodium ions concentration by NaCl dissociation reacting with phenols species adsorbed on GAC surface. Subsequently formed sodium phenate is readily desorbed from the GAC surface, achieving GAC regeneration. In this study, this mechanism is not expected since only tap water without chemical additives will be used. The aim is to achieve regeneration and to produce less polluted waste streams.

2.1.5 Degradation of contaminant species

Enhanced desorption liberates adsorption sites by removing adsorbed species or reversing the adsorption process. Another way to achieve this is by oxidation of adsorbed compounds. It is beneficial to the overall treatment process since that secondary treatment of residual compounds could be avoided or mitigated. Contaminant decomposition means that pollutants are degraded via oxidation to non-toxic products or are completely mineralized. According to Zou et al., (2017), contaminant species can be oxidized directly or indirectly. Direct (anodic) oxidation takes place on the surfaces of anodes. When compounds are adsorbed onto anodes, they transfer one or more electrons to the electrodes and become oxidized (Rajeshwar et al., 1994). The reaction is described in Eqs. (3). Direct anodic oxidation is restricted by the rate of desorption and the rate of mass transfer.



Where R_{ads} is the contaminant compound adsorbed on the anode, P_{ads} is the oxidized product, and z is the number of electrons transferred.

Oxidation of contaminants can also take place by reacting with electrogenerated oxidizing species. This mechanism is named as indirect oxidation. Oxidizing species can be generated at both anode and cathode. Indirect anodic oxidation is achieved by hydroxyl radicals generated within the thin layer on anodes surfaces (Rajkumar & Palanivelu, 2004). For indirect cathodic oxidation, hydrogen peroxides are generated on cathodes by oxygen and protons reaction (Berenguer et al., 2010).

Both direct and indirect oxidation reactions are expected during regeneration in this study. Therefore, several OMP are selected to investigate which of those are favored by direct or indirect oxidation. But their oxidation pathway and oxidation rate will not be the study objectives due to unavailable in-house analysis. Oxidation is only seen as assistance for GAC regeneration.

2.2 Reactor configuration

The structures of electrochemical reactors have different forms to achieve optimized treatment efficiency. The first and basic configuration consists of a packed bed placed between anode and cathode (section 3.4). When the particles are placed into the catholyte (anolyte) compartment, cathodic (anodic) regeneration occurs (section 2.2.2). The electrochemical cell can be divided into two compartments by inserting a membrane to create two compartments (section 2.2.3). The effects of operating parameters are discussed in section 2.3. Table 2 summarizes the relevant studies mentioned in the following discussion.

Table 2 Regeneration efficiencies (RE) of adsorbents achieved for different cell configurations at various applied currents and treatment time.

Adsorbent / Amount	Pollutant	Operating conditions	Applied current [mA]	Treatment time [h]	RE [%]	Reference
Filtrisorb F-400 GAC, 1.2 g	Phenol	Undivided cell, cathodic	50	25	78	(Karimi-Jashni & Narbaitz, 2005)
				10	72	
		Undivided cell, anodic		25	59	
		Divided cell, cathodic		10	78	
WV-A1100 GAC 0.2 g	Toluene	Undivided cell, cathodic	500	3	98	(García-Otón et al., 2005)
Coconut Shell GAC, 0.3 g	Phenol	Undivided, fluidized bed	50	5	85.2	(Zhang, 2002)
Woody GAC 3.0 g	<i>p</i> -nitrophenol	Undivided, fluidized bed	4 mA/cm ²	1.5	92.1	(Zhou & Lei, 2006)
207A GAC 2.0 g	Phenol	Undivided cell, cathodic	1000	3	81	(Berenguer et al., 2010)
		Undivided cell, anodic			39	
F-400 GAC 1.2 g	Phenol	Undivided cell, cathodic	50	3	85	(Roberto M. Narbaitz & Cen, 1994)
		Undivided cell, anodic	50	3	80	
F-400 GAC 1.2 g	Phenol	Undivided cell, fixed bed	10	25	62	(R. M. Narbaitz & Karimi-Jashni, 2009)
			30		65	
			50		77	
			100		76	
GAC	Phenol	Undivided cell, fixed bed	1000	3	97	(Sun et al., 2013)
			2000		90	
			3000		98	
GAC 1.0 g	Phenol	Undivided cell, fixed bed	400	2	42	(Zanella et al., 2017)
			800		90	
			1600		88	
			2400		99	
Activated Carbon Fiber, 0.5 g	Phenol	Undivided cell, fixed bed	100	4	62	(Zhan et al., 2016)
			200		73	
			300		81	
			400		88	
			500		88	
Nyex 100	Atrazine	Divided cell, fluidized bed	400	10 min	60	(Brown et al., 2004)
				20 min	100	
				30 min	190	
				60 min	300	
GAC 6283.2 g	4,4'-diaminostilene-2,2'-disulfonic acid	Undivided, fixed bed	200 A/m ²	1	38	(Wang & Balasubramanian, 2009)
			675 A/m ²		95	
			2533 A/m ²		98	
Field Spent GAC 15.0 g	Wastewater treatment plant	Undivided, fixed bed	1 V/cm	12	66	(Weng & Hsu, 2008)
			3 V/cm		70.1	
			5 V/cm		74.4	

2.2.1 Fixed bed versus fluidized bed

The particle electrode is also named the bed electrode (Fig. 3A). During the design phase of this study, a fixed bed reactor was selected as it can be built easier and with limited resources in the limited time span of this project. The fixed bed design is characterized by a large surface area to volume ratio, and it can be easier translated to a full-scale design (Zhang et al., 2013). In most cases, the particle electrode is placed in direct contact with the anode and/or cathode to enhance the energy efficiency. In this study, however, the design had to account for the limited volume of tested material (0.2 g). To achieve direct contact of GAC with the electrode plates while respecting a minimum distance of 2 cm between the electrode plates (to avoid short circuiting). Increasing the volume of GAC, however, entails using a larger amount of OMP to achieve sufficient loading. The final design contains 0.2 g of the adsorbent in a fixed bed configuration realized by placing the adsorbent particles inside a nylon basket hanging between the plates that have a minimum distance of 2 cm.

A substantial drawback of fixed bed configuration is the limited mass transfer (McQuillan et al., 2018). Desorbed OMP and natural organic matter (NOM) return to the bulk solution through the pore pathways in the adsorbents. In fixed bed configuration, after exiting the granules, desorbed species have to pass through the packed bed to return to the bulk solution. The restricted mass transfer may decrease the concentration gradient between the adsorbents surface and bulk solution, hence limiting the desorption rate (Karimi-Jashni & Narbaitz, 2005). Gaseous bubbles generated during regeneration may be trapped inside the particle bed and decrease current efficiency (Karimi-Jashni & Narbaitz, 2005). To overcome restricted mass transfer in fixed bed configuration, Karimi-Jashni & Narbaitz, (2005) improved the operation by turning it into a semi-batch mode or applying aeration / electrolyte mixing. Considering the thickness of the adsorbents bed (0.5 cm), continuous electrolyte mixing using a magnetic stirrer during the course of regeneration will be adopted in this study. It is thought that the created turbulence will enhance advective mass transfer and can also quickly remove gaseous bubbles trapped on the adsorbents holder (nylon bucket). However, the mixing of electrolytes can also destroy the strong pH front formation, which is highly relevant with desorption (Karimi-Jashni & Narbaitz, 2005) (section 2.2.2).

Another alternative is to realize a fluidized bed which is said to improve mass transfer and enhance regeneration efficiency (García-Otón et al., 2005; Zhang, 2002; Zhou & Lei, 2006). A fluidized bed means that the particles can be mobilized or moved between anode and cathode driven by electrolyte movement or aeration (Fig. 3B). It can be created by external circulation instalments (e.g. pump) or aeration inside the electrochemical cell, depending on the configuration. Other advantages include contact with electrode plates for all particles to achieve oxidation of adsorbed species (Zhou & Lei, 2006). This configuration is not considered in this study due to the difficulty of controlling a fluidized bed at a small scale (Zhang et al., 2013).

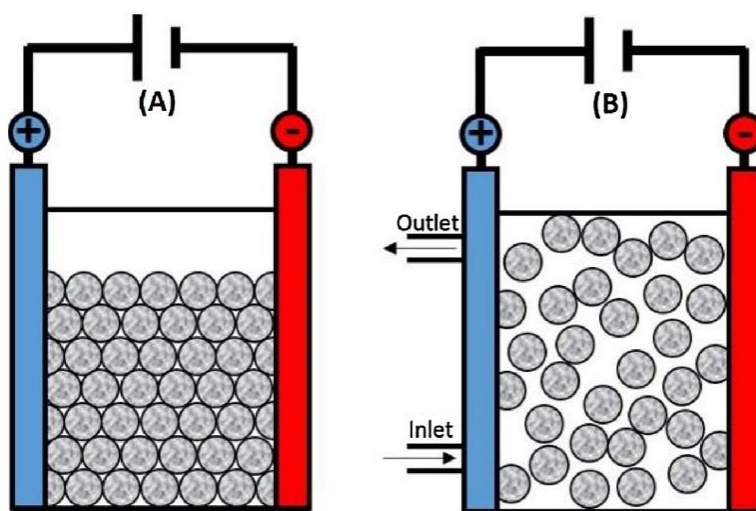


Fig. 3 Electrochemical cell configuration schematic drawing. Fixed bed configuration (A), particles electrode is fixed between anode and cathode. Fluidized bed configuration (B), particle bed's alignment is changed due to flow of electrolyte. (McQuillan et al., 2018).

2.2.2 Cathodic versus anodic regeneration

Electrochemical regeneration can be divided into anodic and cathodic regeneration. Anodic regeneration denotes that the particles are placed near and in contact with the anode (vice versa for cathodic regeneration: Fig. 4). This is to target different regeneration mechanisms: oxidation of adsorbed species during anodic treatment and enhanced desorption during cathodic treatment. The principle reactions taking place on the surfaces of the anode and cathode determine the ambient pH (Eqs. (1) and Eqs. (2)). Low pH values enhance oxidation rates by producing more oxidizing species and promoting direct oxidation on anode surfaces (Nidheesh & Gandhimathi, 2012). High pH (at the cathode) encourages desorption by shifting the adsorptive equilibrium (Semmens et al., 1986).

It is generally reported that cathodic regeneration provides better regeneration efficiencies (Berenguer et al., 2010; Karimi-Jashni & Narbaitz, 2005; Roberto M. Narbaitz & Cen, 1994; H. Zhang, 2002). For example, H. Zhang, (2002) reported a 20% improvement with cathodic regeneration on phenol-loaded GAC compared to anodic regeneration. However, residual phenol was detected after regeneration, while none was detected in the case of anodic regeneration. For cathodic regeneration, phenol desorption is encouraged with extremely high pH conditions. During anodic regeneration, direct oxidation is promoted due to the proximity of desorbed species with the oxidation area. Choosing anodic or cathodic regeneration becomes a problem of selecting dominating mechanisms. Enhanced desorption raises the GAC performance in the subsequent adsorption process, while enhanced oxidation reduces the chance of second treatment of residual solutions (McQuillan et al., 2018).

In this study, regeneration is conducted simultaneously via cathodic and anodic reactions for several factors: (1) Undivided setup could partly include advantages of anodic and cathodic regeneration simultaneously by minimizing GAC bed depth and distance between electrodes; (2) anodic and cathodic regeneration is considered as advanced configurations. Due to the nature of this study as a feasibility test, the optimization of the regeneration setup is not part of this project.

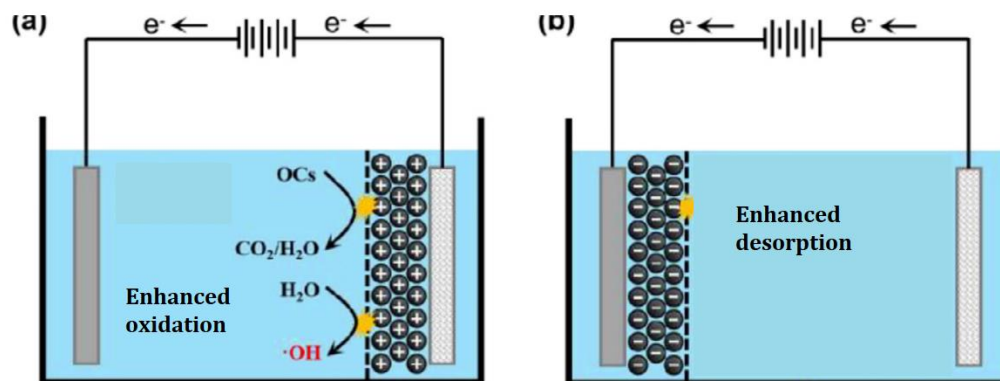


Fig. 4 Schematic drawing of (a) anodic regeneration and (b) cathodic regeneration (altered from W.Zhou et al., 2021).

2.2.3 Undivided versus divided cell

A electrochemical cell can be divided to avoid transfer of ions between anodic and cathodic compartment by inserting an ion-exchange membrane in between anode and cathode (Fig. 5). It is thought that with ion separation a high pH in the cathodic compartment can be maintained and hence enhanced desorption occurs (McQuillan et al., 2018). Narbaitz & Karimi-Jashni, (2012) demonstrated slightly higher regeneration efficiency on phenol loaded GAC with a divided cell. They attributed this to the maintenance of pH 12 in the cathodic compartment. However, this configuration showed an unpromising result by another research team: Berenguer et al., (2010) pointed out the regeneration rate can be limited by membrane separation. The placement of a membrane can, on the one hand, prevent oxidized species from the anode being reduced at the cathode. On the other hand, it constraints the desorbed species migration from the cathodic compartment to the anodic compartment, in which they can be degraded and reduce the overall contaminant concentration in the bulk solution (Berenguer et al., 2010). This is confirmed by the result obtained by Narbaitz & Cen, (1994): even though higher regeneration efficiency can be achieved in the cathodic compartment, residual contaminants were found after regeneration. Practical drawbacks include the difficulty and high cost of setting up membrane separation (McQuillan et al., 2018). Therefore, this study will be conducted with an undivided and simpler configuration.

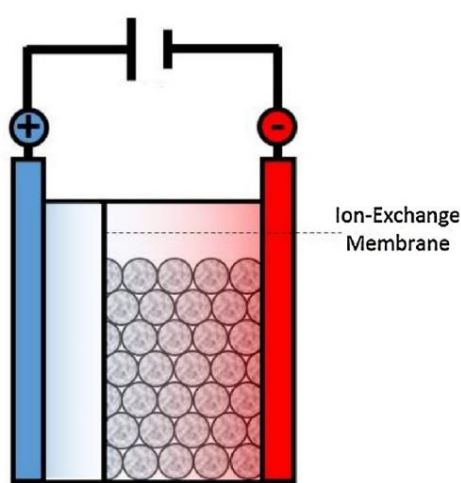


Fig. 5 An ion-exchange membrane is placed inside the electrochemical cell to separate ion transfer between the anodic and cathodic compartment.

2.3 Operating parameters of the electrochemical process

This study focuses on examining the effect of current density and treatment time. As mentioned in the introduction, the application of electrochemical regeneration isn't very common among industries. A comprehensive understanding is required to up-scale the process into industrial practice. Optimization of operating parameters is undoubtedly one of the very first steps. Small changes in operating parameters could lead to significant improvement in regeneration performance.

2.3.1 *Effect of applied current*

The current applied to an electrochemical cell is an important parameter determining the efficiency of regeneration. It provides the driving force for contaminant degradation and controls the oxidation rate (McQuillan et al., 2018). With increased current, both the direct and indirect oxidation (section 2.1.5) rate can be boosted, liberating more adsorption sites. Past studies have shown a positive correlation between regeneration performance and increased applied current (R. M. Narbaitz & Karimi-Jashni, 2009; Sun et al., 2013; Zanella et al., 2017; Zhan et al., 2016). For instance, Zhan et al., (2016) reported a 26% increase in regeneration efficiency on phenol-loaded GAC by raising the applied current from 100 mA to 400 mA. The improvements are due to increased oxidation rate and more oxidation radicals as a result of increased ionic transport (Karimi-Jashni & Narbaitz, 2005). Elevated current density also induces a higher surface charge on GAC and boosts the electrostatic repulsions between adsorbed species and GAC surface, promoting electro-desorption. As such, this study investigates the effect of applied current and, to certain extent how it benefits the desorption of differently charged compounds.

2.3.2 *Effect of treatment time*

Treatment time denotes the time span of spent GAC being electrochemically regenerated in the electrochemical cell. Regeneration begins with the desorption of contaminant species inside the GAC pores, followed by direct oxidation on the electrode surfaces or indirect oxidation by reaction species (Zhang et al., 2015). Higher treatment time allows more desorption and oxidation to take place. More importantly, greater mass transfer is expected to allow more desorbed species to exit the pores and return to the bulk solution (Roberto M. Narbaitz & Cen, 1994). This has been shown in several studies in which they obtained improved regeneration by increasing the treatment time (Berenguer et al., 2010; Brown et al., 2004; Roberto M. Narbaitz & Cen, 1994; Wang & Balasubramanian, 2009; Weng & Hsu, 2008). However, lengthened regeneration time requires more energy consumption. McQuillan et al., (2018) presented concern about striving for little improvement to the expense of uneconomical or inefficient energy consumption.

2.4 PFAS background information

Per- and polyfluoroalkyl substances (PFAS) are a class of synthetic aliphatic compounds which contain multiple fluorine atoms attached to one or more perfluoroalkyl chain groups (Renner, 2001) (PFAS chemical structures, please refer to Table 7). PFAS exhibit unique chemical attributes and recalcitrant properties due to their highly polar and strong carbon-fluorine bonds (Bentel et al., 2019; Rahman et al., 2014). Due to their distinctive physical and chemical properties, PFAS have been extensively used in industries (Takagi et al., 2008), especially in the manufacturing field of firefighting foams, protective coatings, carpet goods and leather textiles. As a result of massive use among industries, persistent PFAS are currently detected in drinking water around the globe (Chen et al., 2017; Dalahmeh et al., 2018; Elmoznino et al., 2018; Eriksson et al., 2017; Gallen et al., 2018; E.Houtz et al., 2018; E. F.Houtz et al., 2016; Pan et al., 2016; Seo et al., 2019; ChaojieZhang et al., 2015).

Regarding their adverse health effects, PFAS have been identified to be potentially carcinogenic (Lindh et al., 2012) and harmful to the immune and reproductive system (Fenton et al., 2021; Panaretakis et al., 2001). Health authorities in different countries formulate regulations to control PFAS uptake (Table 3). In the Netherlands, the Rijksinstituut voor Volksgezondheid en Milieu (RIVM) proposes a standard of 4.4 ng/L for four long-chain PFAS in drinking water (RIVM, 2021). These four compounds were selected based on the criteria of the European Food Safety Authority (EFSA). The U.S. Environmental Protection Agency (US EPA) suggests an advisory level of 70 ng/L for two widely used long-chain PFAS: perfluorooctanoate (PFOA) and perfluorooctanesulfonate (PFOS) (Cordner et al., 2019). These two compounds have also been added to the list of persistent organic pollutants after the 2009 United Nations Stockholm Convention (European Commission, 2019). PFOA and PFOS have been receiving considerable attention in the field of academic research and health regulation (Cantoni et al., 2021). They noted these two compounds were the major PFAS used among industries until their phasing out. Past regulations always targeted these two extensively used PFAS (Cantoni et al., 2021). F.Li et al.,(2020) also made a similar observation and remarked on the lack of attention toward short-chain PFAS. The increasing implementation of regulatory limits on the use of long-chain PFAS results in a worldwide shift to short-chain production (F.Li et al., 2020). As a result, the European drinking water directive proposes a sum concentration limit value of 100 ng/L (European Commission, 2020). This includes 20 long-chain and short-chain PFAS (Table 3).

Accordingly, this study includes two long-chain and one short-chain PFAS to investigate the effect of chain length on adsorption and electrochemical regeneration. The PFAS chain group classification is defined by the number of C atoms. By the EU definition, the long-chain group includes PFAS consisting of more than or equal to seven perfluorinated carbons for the carboxylic functional group; and those which consist of more than six or equal to six perfluorinated carbons for the sulfonate functional groups (Table 3). US EPA's classification deviates from the EU's definition: long-chain PFAS are PFAS with the carboxylic groups consisting of more than eight or equal to eight carbon atoms and long-chain PFAS with the sulfonate groups that consist of more than or equal to seven carbon atoms. The EU's classification is adopted in this study.

Adsorption onto activated carbon has been regarded as an effective way for long-chain PFAS removal (Appleman et al., 2014). This is because of the long non-polar tail, and they adsorb well on carbon via non-polar interactions. However, Rahman et al., (2014) expressed concern that the replacement of short-chain PFAS in industries may impose threats to drinking water systems. On top of that, remediation methods aiming at destroying PFAS are continuously investigated. It is thought that electrochemical processes are promising (Sharma et al., 2022). The authors of the same study proposed that conventional treatment in combination with an electrochemical approach could improve the overall system efficiencies and reduce toxic by-products emissions. With this background, the novel material tested in the present study is considered an appropriate material for PFAS removal due to its mesoporous property and ease of conducting current.

Table 3 Structure, physical-chemical properties and regulation examples for PFAS.

Full name	Abbreviation	Functional group	Formula	MW (g/mol) ^a	Log K _{ow} ^b	pK _a ^c	Chain length	Chain group ^d	Regulation			
									EFAS (NL) ^e	European Parliament ^f	Stockholm Convention ^g	US EPA ^h
Perfluorotetradecanoic acid	PPTeDA	carboxylate	C ₁₄ HF ₂₇ O ₂	714.12	9.32	-5.2	14	long-chain				
Perfluorotridecanoic acid	PPTrDA	carboxylate	C ₁₃ HF ₂₅ O ₂	664.11	8.62	-5.2	13	long-chain		✓		
Perfluorododecanoic acid	PFDoA	carboxylate	C ₁₂ HF ₂₃ O ₂	614.1	7.92	-5.2	12	long-chain		✓		
Perfluoroundecanoic acid	PFUnA	carboxylate	C ₁₁ HF ₂₁ O ₂	564.09	7.22	-5.2	11	long-chain		✓		
Perfluorodecanoic acid	PFDA	carboxylate	C ₁₀ HF ₁₉ O ₂	514.09	6.51	-5.2	10	long-chain		✓		
Perfluorononanoic acid	PFNA	carboxylate	C ₉ HF ₁₇ O ₂	464.08	5.81	-6.51	9	long-chain	✓	✓		
Perfluorooctanoic acid	PFOA	carboxylate	C ₈ HF ₁₅ O ₂	414.07	5.11	-4.2	8	long-chain	✓	✓	✓	✓
Perfluoroheptanoic acid	PFHpA	carboxylate	C ₇ HF ₁₃ O ₂	364.06	4.41	-2.29	7	long-chain		✓		
Perfluorohexanoic acid	PFHxA	carboxylate	C ₆ HF ₁₁ O ₂	314.05	3.71	-0.78	6	short-chain		✓		
Perfluoropentanoic acid	PFPeA	carboxylate	C ₅ HF ₉ O ₂	264.05	3.01	0.34	5	short-chain		✓		
Perfluorobutanoic acid	PFBA	carboxylate	C ₄ HF ₇ O ₂	214.04	2.31	1.07	4	short-chain		✓		
Perfluorodecanesulfonic acid	PFDS	sulfonate	C ₁₀ HF ₂₁ O ₃ S	600.14	6.83	-3.24	10	long-chain		✓		
Perfluorononanesulfonic acid	PFNS	sulfonate	C ₉ HF ₁₉ O ₃ S	550.13	6.13	-3.24	9	long-chain		✓		
Perfluorooctanesulfonic acid	PFOS	sulfonate	C ₈ HF ₁₇ O ₃ S	500.13	5.43	-3.32	8	long-chain	✓	✓	✓	✓
Perfluoroheptanesulfonic acid	PFHpS	sulfonate	C ₇ HF ₁₅ O ₃ S	450.12	4.73	-3.32	7	long-chain		✓		
Perfluorohexanesulfonic acid	PFHxS	sulfonate	C ₆ HF ₁₃ O ₃ S	400.11	4.03	-3.32	6	long-chain	✓	✓		
Perfluoropentanesulfonic acid	PFPeS	sulfonate	C ₅ HF ₁₁ O ₃ S	350.1	3.33	-3.32	5	short-chain		✓		
Perfluorobutanesulfonic acid	PFBS	sulfonate	C ₄ HF ₉ O ₃ S	300.09	2.63	-3.31	4	short-chain		✓		
Perfluoroundecane sulfonic acid	PFUnS	sulfonate	C ₁₁ HF ₂₃ O ₃ S	650.15			11	long-chain		✓		
Perfluorododecane sulfonic acid	PFDoS	sulfonate	C ₁₂ HF ₂₅ O ₃ S	700.16			12	long-chain		✓		
Perfluorotridecane sulfonic acid	PPTrDS	sulfonate	C ₁₃ HF ₂₇ O ₃ S	750.17			13	long-chain		✓		

^a MW: molecular weight (PubChem 2022).^b Octanol-water partition coefficient (PubChem 2022).^c (PubChem 2022).^d The definition of long-chain and short-chain is in accordance of EU authorities (European Commission, 2020). https://ec.europa.eu/environment/pdf/chemicals/2020/10/SWD_PPFAS.pdf^e (Rijksinstituut voor Volksgezondheid en Milieu (RIVM), 2021) <https://www.rivm.nl/sites/default/files/2021-06/Advies%20drw%204-PFAS%20DEP%20beveiligd.pdf>^f (European Commission, 2020). <https://eur-lex.europa.eu/legal-content/EN/TXT/PDF/?uri=CELEX:32020L2184&from=EN>^g Recorded in Category 2B control list. (European Commission, 2019). <https://eur-lex.europa.eu/legal-content/EN/TXT/PDF/?uri=CELEX:32020R0784&rid=1>^h US EPA Health advisory level at 70 ng/L. (Cordner et al., 2019).

3 MATERIALS AND METHODS

3.1 Adsorbent materials

Three samples of adsorbents were provided by BASF. Table 4 lists the abbreviations and properties of the three adsorbent samples. Data and manufacturing procedures were summarized from patent document WO 2014/091447 A1 provided by BASF. JEC SHIRASAGI C2x8/12 (JEC) are microporous activated carbon extrudes (coconut-shell based) which served as the base material for subsequent synthesis of the adsorbent material. Ferromagnetic carbon bodies (FMC) were prepared by applying vacuum (40 mbar) for a minimum of 30 min in a 250mL rotating flask. 58 wt.% of ferric (III) nitrate nonahydrate was sprayed on the carbon extrudes in vacuum extrudes. The extrudes were dried under vacuum at 40 °C for at least 12h. Afterwards, they were in the form of iron impregnated after removing from the vacuum environment. After transporting to a fixed bed, the extrudes were heated at a rate of 5 °C/min to 800 °C under a nitrogen flow of 400 ml/min. After 3h the extrudes were cooled to room temperature and stabilized by slowly applying air. The process turned the materials from microporous to mesoporous (Brandts et al., 2020) due to the recrystallization process. Fe and graphite content were evenly distributed at the same locations. FBC were then treated with 4M HCl for 2h stirring to remove the Fe content. After filtering, HCl treatment was applied again and the extrudes were washed with water, finalizing with 110 °C overnight drying. This acid treated carbon extrudes (ATC) had a 95% reduction in Fe amount from 9.81 to 0.55 wt.%. Graphite content was not affected by the acid treatment. FMC and ATC were tested in the isotherm pre-test with Milli-Q water. It was decided to continue the adsorption and regeneration experiments only with ATC (section 3.3).

Table 4 Abbreviations (JEC for JEC SHIRASAGI C2x8/12, FMC for ferromagnetic carbon bodies, ATC for acid treatment carbon bodies) and adsorbent properties.

Abbreviations	Model	Activation state	Fe amount (wt.%) ^a	BET Surface Area(m ² /g) ^a	N ² Pore Volume (ml/g) ^a	Graphite amount (wt.%) ^{ab}
JEC	JEC SHIRASAGI C2x8/12	Virgin	<0.1	1104	0.08	-
FMC	Ferromagnetic carbon bodies	Virgin	9.81	806	0.47	19.0
ATC	Acid treatment carbon bodies	Virgin	0.55	933	0.53	22.8

^a Data retrieved from Patent: WO 2014/091447 A1. (Hoekstra, J., Brandts, J. A. M., et al. (2014)).

^b Determined by XRD in combination with PONKCS software. (Hoekstra, J., Brandts, J. A. M., et al. (2014)).

3.2 Micropollutants, PFAS and water matrices

3.2.1 Choice of pollutants and preparation of solutions

For adsorption isotherm and kinetic experiments, 17 OMP were selected to provide a wide range of applications and physical-chemical properties. They are classified into four different groups based on their charge at neutral pH: i) neutral, ii) positively charged, iii) negatively charged, and iv) zwitterion (Table 5). Native standards of the 17 OMP were obtained from Sigma-Aldrich with purities >98%. The stock solution was prepared by directly dosing the OMP in powder form in Milli-Q water (Appendix E). All TOC-free glassware used in this study was heated at 550 °C for 4h. After stirring in the dark for two weeks until complete dissolution, the solution was kept in the refrigerator at 4°C until use. Test solutions were made by spiking the OMP stock solution into the designated water matrices to obtain target solvents concentrations. For comprehensive and initial spiked concentrations, see Appendix A. For chemical structures of OMP molecules, see Appendix B.

Table 5 Application and physical-chemical properties of the 17 studied OMP.

Group	Compound	Acronym	CAS no.	Application	MW (g/mol) ^a	Log K _{ow} ^b	Charge at pH 7 ^c	pK _a ^d
Neutral	1H-Benzotriazole	BTA	95-14-7	Corrosion inhibitors	119.1	1.44	0	1.6; 8.6
	5-Methyl-1H-benzotriazole	TTA	136-85-6	Corrosion inhibitors	133.2	1.71	0	2.2; 8.8
	Carbamazepine	CBZ	298-46-4	Anticonvulsant	236.3	2.45	0	13.9
	Hydrochlorothiazide	HCT	58-93-5	Diuretic	297.7	-0.07	0	0.6; 14
	Caffeine	CAF	58-08-2	Stimulant	194.2	-0.07	0	14
	Theophylline	TPL	58-55-9	Stimulant	180.2	-0.02	0	3.5; 8.7
Positively charged	Metoprolol	MTL	37350-58-6	Beta blocker	267.4	1.88	+	9.7
	Propranolol	PPL	525-66-6	Beta blocker	259.3	3.48	+	9.4
	Sotalol	STL	3930-20-9	Beta blocker	272.4	0.24	+	8.2; 9.1
	Trimethoprim	TMP	738-70-5	Antibiotic	290.3	0.91	+	1.3; 7.2
	Metformin	MET	657-24-9	Anti-diabetic	129.2	-2.64	+	12.4
Negatively charged	Diclofenac	DFC	15307-86-5	Anti-inflammatory	296.2	4.51	-	4.1
	Ketoprofen	KET	22071-15-4	Anti-inflammatory	254.3	3.12	-	4.5
	Clofibric acid	CA	882-09-7	Herbicide	214.7	2.57	-	3.5
	Sulfadimethoxine	SDM	122-11-2	Antibiotic	310.3	1.63	-	2.0; 6.7
	Sulfamethoxazole	SMX	723-46-6	Antibiotic	253.3	0.89	-	1.8; 5.8
Zwitterion	Gabapentin	GBP	60142-96-3	Anticonvulsant	171.2	-1.1	+/-zwitterion	3.7; 10

^a MW: molecular weight (PubChem 2022).

^b Octanol-water partition coefficient (PubChem 2022).

^c Neutral (0), positive (+), negative (-).

^d (PubChem 2022).

^e Estimated values retrieved from SPARC (ARChem, <http://www.archemcalc.com/>).



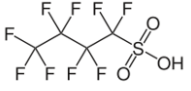
For the OMP regeneration experiment (section 3.4), several OMP were selected to conduct initial adsorption and re-adsorption experiments to evaluate regeneration efficiency. A higher OMP dosage was required to achieve higher OMP loading on the adsorbents. The OMP selection criteria were mainly based on diversity in charged groups and sufficient availability of OMP. An initial concentration of 5 mg/L for both initial adsorption and re-adsorption was utilized. The experiment with multiple cycles of regeneration were conducted with seven OMP. Experiments with varying operating parameters were conducted with nine OMP (listed in Table 6).

Table 6 Studied OMP in multiple cycles of regeneration experiment and varying operating parameters experiments.

Group	Compound	Acronym	Multiple cycles of regeneration experiment	Varying operating parameters experiments
Neutral	1H-Benzotriazole	BTA		
	5-Methyl-1H-benzotriazole	TTA		
	Carbamazepine	CBZ		✓
	Hydrochlorothiazide	HCT		
	Caffeine	CAF	✓	✓
	Theophylline	TPL		
Positively charged	Metoprolol	MTL	✓	✓
	Propranolol	PPL		
	Sotalol	STL	✓	✓
	Trimethoprim	TMP		
	Metformin	MET	✓	✓
Negatively charged	Diclofenac	DFC		
	Ketoprofen	KET	✓	✓
	Clofibric acid	CA		
	Sulfadimethoxine	SDM		✓
	Sulfamethoxazole	SMX	✓	✓
Zwitterion	Gabapentin	GBP	✓	✓

One set of regeneration experiments was also conducted on PFAS-loaded adsorbents. All PFAS reference standards were obtained from Sigma-Aldrich. Three PFAS were selected to investigate the effect of chain length, including two long-chain PFAS (PFHpA and PFOA) and one short-chain PFAS (PFBS). Table 7 reports the classification and characteristics of the selected PFAS. PFAS in powder or solid form were directly dosed into the water matrix to obtain the target initial concentration.

Table 7 Physical-chemical properties and structures of three studied FPAS.

Full name	Abbreviation	Functional group	Formula	Structure	MW (g/mol) ^a	Log K _{ow} ^b	pK _a ^c	Chain length	Chain group ^d
Perfluoroheptanoic acid	PFHpA	carboxylate	C ₇ HF ₁₃ O ₂		364.06	4.41	-2.29	7	long-chain
Perfluorooctanoic acid	PFOA	carboxylate	C ₈ HF ₁₅ O ₂		414.07	5.11	-4.2	8	long-chain
Perfluorobutanesulfonic acid	PFBS	sulfonate	C ₄ HF ₉ O ₃ S		300.09	2.63	-3.31	4	short-chain

^a MW: molecular weight (PubChem 2022).

^b Octanol-water partition coefficient (PubChem 2022).

^c (PubChem 2022).

^d The definition of long-chain and short-chain is in accordance of EU authorities (European Commission, 2020).
https://ec.europa.eu/environment/pdf/chemicals/2020/10/SWD_PFAS.pdf

3.2.2 Analytical method

High performance liquid chromatography combined with tandem mass spectrometry (LC-MS) was used for OMP quantification. Through ACQUITY UPLC®BEH C18 column (1.7 μ m particle size, 2.1 \times 50 mm, Waters, Ireland) the liquid chromatography separates the sample components. Pumping was performed by an ACQUITY UPLC I-Class Plus System (Waters, USA) at a flow rate of 0.35 ml/min. For gradient elution, ultrapure water and acetonitrile (LC-MS grade, Biosolve, France) phases were used. Both were acidified with 0.1 % LC-MS grade formic acid (Biosolve, France). Tandem mass spectrometry was performed on Xevo TQ-S micro (Waters, USA), separating ionized molecules with electrospray ionization in positive and negative modes and detecting them by corresponding deuterated internal standards. The calibration levels are from 0.0025 to 25 μ g/L to 10 μ g/L.

TOC analysis was performed by a SHIMADZU TOC-VCPH/CPN analyzer. Briefly, 30 mL of sample was filtered by Whatman® SPARTAN® RC 30 syringe filter. Next, 1.6 ml of 2M analytical grade hydrochloric acid was added to the sample vial. A TOC standard (10 ppm) was prepared to ensure the measurement quality.

Surface area and pore volume analyses were conducted by the N₂ adsorption-desorption methods. 0.1 g of sample was dried for 15 h at 105 °C before measurement. N₂ adsorption was performed at -196.15°C with a Micrometrics TriStar II unit. The surface area (m²/g) was calculated by Brunauer-Emmett-Teller (BET) method. Micropore and mesopore volume (cm³/g) were calculated by t-plot and Barrett-Joyner-Halenda (BJH) desorption.

PFAS were analyzed externally at Het Waterlaboratorium. Samples were diluted on the day of sampling. This preservative ensured that the composition of the samples was immediately suitable for injecting into the UHPLC. An exact amount of isotope-labeled internal standards was added to the preserved water sample on the day of analysis, followed by filtration through a 0.45 μ m filter (Whatman Spartan 30). 100 μ L of the filtrate was applied to a MM column. After the chromatographic separation, PFAS were detected with a TQ- MS in negative ionization mode according to the MRM principle. Afterwards, the concentrations were evaluated by linear calibration with eight calibration points ranging from 0 – 50 ng/L. The reporting limits are 0.2 ng/L (PFHpA), 0.5 ng/L (PFOA) and 0.2 ng/L (PFBS).

3.2.3 Water matrices

For isotherm and kinetic adsorption experiments (sections 4.1 and 4.2), three water matrices were used, characterized by their different organic content: Milli-Q water (MQ), Delft tap water (TW) and RWZI Harnaschpolder wastewater treatment plant effluent (WW). Table 8 shows the characteristics of the three tested water matrices. The background NOM concentration was measured as dissolved organic carbon (DOC) concentration and as UV-absorbance at a wavelength of 254 nm. WW was filtered by 1 μm cartridge filters. OMP stock solution of 1 mg/L was spiked in all three water matrices to target an initial concentration of 10 $\mu\text{g/L}$ OMP in the test solutions. All regeneration experiments were carried out in TW. The same source of TW was used as in the kinetic and isotherm adsorption experiments. The OMP powder was dosed directly into the water matrices to make test solutions at OMP concentrations of 5 mg/L. In all cases, adsorbent removal calculations were based on actual measurements and not theoretical dissolved concentrations. To account for losses due to volatilization and/or adsorption on glassware and caps, control bottles without adsorbents were included in the adsorption experiment, spiked with OMP stock solution. Standard deviations of all 17 OMP in 312 hours of control were $< 1.5 \mu\text{g/L}$ in all cases (at initial concentrations of 10 $\mu\text{g/L}$), indicating no significant change due to losses.

Table 8 Characteristics of the three tested water matrices.

Water type	Acronym	DOC (mg/L)	pH (-)	Conductivity ($\mu\text{S/cm}$)	UV254 (A/cm)	SUVA254 (L/mg.m)
Milli-Q water	MQ	0.21 ± 0.05	7.70 ± 0.23	1.97 ± 0.74	-	-
Tap water	TW	4.97 ± 0.52	7.98 ± 0.01	448.33 ± 1.53	0.047 ± 0.001	0.95 ± 0.12
WWTP second effluent	WW	13.93 ± 1.22	8.18 ± 0.02	1000.00 ± 1.73	0.273 ± 0.001	1.96 ± 0.04

3.3 Adsorption experiments

Adsorption isotherms and kinetics on OMP removal were measured by the bottle point technique (Worch, 2012). Fig. 6 describes the process of carbon preparation and adsorption experiments in flow charts. Dry adsorbents were washed with deionized water before the experiments and dried at 105°C. Dried adsorbents were stored in the desiccator before use. To pre-wet the adsorbents, all carbon particles were weighed into bottles, and 10 mL of ultrapure water were added. Vacuum was applied for 15 min to remove air bubbles in the adsorbents' pores.

In all cases, 500 mL glass bottles were used as adsorption batch reactor, filled with 500 mL spiked solution and placed in the dark. The bottles were shaken by VWR® Advanced Orbital Shakers (Model 10000) at 120 rpm and room temperature for 312h. Both isotherm and kinetic experiments were spiked at 10 µg/L of each OMP. Kinetic points were sampled (10 mL) in polypropylene tubes at increasing contact times (24, 48, 120, 312h), and the last points were taken as isotherm points. For the isotherm experiment, five adsorbent doses were used, spanning from 30 mg/L to 500 mg/L in all three water matrices. The minimum adsorbent dosage was determined to be at least 30 mg/L because a minimum of three pellets were required in each bottle (5 mg per pellet). Control bottles with the same adsorbate concentrations and no adsorbent dose were included for each water matrix case to ensure no significant loss due to adsorption on glassware and caps. They were sampled at the same time intervals with batch reactor bottles, and averaged measured concentrations were taken as initial adsorbates concentrations. Pre-test was conducted with one duplicate in one condition (adsorbent dosage at 100 mg/L, standard deviation ranged from 0.0029 to 0.1185 µg/L). Adsorption experiments were conducted without duplicates due to limited LC-MS measurement availability. In all cases, samples were stored immediately at 4 °C and filtered through ADVANTEC® glass fiber membrane filters (GF-75, 25mm/0.3 µm, SWINNEX® 25 mm filter holder).

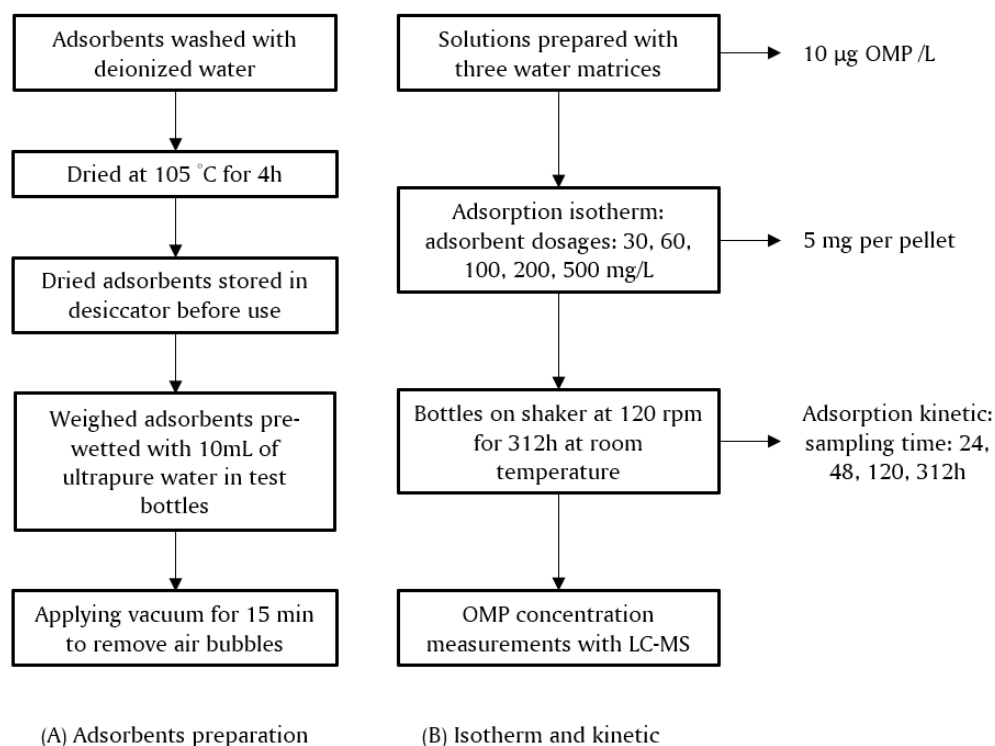


Fig. 6 Flow charts of (A): adsorbents preparation and (B): adsorption isotherm and kinetic experiments

Pre-tests (isotherm test with conditions identical to the above description) were performed with both materials, FMC and ATC, in separate bottles with Milli-Q water. Iron flocs were formed on the surface of FMC. The solution appeared to be yellowish after the pre-test due to the reaction of iron content in FMC (Fig. 6). It was therefore decided to continue the adsorption and subsequent regeneration experiment with ATC only. The presence of zero-valent iron in the carbon particles may cause complex interaction during adsorption and regeneration. Due to the nature of this study as a feasibility test and time limitation, ATC was considered to be the proper and simple version of the novel material in this study.

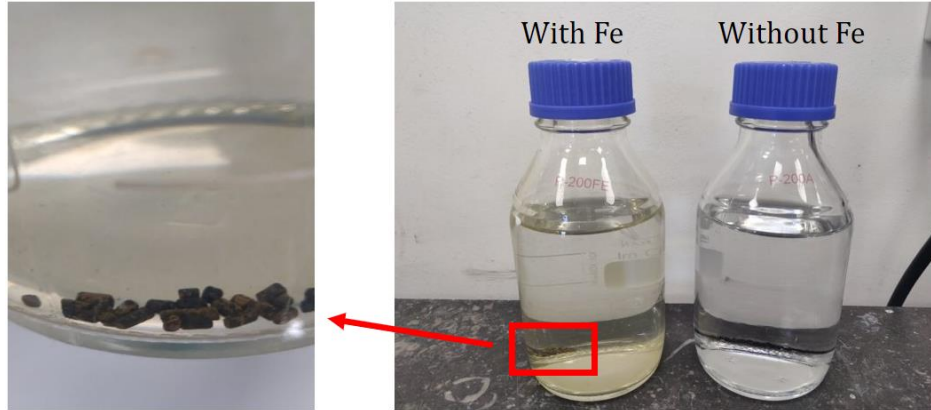


Fig. 7 Left: Zoom in of FMC after pre-test in Milli-Q water. Iron flocs were formed on the surface of FMC pellets. Right: Solution containing FMC appeared to be yellowish, while solution containing GWC remained transparent.

3.4 Electrochemical regeneration experiments

Electrochemical regeneration of this novel material was investigated in an undivided fixed bed electrochemical cell. Fig. 8 and Fig. 9 show the electrochemical cell schematic and picture, respectively. Two $4 \times 4 \text{ cm}^2$ titanium plates were used as anode and cathode, with a working area of 12 cm^2 . A distance of 2 cm was kept between anode and cathode to prevent short-circuiting. 0.2 g of adsorbent was used to ensure adequate bed volume. Higher adsorbent dosage was not considered due to inadequate adsorbate. The thickness of adsorbents refrained direct contact with electrodes plates. A DC power supply was utilized to provide constant current by manipulating cell voltage during regeneration. Pollutant-loaded adsorbents were filled into a nylon bucket without direct contact with the electrodes surface (a distance of 0.5 cm was always kept). Delft tap water was used as an electrolyte without chemical additions (characteristics can be found in Table 8). During the course of regeneration, the electrolyte solution was stirred continuously by a magnetic stirrer (Heidolph MR 82) at 200 rpm to facilitate the mass transfer.

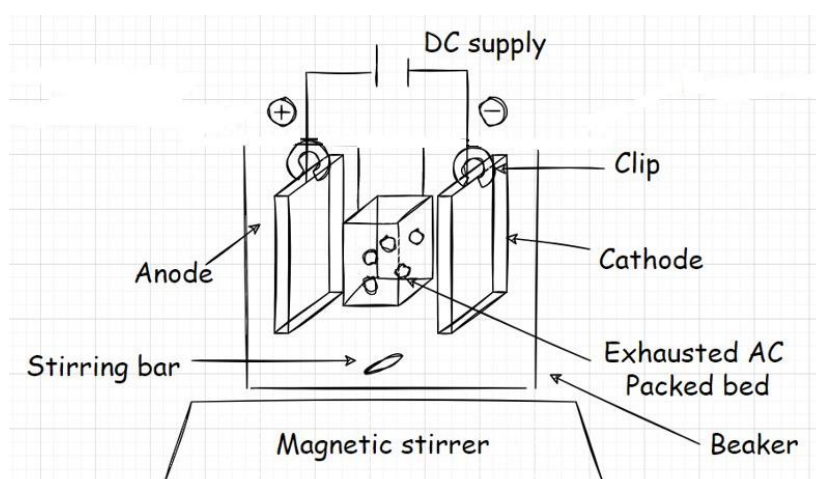


Fig. 8 Electrochemical cell schematic.

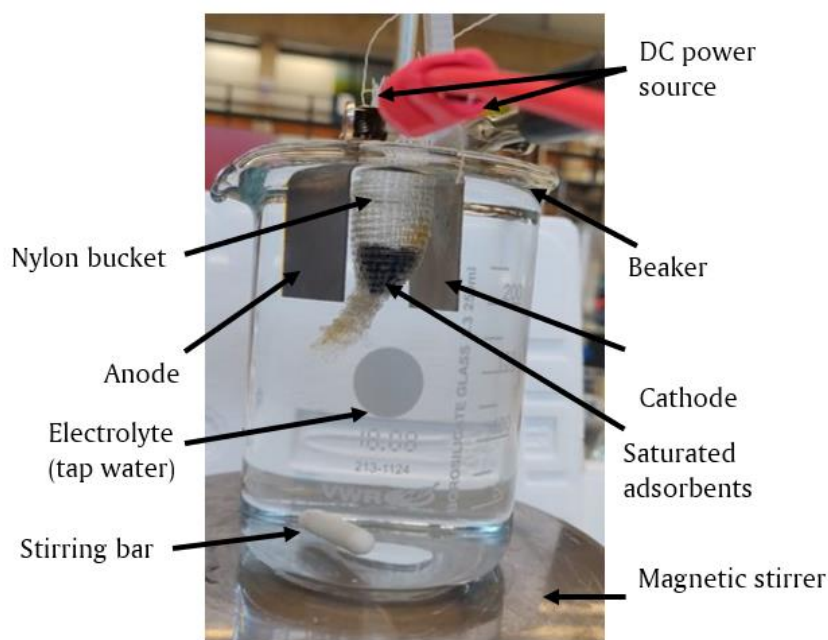


Fig. 9 A picture of electrochemical cell used in the regeneration experiment in all cases. This setup was realized according to schematic shown in Fig. 8.

Investigation of regeneration efficiency of this novel material (only on the version without iron: i.e. ATC, as stated in section 3.3) was conducted with subsequent cycles of adsorption and regeneration. Two batches of ATC with the same mass (200 mg) underwent six cycles of adsorption simultaneously. One batch was regenerated in between each adsorption cycle. Another batch served as a control group with no regeneration, and it was drained and stored separately before the next cycle of adsorption. The standard procedure is described in Table 9.

Table 9 Standard procedure of regeneration experiment.

Step	
1	Initial adsorption
1.1	A known mass of material (200 mg) was added to Delft tap water containing known concentration of adsorbates. For OMP regeneration. 200 mL solution with a concentration of 5 mg/L was used. For PFAS, 50 mL solution with a concentration of 100 mg/L.
1.2	Place all the contents in step 1.1 in a batch reactor. Place the batch reactor on a shaker at 120 rpm for a fixed period of time. 120h and 72h contact time were adopted for OMP and PFAS experiment respectively.
1.3	After designated contact time. A sample of treated liquid is taken and measured. For OMP, 20 µL samples were taken, diluted and measured in-house. For PFAS, 10 mL samples were taken and sent to Het Waterlaboratorium for dilution and measurement.
1.4	By mass balance the initial adsorbent loading (q_i) is determined.
2	Electrochemical regeneration
2.1	Load all the carbon content in step 1 into the electrochemical cell.
2.2	Apply DC current to the electrochemical cell for 3h for both OMP and PFAS regeneration.
2.3	Take samples (10 mL from electrolyte, add 10 mL of tap water afterwards to maintain initial electrolyte volume) at regular time intervals during regeneration. Results are shown in section 0.
2.4	Drain off and store used electrolyte. All contents of electrochemical cell (i.e. electrodes, nylon bucket, stirring bar and beaker) were rinsed with deionized water for next cycle of regeneration.
3	Re-adsorption
3.1	Repeat step 1.1-1.4 by regenerated adsorbents (i.e. contents from step 2 with no further treatment).
3.2	By mass balance the adsorbent loading after regeneration (q_r) is determined.
3.3	The regeneration efficiency (RE) is defined by the equation:
$RE = \frac{q_r}{q_i} \times 100\%$ <p style="text-align: right;">Eqs. (4)</p> <p>where, q_i is the initial adsorbent loading (mg/g) and q_r the adsorbent loading after regeneration (mg/g).</p>	

Experiments with varying operating parameters were conducted with the above standard procedure. Only one cycle of regeneration was conducted for each condition. The applied current applied varied between 10 – 80 mA at a fixed treatment time of 1h. The regeneration time was set between 0.5 – 5 h at a fixed current of 60 mA. The studied OMP are listed in Table 6. An overview of all performed experiments can be found in Appendix F.

3.5 Adsorption isotherm and kinetic models

Adsorption isotherm data were fitted by the Freundlich equation. This empirical equation describes the adsorption process and equilibrium data for a heterogeneous surface (Freundlich 1906). The Freundlich equation was chosen because the description of low OMP concentration (i.e. $\mu\text{g/L}$ to ng/L) adsorption in water is possible (Xu et al 2013 from Hong). Eqs. (5) and Eqs. (6) show the nonlinear and linear forms of the Freundlich equation.

$$q_e = K_F C_e^n \quad \text{Eqs. (5)}$$

$$\log q_e = \log K_F + n \log C_e \quad \text{Eqs. (6)}$$

Where q_e ($\mu\text{g/mg}$) is the equilibrium uptake of contaminant species in the solid phase; $K_F [(\mu\text{g/mg})/(\mu\text{g/L})^n]$ is the Freundlich constant which characterizes adsorption capacity (Worch, 2012); C_e is the adsorbate concentration in solution at equilibrium and; n (dimensionless) is the Freundlich intensity parameter, which is an indicator of adsorption affinity (Worch, 2012), or a measure of surface heterogeneity (Tran et al., 2017).

Kinetic data were fitted by the Pseudo-second-order (PSO) equation. It was initially proposed by Blanchard et al., (1984) and further developed into linear form by Ho & McKay (1998). PSO was selected to describe adsorption kinetics because it was said to be an appropriate representation for the majority of adsorbent adsorbate systems (Ho & McKay, 1999). Eqs. (7) and Eqs. (8) show the initial nonlinear and linear forms of the PSO equation. q_e was calculated from the plot of $1/q_t$ versus time $1/t$ by Eqs. (8).

$$q_t = \frac{q_e^2 k_2 t}{1 + k_2 q_e t} \quad \text{Eqs. (7)}$$

$$\frac{1}{q_t} = \left(\frac{1}{k_2 q_e^2} \right) \frac{1}{t} + \frac{1}{q_e} \quad \text{Eqs. (8)}$$

Where q_t ($\mu\text{g/mg}$) and q_e ($\mu\text{g/mg}$) are uptakes of contaminant species at any time t (h) and at equilibrium, respectively; and k_2 [$\text{mg}/(\mu\text{g.h})$] is the second-order rate constant.

4 RESULTS AND DISCUSSION

4.1 OMP adsorption capacity in different water matrices

The Freundlich model fitted well to the isotherm data of all experiments with average R^2 values ranging from 0.77 to 0.99 (model coefficients are reported in Table 10). Several compounds were assumed to be degraded because gradual drops of concentration in the control bottles were recorded. Freundlich data plots and interpolation lines are shown in Fig. 10 for CBZ, STL, and SMX, each of which is charged OMP as described in Section 3.2. For all other OMP plots, see Appendix C.

Table 10 Adsorption isotherm parameters for ATC applying the Freundlich model.

Isotherms		Model Coefficients								
		Milli-Q water			Tap water			WWTP effluent		
		K_F (ug/mg)			K_F (ug/mg)			K_F (ug/mg)		
Group	OMP	$1/(ug/L)^n$	n [-]	R^2	$1/(ug/L)^n$	n [-]	R^2	$1/(ug/L)^n$	n [-]	R^2
Neutral	BTA	0.24	0.32	0.92	_b	_b	_b	0.04	0.68	0.83
	TTA	0.25	0.39	0.99	_b	_b	_b	_b	_b	_b
	CBZ	0.27	0.35	0.99	0.08	0.53	0.96	0.03	0.77	0.83
	HCT	_a	_a	_a	_a	_a	_a	_a	_a	_a
	CAF	0.29	0.42	0.99	0.05	0.87	0.83	_b	_b	_b
	TPL	0.37	0.25	0.91	0.11	0.57	0.93	_b	_b	_b
Positively charged	MTL	0.19	0.44	0.86	0.09	0.56	0.92	_b	_b	_b
	PPL	0.19	0.54	0.77	0.10	0.44	0.93	0.06	0.94	0.84
	STL	0.14	0.22	0.87	0.08	0.52	0.95	0.02	0.84	0.82
	TMP	0.18	0.32	0.90	0.07	0.43	0.95	0.02	0.78	0.83
	MET	0.00	3.50	0.80	_b	_b	_b	_b	_b	_b
Negatively charged	DFC	0.20	0.40	0.93	0.05	0.43	0.96	0.01	0.79	0.84
	KET	0.17	0.53	0.78	0.04	0.44	0.92	0.01	0.99	0.89
	CA	_a	_a	_a	0.04	0.29	0.81	0.01	0.90	0.95
	SDM	0.18	0.34	0.99	0.03	0.30	0.84	0.01	0.82	0.75
	SMX	0.21	0.37	0.89	0.04	0.46	0.96	0.01	0.75	0.90
Zwitterion	GBP	0.09	0.27	0.98	0.03	0.42	0.91	_b	_b	_b

^a Invalid results due to inaccurate measurement.

^b Invalid results due to degradation.

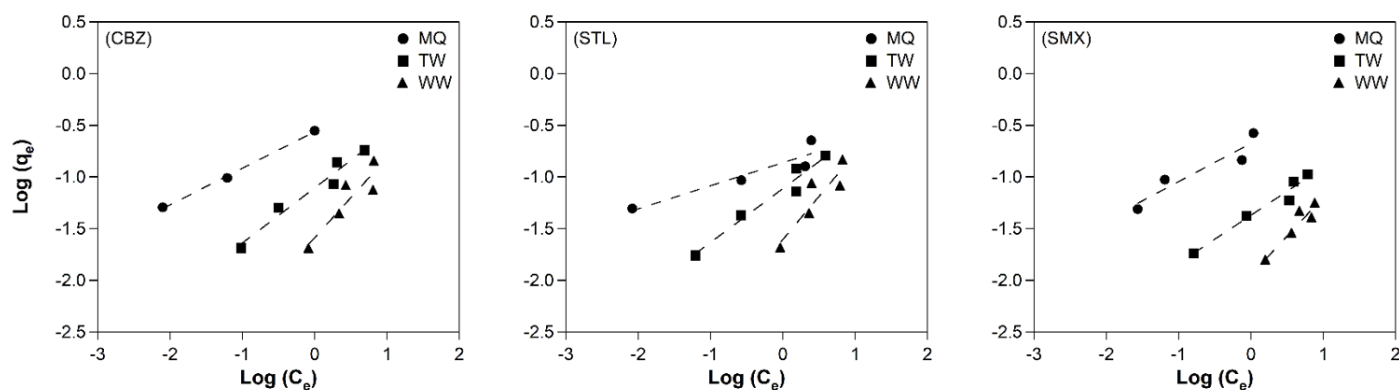


Fig. 10 Isotherms for carbamazepine (CBZ), sotalol (STL) and sulfamethoxazole (SMX) in three test solutions: Mill-Q water (MQ), tap water (TW) and WWTP effluent (WW).

To characterize the strength of adsorption of the OMP, the Freundlich constant K_F was obtained from the model. The constant K_F is an indicator of adsorption capacity (Worch, 2012) and is considered to be comparable in case of similar Freundlich parameters n (a quantification of adsorption affinity). In this study, the n values for all solutes (except for metformin in MQ: 3.50) were less than 1 (MQ: 0.22 – 0.54, TW: 0.29 – 0.87, WW: 0.68 – 0.99), representing a concave shape of isotherms which indicates high adsorption affinity between pollutants and GAC (Lompe et al., 2018). However, the n values obtained in the three water matrices were significantly different from each other ($p < 0.05$). The box plot summarizes adsorption performance for all OMP in three solutions (Fig. 11). The difference of n values among three solutions indicates descending adsorption affinity: MQ > TW > WW, hinting the K_F values were not comparable to each other. The isotherm data plot (for example, Fig. 10 (STL)) visualizes a similar conclusion: the slopes of three interpolation lines are different.

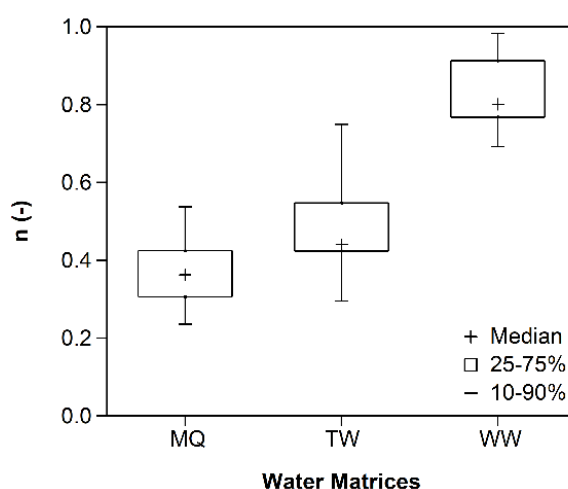


Fig. 11 The n values obtained from isotherm data by fitting the Freundlich model.

The difference in adsorption affinity in the various water matrices is likely to be caused by varying NOM background concentrations, indicated by DOC values (Table 8). By testing pollutants uptake in tap water and WWTP effluent, the model coefficients indirectly incorporate the competition effect (Piazzoli & Antonelli, 2018). The presence of NOM hinders OMP adsorption onto activated carbon (Q. Li et al., 2003). This phenomenon is acknowledged as direct competition and pore blocking (Q. Wang et al., 2022). NOM competes with other adsorbates (OMP in this adsorption experiments) for adsorption sites, and they block the access to the micropores on the adsorbents instead of entering (Pelekani & Snoeyink, 1999). Both of these mechanisms explain the significant drop in OMP uptake in water matrices with NOM (i.e. TW and WW). The drop of adsorption affinity of most OMP (25 - 75% shown in box plot Fig. 11) were consistent with the corresponding NOM concentration in solutions. Interpolation of model coefficients might be possible for further adsorption model development or pilot setup design.

Even though inter-water matrices K_F values comparison is not possible, intra-water matrices K_F values could still be compared because of similar NOM characteristics and concentration. In the case of MQ (i.e. without NOM), hydrophobicity (expressed by $\text{Log } K_{ow}$) of OMP was a leading property that affected adsorption capacity (Fig. 12). Hydrophobic compounds tend to have higher adsorbability (Westerhoff et al., 2005). Hydrophilic compounds are inclined to remain in the aqueous phase and thus exhibit low removals as a result. GBP and MET adsorption are particularly poor even without NOM competition. They exhibit low $\text{Log } K_{ow}$ values (-1.1 and -2.64, respectively, Table 5). Their hydrophilic properties are likely due to the absence of aromatic rings (de Ridder et al., 2010). The lack of aromatic rings in the structure (Appendix B) weakens the $\pi-\pi$ bond interactions between solutes and adsorbents surfaces (Peng et al., 2016).

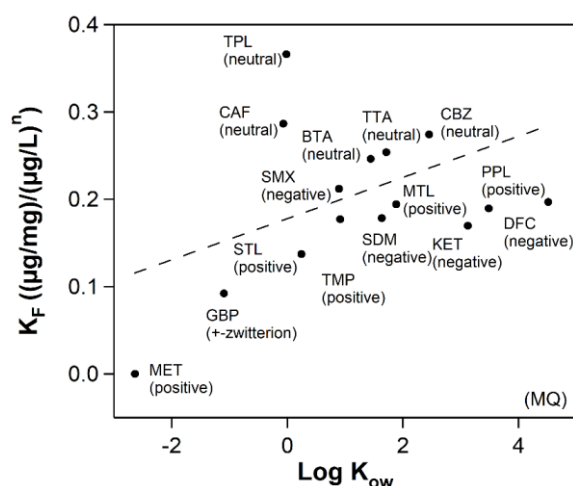


Fig. 12 Freundlich constants K_F -values versus OMP properties in MQ water.

This result is consistent with the conclusion made by Delgado et al., (2012), in which they pointed out that the octanol-water partition coefficient could act as an appropriate measure to predict adsorbability. On the other hand, they also mentioned that it cannot be a sole indicator to describe adsorption activities. This reduces the complexity of the interaction between adsorbents and adsorbates as a pure hydrophobic interaction. Other factors, for instance, properties of the carbon and contaminant compounds, should be taken into account. In this case, the charges of OMP were observed to be another factor affecting adsorption capacities. An ANOVA test was performed, and the K_F of neutral OMP are significantly higher than that of positively or negatively charged compounds ($p < 0.05$). The charges of OMP are annotated on the figure for better visualization, and a linear regression line was fitted. The K_F values of all five neutral compounds were higher, whereas the charged compounds showed a lower adsorption capacity. The better adsorption of neutral compounds matched the expectation from BASF (Brandts et al., 2020). They have indicated that the graphite content in the material would attract neutral components. No significant difference was found among the K_F values of positively and negatively charged OMP.

The observation of OMP adsorption in MQ did not fully match observations in TW and WW. In the presence of NOM, no insight was gained by comparing hydrophobicity. Instead, charge interaction became the dominant factor determining OMP uptakes (Fig. 13). Both neutral and positively charged compounds were well adsorbed. NOM is known to have an influence on the removal of charged adsorbates (DeRidder et al., 2011). Their study evaluated the effect of NOM coverage on charged pharmaceuticals removal. The accumulation of NOM on the adsorbent surface leads to significantly higher removal of positively charged compounds than that of negatively charged species. This phenomenon was also observed in the present study. K_F values of positively charged OMP were statistically higher than those of the negatively charged ($p < 0.05$), in both TW and WW as test solutions. At neutral pH, NOM is negatively charged (Newcombe & Drikas, 1997). A layer of negatively charged NOM is formed on the GAC surface due to adsorption. This promotes electrostatic attraction to cation and repulsion to anion (DeRidder et al., 2011) and explains the uptake difference between the positively and negatively charged OMP. This phenomenon is thought to be particularly significant for this material. Due to its mesoporous property, BASF obtained better performance for humic acid (2-7 nm) adsorption within 24h. Fast NOM accumulation forms a layer of negatively charged sub-surface on the carbon and attracts positively charged OMP. Furthermore, there was no significant difference in the comparison of neutral and positively charged compounds (TW: $p = 0.78$; WW: $p = 0.83$). Isotherm results showed that this material favored both neutral and positively charged components.

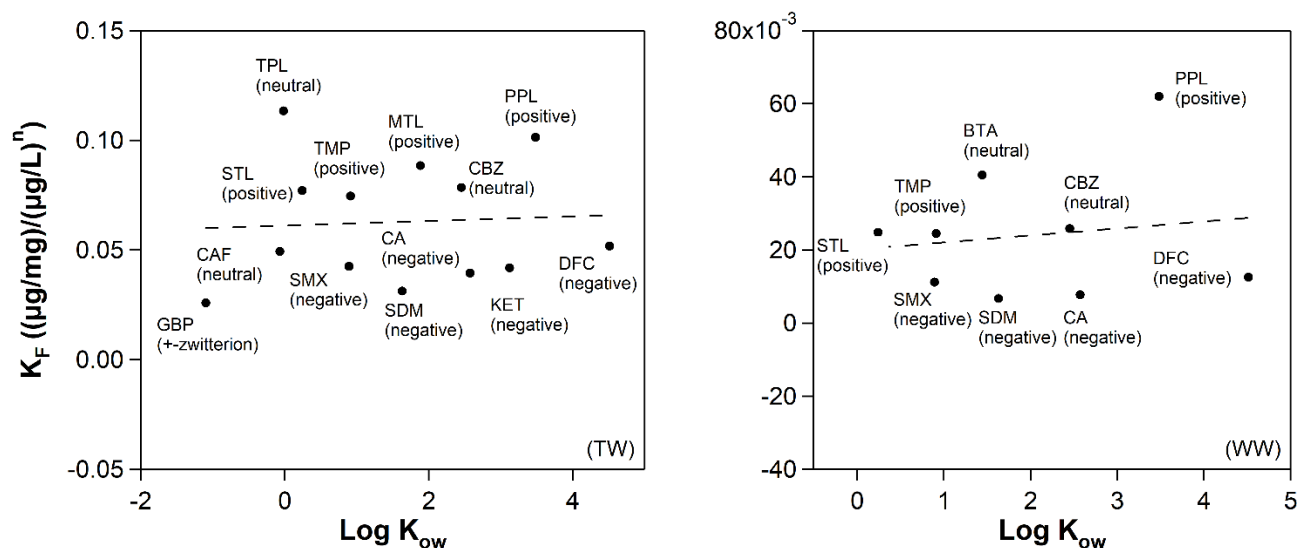


Fig. 13 Freundlich constants K_F -values versus OMP properties in TW and WW.

4.2 OMP adsorption kinetics in different water matrices

Kinetic experiments were simultaneously conducted with the isotherm experiments; thus the testing conditions were identical (initial adsorbent and adsorbate dose and water matrices). The PSO model fitted well to the kinetic data for all three water matrices with R^2 values ranging from 0.87 to 1.00 (Table 11). For the kinetic data from the adsorbent dose of 200 mg/L, the model fitted the best ($R^2 = 1.00$). It was therefore selected to be the representation of the kinetic experiments results. Fig. 14 shows the adsorption profiles of CBZ, STL and SMX, each of which are charged OMP as described in Section 3.2. For all other OMP plots, see Appendix D. >82% removal of all OMP was reached after 120 hours for MQ, >72% for TW and 43% WW. Under this condition, equilibrium was achieved after a maximum of 150h for all three water matrixes. Kinetic constants k_2 varied between 0.84 - 0.90, 0.31 – 0.93 and 0.35 – 1.25 mg/(μ g h) for MQ, TW and WW, respectively (Fig. 15). Without competition (test solution as MQ), the k_2 values of different OMP were similar to each other (average $k_2 = 0.87 \pm 0.02$, unit: mg/(μ g.h). In the condition with the presence of NOM (test solution as TW and WW), the k_2 values deviate from each other (TW: 0.60 ± 0.19 and WW: 0.61 ± 0.33) and were significantly lower than those of MQ ($p < 0.05$). The significant drop in k_2 is in alignment with different n values reported in Section 4.2, demonstrating the same effect that NOM presence causes intraparticle pore blockage and limits the rate of adsorption process (Yu et al., 2012).

Table 11 Kinetic parameters (PSO model) for OMP adsorption onto ATC (200 mg/L) for 312h

Kinetics		Model Coefficients					
		Milli-Q water		Tap water		WWTP effluent	
Group	OMP	k_2 mg/(ug.h)	R^2	k_2 mg/(ug.h)	R^2	k_2 mg/(ug.h)	R^2
Neutral	BTA	0.86	0.86	_b	_b	0.43	1.00
	TTA	0.88	0.88	_b	_b	_b	_b
	CBZ	0.88	0.88	0.46	1.00	0.37	0.99
	HCT	_a	_a	_a	_a	_a	_a
	CAF	0.86	0.86	0.65	0.99	_b	_b
	TPL	0.85	0.85	0.31	0.99	_b	_b
Positively charged	MTL	_a	_a	0.48	1.00	_b	_b
	PPL	0.88	0.88	0.62	0.99	0.41	0.95
	STL	0.84	0.84	0.41	0.99	0.35	0.99
	TMP	0.88	0.88	0.58	1.00	0.60	0.97
	MET	_a	_a	_b	_b	_b	_b
Negatively charged	DFC	0.90	0.90	0.48	1.00	0.51	0.99
	KET	0.84	0.84	0.83	1.00	0.50	0.98
	CA	_a	_a	0.69	1.00	1.15	0.96
	SDM	0.89	0.89	0.86	1.00	1.25	0.96
	SMX	0.88	0.88	0.46	1.00	0.53	0.97
Zwitterion	GBP	0.88	0.88	0.93	1.00	_b	_b

^a Invalid results due to inaccurate measurement.

^b Invalid results due to degradation.

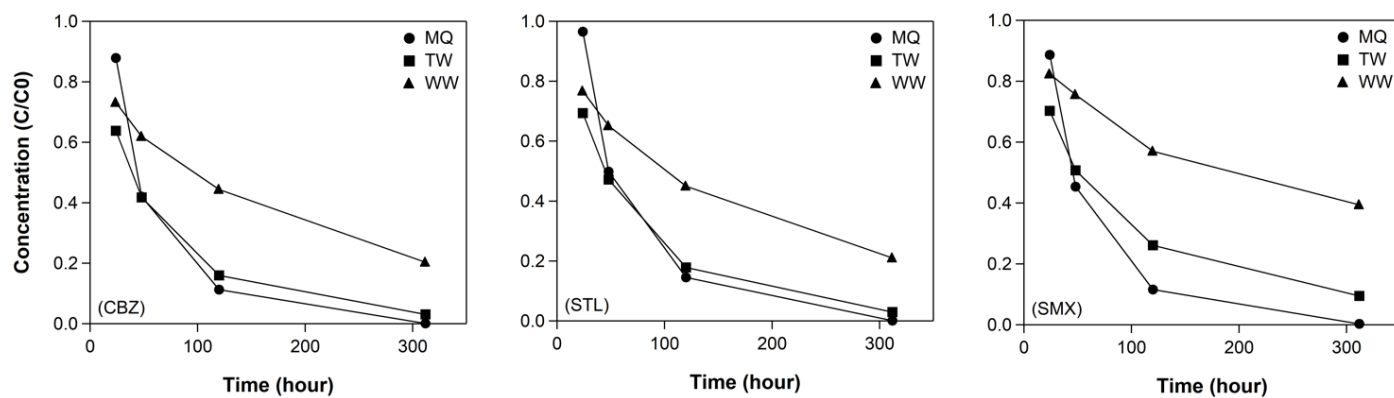


Fig. 14 Adsorption kinetic profiles of CBZ, STL and SMX (adsorbent dose: 200 mg/L).

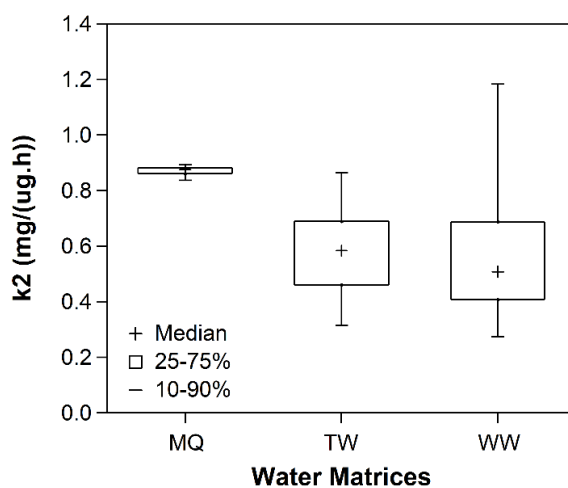


Fig. 15 PSO constants k_2 at GAC dose of 200 mg/L from three water matrices: Milli-Q water (MQ), tap water (TW) and WWTP effluent (WW). The k_2 values of MQ were significantly larger than those of TW and WW ($p < 0.05$).

No insight was gained by correlating the k_2 values with OMP properties, including molecular weight, hydrophobicity and charge. The k_2 constants were best correlated with the Freundlich constants K_F , which describe the comprehensive adsorption capacity of OMP. Fig. 16 shows the plot of k_2 values as a function of the Freundlich constants. OMP with higher adsorbability show a slower adsorption rate. This is probably attributed to more micropores responsible for OMP adsorption and longer intra-particles diffusion time is required for adsorbates transport. For those OMP with poor adsorbability, less loading on adsorbents results in faster equilibrium.

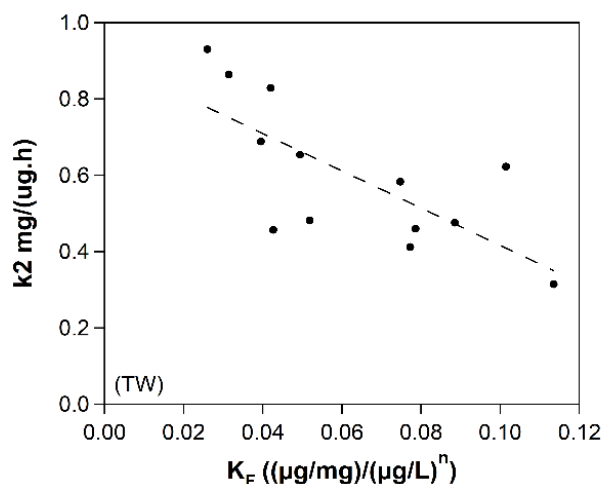


Fig. 16 PSO constants k_2 as a function of the Freundlich model constants K_F in TW.

In section 4.1, it was described that NOM accumulation on the carbon surface forms a negatively charged layer and assists the adsorption of positively charged species. The plot in Fig. 16 is separated into three charged groups to study this effect in kinetics (Fig. 17). For neutral and negatively compounds, their adsorption rates followed the same trend as described in the last paragraph. However, the k_2 values of positively charged compounds were in positive correlation with their adsorption capacities. It is speculated that their adsorbability was influenced by the negatively charged NOM layer (increased electrostatic attractive forces).

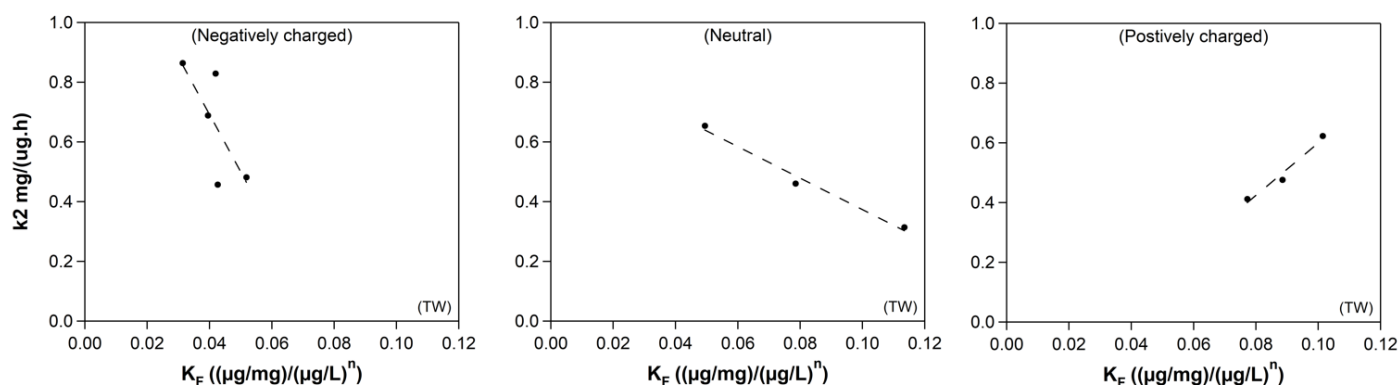


Fig. 17 k_2 values in TW as a function of OMP K_F values and charge at pH 7 (positively charged, negatively charged and neutral). Zwitterion compound (GBP) is not included.

4.3 Adsorption performance comparison between the novel adsorbent and regular GAC

OMP adsorption performance of ATC was compared with Filtrasorb F400 GAC data from previous work. F400 is a type of GAC that has been widely used among adsorption studies and worldwide treatment systems. Table 12 lists k_2 values of the PSO model of two adsorbents. Initial OMP concentrations were identical in all cases. Groundwater was used in previous work with a background DOC concentration of 2.3 mg/L (compared with TW: 5 mg/L in this study). In both MQ and TW cases, the adsorption rates of ATC were significantly higher than those of F400 ($p < 0.05$). Even in the case of higher NOM concentration, ATC was more capable of coping with the effects of direct competition and pore blocking. This is attributed to its mesoporous property that allows certain mass transfer even with NOM blockage. For the isotherm data, an initial adsorbate dose of 50 $\mu\text{g/L}$ was used, five times higher than this study. Table 13 lists the Freundlich model coefficients comparison. The n values in MQ cases were similar, which allows K_F values to be comparable. The adsorption capacity of F400 is significantly higher than that of ATC. This is most likely due to the lower micropore volume of ATC (0.33 ml/g), while F400 was reported to contain 0.40 ml/g of micropores (Diamantopoulou et al., 2010). The difference could also be caused by different initial adsorbate concentrations and contact time. It is thought that this weakness can be counterbalanced by its high adsorption rate, since the internal diffusion rate also determines how efficient the system is. Combining with its potential to be regenerated in-situ, it was therefore still recommended to continue further investigation on this novel material.

Table 12 Comparison of kinetic constants between F400 FAC and ATC. (Krijn, 2021).

OMP	PSO model constant k_2 [mg/(ug.h)]			
	Groundwater / TW		MQ	
	F400 GAC	ATC	F400 GAC	ATC
BTA	0.000	-	0.003	0.864
CBZ	0.295	0.460	0.004	0.878
CAF	-	0.654	0.008	0.864
STL	0.276	0.412	0.002	0.837
DFC	0.402	0.482	0.004	0.900

Table 13 Comparison of Freundlich model constants between F400 FAC and ATC. (Krijn, 2021).

OMP	Freundlich model coefficients				n [-]			
	K_F [(ug/mg)/(ug/L) ⁿ]		MQ		Groundwater / TW		MQ	
	F400 GAC	ATC	F400 GAC	ATC	F400 GAC	ATC	F400 GAC	ATC
BTA	1.68	-	2.94	0.24	0.32	-	0.37	0.32
CBZ	1.10	0.08	3.09	0.27	0.34	0.53	0.30	0.35
CAF	1.16	0.05	2.50	0.29	0.33	0.87	0.32	0.42
STL	1.60	0.08	2.49	0.14	0.28	0.52	0.32	0.22
DFC	1.00	0.05	2.04	0.20	0.26	0.43	0.25	0.40

4.4 OMP regeneration efficiency profile in multiple cycles of adsorption and regeneration

Fig. 18 shows the seven OMP regeneration profiles over six adsorption cycles with regeneration conducted in between. Each regeneration efficiency ($RE = q_{\text{regenerated}}/q_{\text{initial}} \times 100\%$) obtained is represented by a black column. In each cycle, a control experiment was conducted in which no regeneration took place. Those results are shown with white columns. After six cycles of adsorption and regeneration, the highest RE was achieved on CAF with all of them $>82\%$. For three positively charged OMP (i.e. MET, MTL and STL), their RE decreased steadily and remained $>65\%$ RE after the last cycle. For negatively charged OMP (i.e. KET and SMX), slightly lower RE was observed on the last cycle (60% and 48%). Regeneration performed the worst on GBP (zwitterion), for which RE dropped rapidly over six cycles, and no more than 20% of pristine loading was recovered in the last cycle. The most significant regeneration performance was observed on MET, for which 58% of the initial loading capacity was recovered in the fifth cycle. MET exhibited the lowest K_{ow} and is highly hydrophilic. The hydrophilic effect is in cooperation with electrodesorption force and thus resulted in outstanding RE. It is noticed that for certain compounds (for example, KET), RE exceeded 100%. This could be due to the lack of duplicate experiments or measurement errors. Inadequate mixing of the stock solution may also increase the initial concentration, which results in higher loading.

Before the experiment, it was expected that the loading on non-regenerated adsorbents would drop drastically. Available sites on carbon surface would be occupied by previously loaded OMP. However, a significant decrease in RE was not observed on every OMP, only on GBP and MET (Fig. 18: RE: 6.7% and 27.3% after the last cycle, respectively). For the other OMP, loading of $>50\%$ was still achieved. It is speculated that the initial adsorbate dose was not high enough to fully saturate the adsorbent. The regeneration effect was, therefore, not different from other OMP.

It is observed that loading could almost never be fully recovered. Over six cycles of adsorption and regeneration, RE of all OMP gradually decreased and reached a steady state (except GBP). Weng & Hsu, (2008) and Zanella et al., (2017) have pointed out that some adsorption sites cannot be restored by the electrochemical process. Accumulation of degradation products of contaminants may block the pores or pathway, limiting the mass transfer of desorbed species or re-adsorption efficiency. Degraded or newly-formed products could also be adsorbed again on already regenerated adsorption sites (DeOliveira Pimenta & Kilduff, 2006; Grant & King, 1990; Vidic & Suidan, 1991). On top of that, permanent loss of adsorption capacity could attribute to poor NOM desorption. Narbaitz & McEwen, (2012) investigated NOM regeneration for field spent GAC and obtained a maximum RE of 17%. They emphasized the relation between limited NOM desorption and poor RE. NOM blockage causes already desorbed species to stay in the pores, and those sites are not available for the next cycle of regeneration. It is suggested to perform cathodic regeneration to assist NOM desorption from spent carbon particles. Negatively charged carbon surfaces produce electrostatic repulsion and facilitate NOM desorption and mass transfer. The presence of NOM on the EC process should receive more attention in future studies.

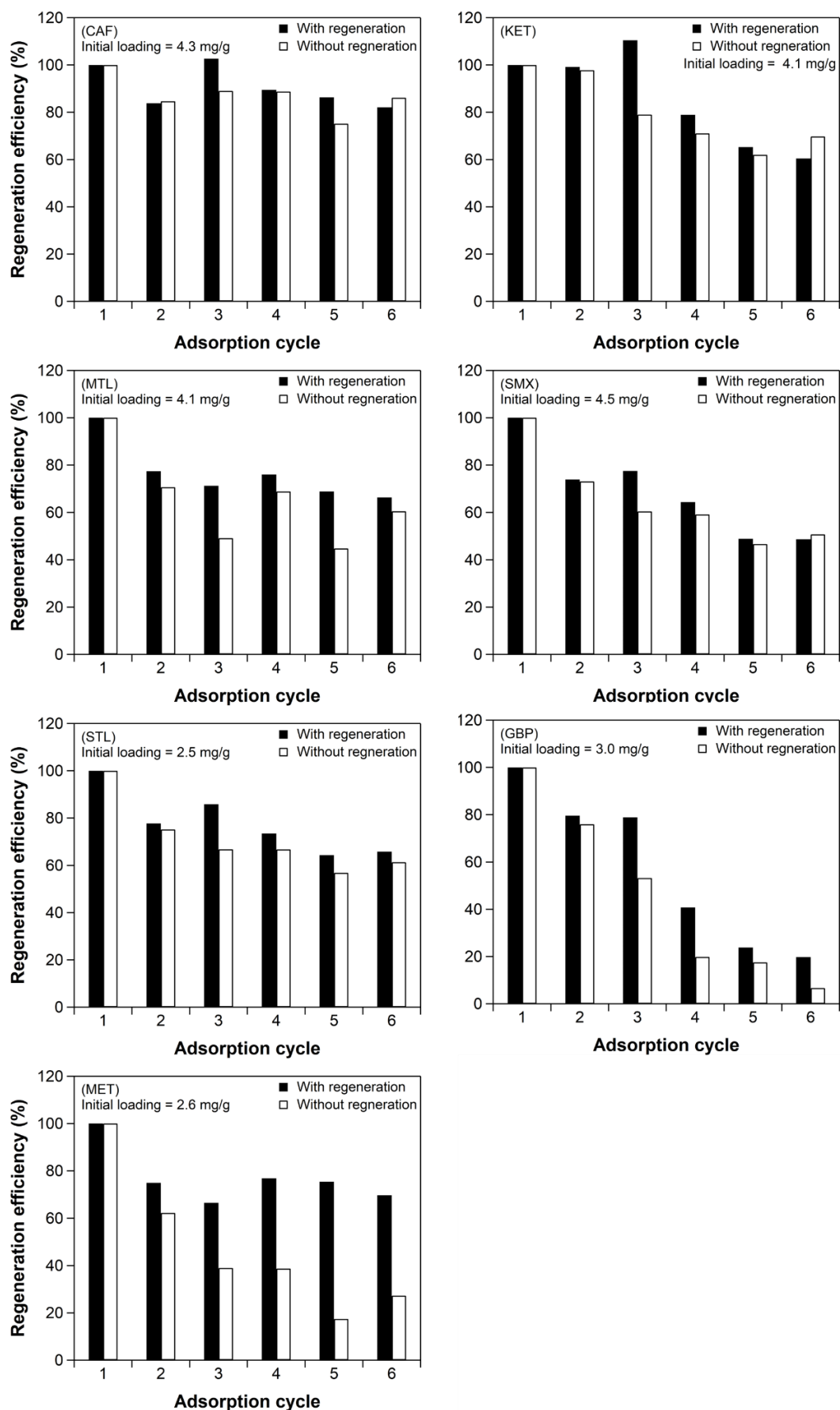


Fig. 18 Seven OMP regeneration profile over six adsorption cycles. Black columns represent RE with regeneration in between each adsorption and white columns represent those without. RE in the first adsorption cycles are regarded as threshold and are always 100% (initial loading divided by itself). Values in mg/g represent the initial loadings of the adsorbent .

4.5 Performance of cell configuration

Electrochemical regeneration of carbon-based material involves two main mechanisms: enhanced desorption and degradation of contaminant species. Depending on the electrochemical cell configuration, these mechanisms could be strengthened or weakened and result in variation of RE on different species. Due to the nature and practical limitations of this study, all conditions of the regeneration experiments were only conducted with one configuration.

Neither an anodic nor a cathodic compartment was realized in the setup. In all cases, OMP-loaded adsorbents were placed and hung in between the electrodes without touching them. The adsorbent was always kept at a distance of five mm from both electrodes. Thus, it is postulated that the loaded GAC did not experience a change in ambient pH. Therefore, under this configuration pH induced desorption was suspected to be less profound or even absent due to the constant circulation of electrolytes during regeneration.

Without separation of the compartments, the adsorbent's polarity is simultaneously anodic and cathodic. The most relevant and strongest desorption mechanism under this configuration is likely to be electrodesorption. Fig. 19 groups the RE obtained for all seven OMP according to their charge at pH 7. Each data point represents the percentage of restored loading compared to the first adsorption cycle.

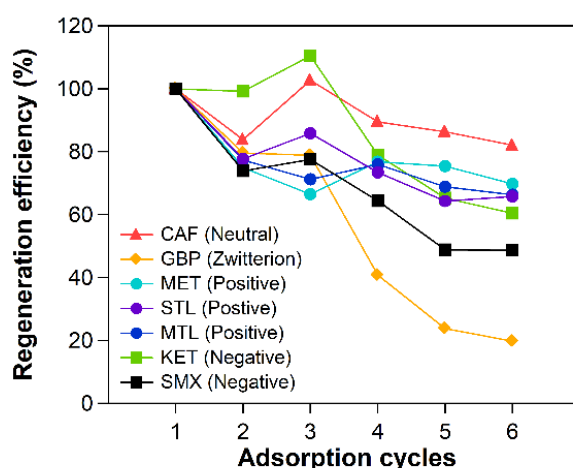


Fig. 19 Regeneration efficiency over six cycles of adsorption and electrochemical regeneration of seven OMP loaded ATC. In all cases, adsorption was performed by adsorbent dosage of 200 mg and adsorbate dosage of 5 mg/L. Electrochemical regeneration was performed with current density of 30 mA for three hours, with tap water as electrolyte. Each data point represents the RE of each cycle. Neutral and zwitterion compounds are represented respectively by triangles and rhombuses. Positively charged and negatively charged compounds are grouped and marked with dots and squares.

By applying an electric field to the adsorbent bed, carbon is polarized and exhibits a positive charge on one side and a negative charge on another side (Zhang et al., 2013). Surface charge on carbon induced electrostatic repulsion of similarly charged species (McQuillan et al., 2018). This could be the explanation for moderate RE of charged contaminants (Fig. 19). On the charged surface of carbon pellets, only similar charged species were desorbed because of electrostatic repulsion, whereas oppositely charged species were held by electrostatic attraction. Slightly higher RE on positively charged species is probably due to limited NOM regeneration (Roberto M. Narbaitz & McEwen, 2012). Positively charged contaminants attached to NOM were carried out simultaneously with desorbed NOM. For uncharged molecules (i.e. CAF in this case), its RE was higher than those of charged contaminants. This is in agreement with the finding by Bán et al., (1998), in which they demonstrated electrodesorption could also be applied to uncharged species. Electrodesorption as the main mechanism of regeneration may also provide an explanation for poor GBP regeneration performance. GBP is a zwitterion which holds the same number of positively and negatively charged functional groups (Skoog et al. 2013). It always contains a similar charge with the carbon surface and is not favored by electrostatic repulsion, hence limiting the desorption rate.

Another relevant mechanism for enhanced desorption was absent under this configuration: ionized species. The use of electrolytes such as NaCl, has been proven to facilitate the desorption process of activated carbon (Zhang, (2002), Narbaitz & Cen, (1994), (Savlak & Belgin, (2014)). NaCl dissociates during regeneration into sodium cation and chloride anion. The ions react with contaminants and form more soluble compounds. In this study, tap water without additives was used as electrolytes. Ions from tap water are not sufficient for regeneration.

4.6 Effect of surface chemistry modifications

A steady drop of RE for seven OMP was recorded over six adsorption and regeneration cycles. For CAF, KET and SMX (Fig. 18), slightly lower RE with the process of regeneration was observed in the last adsorption cycle than those without. This may indicate a permanent loss of adsorption capacity on the carbon surface instead of an irreversible adsorption process. Modification of surface chemistry on the adsorbent surface could be a factor of such capacity loss. CAF, KET and SMX contain aromatic ring structures. Mattson et al., (1969) introduced the donor-acceptor adsorption mechanism between carbon surface and adsorbent structure. Carbonyl oxygen on carbon surface acts as electron donor, and aromatic ring of solvent act as electron acceptor. The carbonyl oxygen could be oxidized electrochemically to carboxylic acid oxygen (Mehta & Flora, 1997), characterized by a smaller dipole moment than carbonyl oxygen (Sinha & Dogra, 1989). As a result, carboxylic acid oxygen as a weaker electron donor contributes to a decrease in adsorption capacity after electrochemical regeneration. The oxidation rate, in general, depended on the applied current, and this may suggest adopting low current density facilitates a more long-term use of material without considerable change in chemical stability. This hypothesis could be verified by Fourier Transform Infrared Spectroscopy (FTIR) in future studies.

4.7 Effect of operating parameters: applied current and treatment time

The regeneration efficiency for most of the OMP (except GBP) was not sensitive to changes in current. Fig. 20 shows the change of regeneration efficiency for three OMP from different charged groups. RE was not correlated with manipulated current applied and fluctuated between 60 to 80 %. The increase of current did not improve RE. This is in line with and in disagreement with past studies simultaneously. Ferrández-Gómez et al., (2021) observed unimproved RE on spent activated carbon by increasing current density from 0.025 to 0.075 A/cm². They speculated the increased formation of air bubbles had a deteriorated effect on regeneration performance. Zanella et al., (2017) also obtained stabilized RE on phenol-loaded carbon by increasing the current from 1.6 to 2.4 A. They noted that, increased current could advance the overall transport process within pores, it might elevate the number of cations and anions in bulk solution. The increased number of ions exhibit stronger electrostatic repulsion and hinders desorbed species from returning to the bulk solution. Stagnant improvement in RE may indicate that the current applied in the experiments could be reduced. This will be further discussed in Chapter 6.

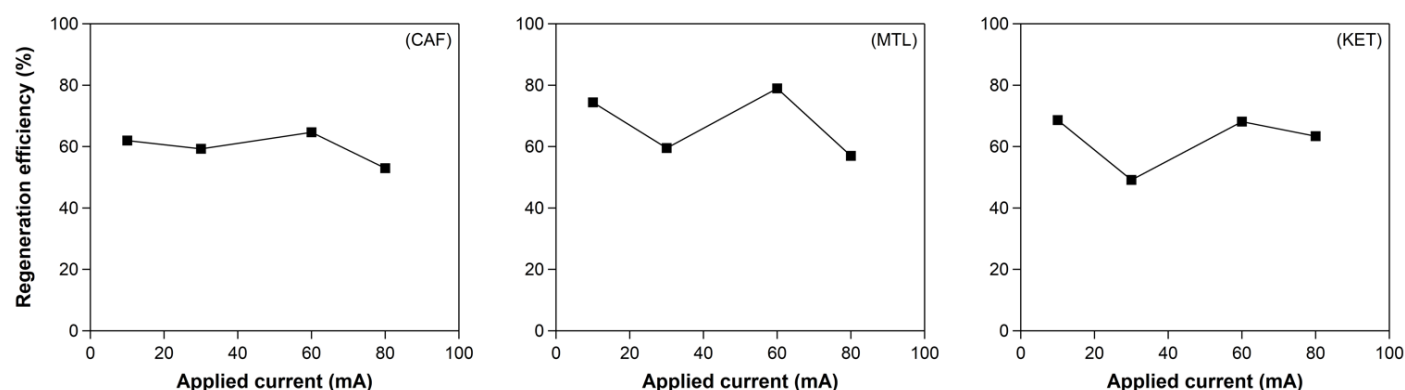


Fig. 20 The effect of applied current on regeneration efficiency for CAF (neutral), MTL (positively charged) and KET (negatively charged). In all cases, the operating condition remained unchanged except for current applied (10, 30, 60, 80 mA). Current was kept steadily during the course of regeneration by controlling cell voltage.

However, it is also suggested that a better regeneration can be achieved by raising the applied current due to electrochemical polarization (Foo & Hameed, 2009; M. Zhou & Lei, 2006). GBP showed a higher sensitivity to the applied current with greater variation in this study (Fig. 21). RE dropped under 30% at 30 mA and performed the best at 60 mA with over 80% capacity restoration. GBP is characterized by its zwitterion property, and this result implies its desorption mechanism was highly relevant to electrodesorption and polarization effect. The different magnitude of variation between GBP and other OMP indicates the effect of applied current could also be relevant to the solvent properties.

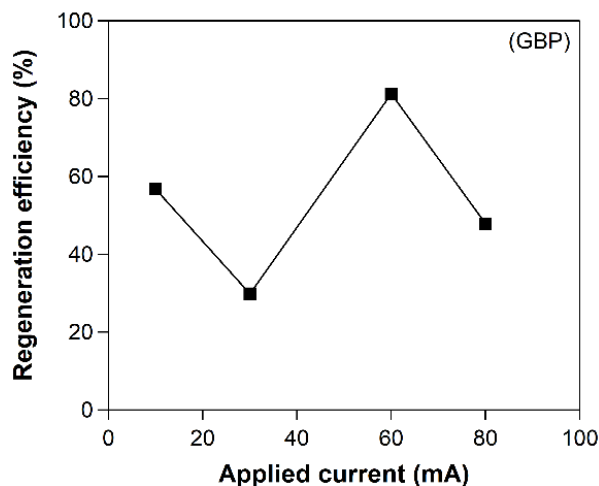


Fig. 21 The effect of current applied on regeneration efficiency for GBP (zwitterion). Stronger variation was observed.

Another implication is that this material could be regenerated with low energy consumption. In the varying current experiment, around 60% of RE for most of the OMP could be achieved at 10 mA for 1h of treatment time. The achieved RE achieved was comparable with past studies in which regenerated phenol-loaded GAC and coconut shell at 10-15 mA: 62-76% RE were obtained for over 5-25h treatment time (R. M.Narbaitz & Karimi-Jashni, 2009; Roberto M.Narbaitz & Cen, 1994; H.Zhang, 2002). This is attributed to the low resistance of this adsorbent material. Higher current efficiency facilitates desorption and production of reaction species (McQuillan et al., 2018). Less treatment time is then required to achieve similar RE and results in a five-fold decrease of energy spent. This seems to be a promising test result for this novel material. However, a lower energy requirement may not be directly applied to multiple cycles of regeneration due to accumulated OMP loading and NOM competition.

Another factor of energy consumption is the treatment time needed for electrochemical regeneration. A longer time span could ultimately affect the overall energy performance. Experiments with varying treatment time were conducted to investigate to which extent an increase in regeneration time could obtain a better RE performance. A stable current of 60 mA was applied as it generally yielded the highest RE in the varying current experiment. Fig. 22 shows the change of regeneration efficiency for three OMP from different charged groups.

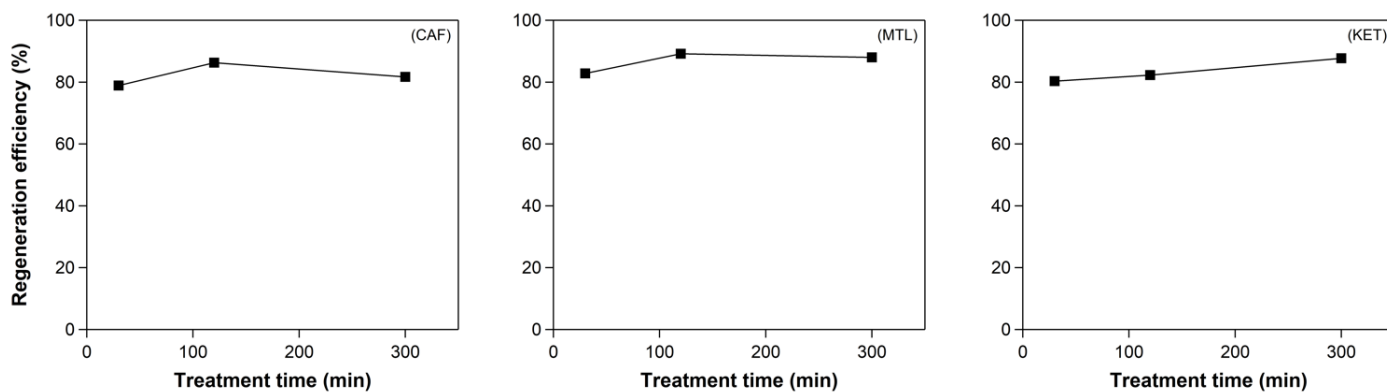


Fig. 22 The effect of regeneration time on regeneration efficiency for CAF (neutral), MTL (positively charged) and KET (negatively charged). In all cases, the operating condition remained unchanged except for regeneration time (30, 120, 300 min). Current was kept steadily during the course of regeneration by controlling cell voltage.

Prolonged treatment time is generally thought to be beneficial to improve regeneration efficiency (Berenguer et al., 2010; Brown et al., 2004; Roberto M. Narbaitz & Cen, 1994; L. Wang & Balasubramanian, 2009; Weng & Hsu, 2008). The regeneration mechanism is supposed to be desorption followed by species degradation. Increased regeneration time allows more mass transfer for contaminants to arrive at electrodes surface, where direct oxidation takes place (McQuillan et al., 2018). Improvement of RE was observed in this experiment, but the benefits were low and inconsistent among different OMP. 2 – 11% RE improvement (except for SMX and SDM) was recorded by increasing treatment time from 30 to 100 min. It could be due to improved NOM regeneration. Weng & Hsu, (2008) reported extended treatment time not only enables more desorption or oxidation but also increases the leach of NOM from spent GAC. Increased liberation of NOM could mitigate pore blocking and allow desorbed species to return to the bulk solution. GBP was the most sensitive compound with increasing regeneration time (Fig. 23). Its RE growth was consistent with prolonged treatment time, increasing from 47% to 71%. It seems that GBP has a high sensitivity towards the operating conditions, probably own to its zwitterion property.

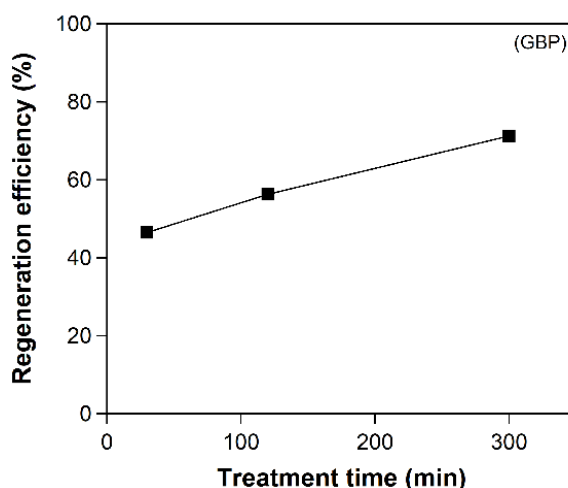


Fig. 23 The effect of regeneration time on regeneration efficiency for GBP (zwitterion).

At regeneration time of 300 min, CAF, MTL and CBZ showed a subtle decline in RE. For the rest of OMP, a maximum of 90% RE was achieved, implying complete regeneration was not likely to take place even with optimized operating parameters. It is suggested to improve the cell configuration first since it affects the most fundamental mechanisms. Most of the OMP showed stabilizing improvements with increased treatment time. This is similar to the results obtained by (Berenguer et al., 2010). They reported that the RE of phenol-loaded GAC tends to stabilize after a certain period of regeneration time. They speculated that extended time would also enable re-adsorption of oxidized products. McQuillan et al., (2018) pointed out the importance of strike the balance between regeneration efficiency improvement and energy consumption. It is uneconomical to spend lots of input to gain small improvement, as the results showed low marginal benefits. Less than 5% of RE improvement was obtained by lifting treatment time from 120 to 300 min. It is considered to be unwise to spend 2.5 times more energy to attain such a small boost.

In short, from the perspective of minimizing energy input, regeneration on this material showed promising performance: except for GBP, > 62% of RE was achieved for all OMP for 30 min of treatment time. García-Otón et al., (2005) achieved approximately 90% of RE on toluene-loaded GAC (the same amount of adsorbents as this study) by applying a current of 1300 – 2400 A for 3h, and with the aid of a chemical electrolyte. This novel material has shown the potential to be electrochemically regenerated with reduced energy and time span, making it more feasible for in-situ operation.

4.8 OMP concentration profile

Carbon regeneration is achieved by liberation of exhausted adsorption site through contaminants desorption and degradation (hypothesized to take place simultaneously in this study). During the design phase of this study, it was first thought that the effectiveness of regeneration could be determined by the mass of desorbed / residual contaminants in the electrolyte after regeneration. This is defined as stripping efficiency Eqs. (9).

$$\text{stripping efficiency} = \frac{\text{Mass of desorbed species}}{\text{Initial mass of loaded species}} \times 100\% \quad \text{Eqs. (9)}$$

In this formula, the efficiency of the electrochemical process is determined by the mass percentage of desorbed species overloading in the previous adsorption process. It was not adopted eventually due to several factors: (1) stripping efficiency does not represent the loading capacity of the material directly. Mass of residual contaminants does not translate to the availability of adsorption sites. Liberated adsorption sites might be blocked by poorly-desorbed NOM (Roberto M.Narbaitz &McEwen, 2012) or degraded by-products (Weng &Hsu, 2008; Zanella et al., 2017), meaning those liberated sites are not readily accessible for subsequent adsorption; (2) Efficiency could be underestimated. Degradation of contaminants species is assumed to take place on the surface of electrodes (direct oxidation), in bulk solution and inside the carbon pellets (indirect oxidation). Degradation by-products of studied OMP cannot be measured in-house and are out of the focus in this study. According to Eqs. (9), degraded species are regarded as adsorbed species remaining in adsorption sites, and efficiency is deviated; (3) Measurement only caters for concentrations of desorbed species in bulk solution. Desorbed contaminants could remain inside the carbon pellets. Continuous sampling was conducted during the adsorption cycles. It was occasionally observed an increased OMP concentration in solutions. Desorbed but trapped species might escape and compete with the original presence of OMP. Eqs. (4) is able to take this phenomenon into account by considering the actual loading.

However, residual OMP concentrations were still measured by sampling from the electrolytes during 3h of electrochemical regeneration. The measurement is an indicator of the degradation efficiency of the electrochemical cell. It is beneficial to eliminate pollutants in the electrolyte to sustain the electrochemical process. The profile of seven residual OMP concentrations was recorded as a function of regeneration time (Fig. 24). Desorbed species were classified into three groups according to their change during regeneration.

Group (a) is characterized by two distinctive regions: a sharp increasing region in which desorption rate is dominating; and a subsequent rapid drop region in which degradation rate is surpassing. Peak concentration occurred within 50 min for GBP, which was the earliest among all seven OMP. The earliest decrease of desorption was in line with its poor regeneration performance (Fig. 18 (GBP)), implying electrochemical regeneration might not be effective for GBP desorption. For STL, the peak concentration was also recorded early among all studied OMP. This was likely contributed by its easily degradable property. STL showed approximately 10% of RE in continuous regeneration cycles (Fig. 18 (STL)), which was equivalent to the desorbed mass of 50 μg . The peak concentration recorded was, however, at a maximum of 0.3 μg . Its low concentration profile indicated most of the desorbed STL were indirectly oxidated before returning to the bulk solution. For MET, its concentration profile was consistent to its regeneration profile (Fig. 18 (MET)). The rise of concentration is rapid and delayed at regeneration cycles 4 and 5, corresponding to its significant difference in the regeneration profile. A rapid drop in concentration was recorded after the peak, indicating MET is a promising candidate for the electrochemical process. These three compounds were fully degraded after the electrochemical treatment, hinting no secondary treatment is required. The pattern in group (a) concentration profile was in resemblance to results obtained by Berenguer et al., (2010) and H.Zhang, (2002). They monitored the concentration of phenol-loaded GAC during electrochemical regeneration, suggesting this is a desorption-dependent process. The rise before the occurrence of peak concentrations is caused by the time lag between desorbed species entering the bulk solution and being oxidized when in contact with electrodes surfaces (McQuillan et al., 2018). The delayed time span reveals that compounds in group (a) are favored with direct anodic oxidation.

Group (b) is characterized by their steady increasing concentration profiles. In general, the rise was gradual and exhibited a correlation with accumulated OMP loading between each cycle. A drop of concentration in the bulk solution was barely observed, hinting at the possibility that direct oxidation on the electrode surfaces does not favour the degradation of CAF, MTL and KET. Major degradation was contributed by indirect oxidation. An electrochemical process targeting these species is suggested to focus on the generation of oxidation species.

Group (c) contains only SMX, which showed an irregular pattern in different regeneration cycles. A stabilized profile indicated desorption of SMX was counterbalanced by degradation.

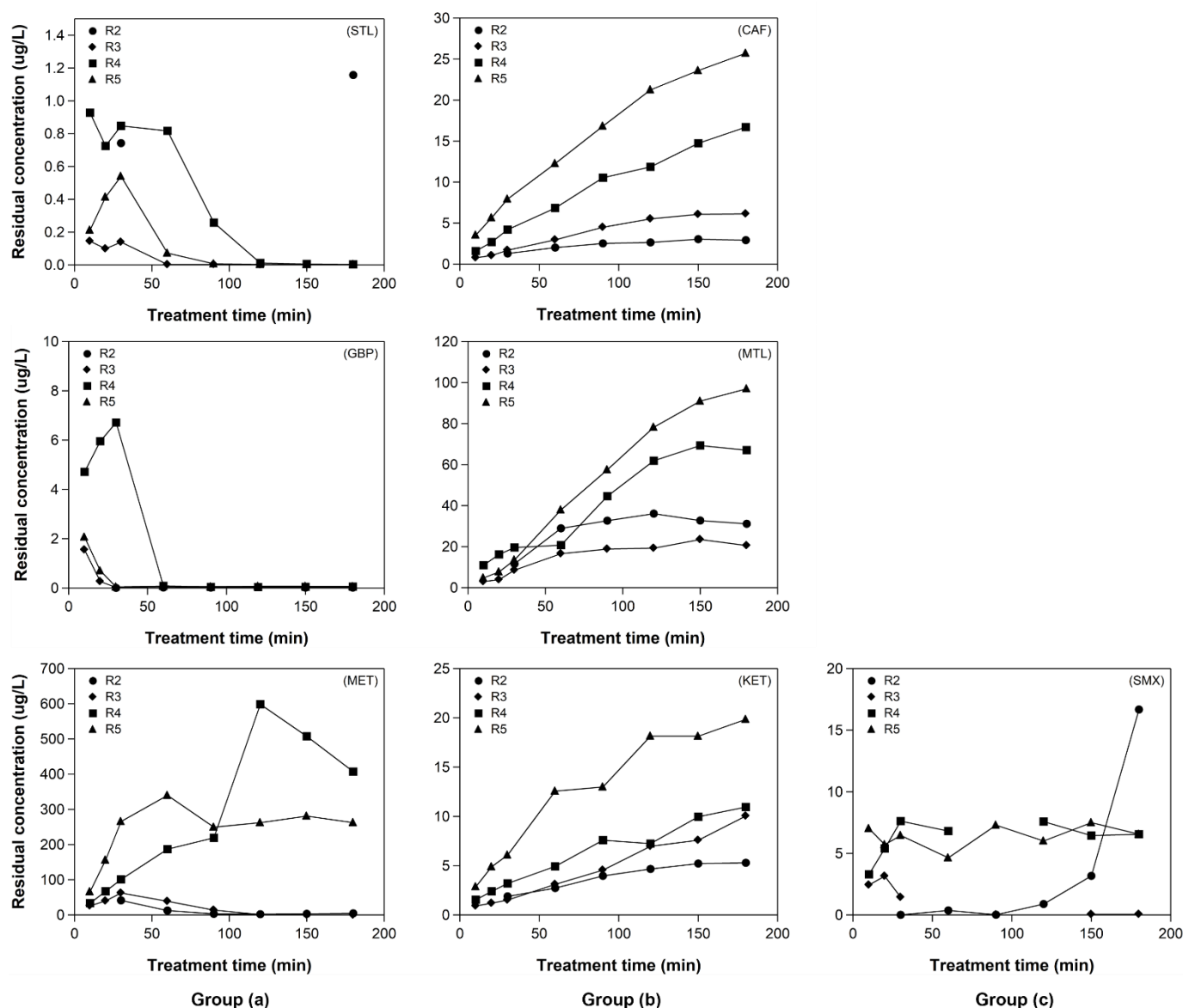


Fig. 24 Profile of seven residual OMP concentrations as a function of regeneration time. Sampling were conducted during the course of regeneration from 300 mL of electrolyte. Each line represents concentration change in each cycle of regeneration. Number after R denotes regeneration after which adsorption cycle (e.g. R3 denotes after adsorption cycle 3). Degradation of seven OMP are classified into three groups: (a) More easily degradable; (b) gradual increases; (c) other.

4.9 Impact of regeneration on adsorbent durability

The surface area and pore volume analyses were conducted to evaluate the physical stability of the material after applying electrochemical regeneration. Table 14 lists the pore size distribution of three samples. The virgin state represents pristine ATC. The second sample received 15h of electrochemical regeneration with the applied current and treatment time identical to the regeneration experiment (name the conditions here again). It serves as a threshold to evaluate how continuous cycles of adsorption and regeneration affect the material durability and pore size distribution. The third sample was used in the multiple cycles of regeneration experiment, ending with the final re-adsorption step. All samples were dried for 15h at 105 °C before the N₂ adsorption test.

Table 14 Characterization of surface area and pore volume of ATC before and after regeneration.

Model	Activation state	BET Surface Area (m ² /g)	N ² Pore Volume (ml/g)	Micropore volume (ml/g)	Mesopore volume (ml/g)	Micropore volume fraction (%)	Mesopore volume fraction (%)
ATC	Virgin	957	0.55	0.33	0.22	60.2	39.8
	Regenerated without adsorption	862	0.45	0.30	0.15	66.8	33.2
	Regeneated with adsorption	478	0.32	0.15	0.16	48.6	51.4

After undergoing the electrochemical process, the carbon particles had a 10% and 18% decline in surface area and total pore volume, respectively. The loss of pores was mostly due to a 32% drop in mesopore volume, while micropore volume only decreased by 10%. It is speculated the major loss of surface area and mesopores volume is caused by a reaction taking place on the carbon surface. Upon applying current to carbon surface, it forms microelectrodes and acts as a catalyst to facilitate the decomposition of hydrogen peroxides into hydroxyl radicals (H. H.Huang et al., 2003; Lücking et al., 1998; Miller &Valentine, 1995). Contaminant species are oxidized on the surface of carbon particles as a result. The reactions are described in Eqs. (10) and Eqs. (11). Outer walls that contribute to the mesopore volume could therefore be destroyed during the course of the electrochemical process. The loss of micropores might partly contribute to the permanent loss of adsorption capacity as micropores are responsible for OMP removal.



After 15h of the electrochemical process, the disintegration of the pellets was not observed, and no powders were formed. The carbon particles can remain intact and unchanged in shape due to 90% of the surface area being conserved. Considering the potential of this material to be regenerated in shorter treatment time (section 4.7), it is promising to apply it on continuous regeneration at an appropriate current; thus the burden on the carbon surface could be minimized.

The pore size distribution after re-adsorption is in agreement with the results discussed in sections 4.1 and 4.4. NOM blockage caused a 50% reduction in micropore volume. Accumulation of NOM in pores is more concerning than physical durability. Upon cycles of adsorption and regeneration, a decline in adsorption capacity is more likely due to the poor regeneration performance for NOM. However, this drawback is shared by all other porous adsorbents. Increased mesopores of this material may mitigate this effect, making it more suitable to conduct regeneration. It is suggested to conduct cathodic regeneration to assist NOM desorption in further study.

4.10 PFAS regeneration efficiency profile in multiple cycles of adsorption and regeneration

Fig. 25 summarizes the regeneration efficiency of three tested PFAS in four cycles of adsorption and regeneration. Regeneration performed the best for PFOA (long-chain): >72% of RE was achieved steadily in all regeneration cycles. Continuous drops of RE were observed on the other two PFAS: a gradual decrease from 83% to 58% was recorded for PFHpA (long-chain); a significant reduction from 62% to 10% was observed for PFBS (short-chain). The initial loading showed no significant difference between long-chain and short-chain PFAS.

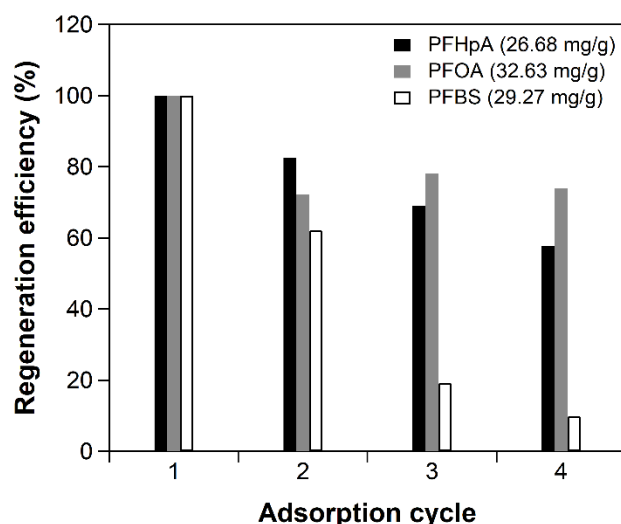


Fig. 25 Regeneration efficiency of three tested PFAS (long-chain: PFHpA and PFOA; short-chain: PFBS) in four cycles of adsorption and regeneration. In all cases, adsorbent dosage of 200 mg was adopted (identical to OMP regeneration experiment). Bracket values report the initial loading of PFHpA, PFOA and PFBS in the first adsorption cycle.

The difference in the obtained RE could be explained by the effect of hydrophobicity of PFAS. Park et al., (2020) pointed out the relationship between carbon pore size and PFAS hydrophobicity. They concluded mesopores are more important for hydrophobic PFAS, and micropores are more responsible for hydrophilic PFAS adsorption. The hydrophobicity of three tested PFAS is in line with the regeneration performance obtained in this study: PFOA>PFHpA>PFBS. The Log K_{ow} of the compounds are 5.11, 4.41 and 2.63, respectively. During the course of the electrochemical process, the liberation of mesopores is considered faster due to their proximity to the granule's surface. Oxidation species such as hydroxyl radicals are able to enter mesopores faster than they enter micropores. Desorbed species can return to the bulk solution through the wider pathway from mesopores compared to micropores. The higher availability of mesopores facilitates adsorption of hydrophobic PFAS (PFOA and PFHpA in this experiment). This also explains the drastic decrease of RE for hydrophilic PFBS due to less regenerated micropores. Micropores are of higher importance for hydrophilic PFAS adsorption (Park et al., 2020). Micropores regeneration could be limited by two factors: poor regeneration of NOM (Roberto M. Narbaitz & McEwen, 2012), which blocks the pathway to micropores; degraded species limiting mass transfer (Weng & Hsu, 2008; Zanella et al., 2017) and hence a lower regeneration rate of micropores.

The possibility of re-adsorption of degraded PFAS may also restrict the micropores availability in subsequent adsorption. Kim et al., (2020) proposed a degradation pathway of PFOA in which short-chain perfluorocarboxylates (PFHpA, PFHxA and PFPeA) appeared as organic by-products. They proposed during the decomposition of PFOA, the breaking down of C-C bond forms short-chain species. Zhuo et al., (2011) also recorded the presence of short-chain perfluorocarboxyl anions (CF_3COO^- , $C_2F_5COO^-$, $C_3F_7COO^-$, $C_4F_9COO^-$, $C_5F_{11}COO^-$, and $C_6F_{13}COO^-$) for PFOA degradation. It is speculated that the presence of short-chain degradation products may adsorb to regenerated micropores, reducing the availability of micropores in the next adsorption cycle. They could become competitors with PFBS for micropores if they do not return to bulk solution before the end of electrochemical treatment. This explanation is also consistent with the mild decrease of RE for PFHpA since that more PFHpA is formed by PFOA degradation. An increasing amount of PFHpA may compete for limited adsorption sites during the subsequent adsorption cycle.

A maximum RE of 83% was obtained by the second adsorption cycle for PFHpA, indicating the phenomenon of permanent loss of adsorption capacity mentioned in the previous OMP regeneration discussion could take place in the case of PFAS adsorption. The reasons behind this are speculated to be similar to OMP regeneration (section 4.4). On top of that, it is thought that PFAS is more difficult to desorb than those OMP used in this study, especially for long-chained PFAS: PFOA and PFHpA have higher Log K_{ow} values (5.11 and 4.41, Table 7), whereas all OMP in this study exhibit lower hydrophobicity (except for DFC). A higher hydrophobicity of PFAS implies a more advanced desorption condition is required to overcome the hydrophobicity effect. However, it is assumed that it is compensated by the effect of initial loading concentration. For PFAS regeneration, an initial concentration of 100 mg/L was used, whereas for OMP regeneration, only 5 mg/L was adopted. PFAS concentration gradient may assist the mass transfer towards the bulk solution (Zanella et al., 2017). The concentration gradient and ionic migration are both contributing to the transport of desorbed anionic PFAS species to the positively charged anode. PFAS species then experience direct and indirect anodic oxidation. It should also be noted that the contact time (72h) in adsorption cycles 2, 3, and 4 is less than which in the initial adsorption cycle (87h). Higher RE is expected for identical adsorption duration.

Residual PFAS concentrations were measured by sampling at the end of the first and last regeneration electrolyte (Table 15). Increased residual concentrations were observed over the course of regeneration cycles, with the least concentration for PFOA, followed by PFHpA and PFBS. One probable reason could be more PFAS are desorbed after cycles of adsorption. Residual PFAS after the electrochemical process could be one of the indicators of PFAS degradation rate: lower residual left in the electrolyte denotes a faster degradation rate. In this study, PFOA has the fastest degradation rate, followed by PFHpA and PFBS. This sequence is in line with the chain length of corresponding PFAS: PFAS (8), PFHpA (7), PFBS (4). Lin et al., (2012); Trautmann et al., (2015) reported similar observations that PFAS degradation rates are correlated with increasing chain length. According to the reaction pathway proposed by Kim et al., (2020), PFOA enters this pathway first by donating an electron to the anode, forming a PFOA radical ($C_7F_{15}COO\cdot$) (Eqs. (12)).



Zhuo et al., (2012) suggested long-chain hydrophobic PFAS are promoted to adsorb on the electrode surface; thus increasing the reaction rate. However, in this study (where different electrode materials were used), due to limited data points and different uptake of three PFAS, further research is needed to confirm the correlation.

Table 15 Residual PFAS concentration profile by the end of regeneration.

	PFHpA (mg/L)	PFOA (mg/L)	PFBS (mg/L)
1 st regeneration	0.58	0.22	2.1
3 rd regeneration	2.4	1.3	6.2

5 CONCLUSIONS

This chapter concludes the overall adsorption and regeneration performance of ATC by answering the initial research questions. According to the nature of this feasibility study, the performance of the novel adsorbent is comprehensively evaluated, and further suggestions for its application are given.

- **What are the adsorption capacity and kinetics of the selected OMP by the novel iron-graphitic activated carbon in different water matrices (tap water and wastewater treatment plant (WWTP) effluent)?**

The material was able to adsorb a great variety of OMP, including different charges and hydrophobicity. Its graphite content promoted the adsorption of neutral compounds. A negatively charged layer formed by NOM accumulation on the adsorbent surfaces assisted the adsorption of positively charged compounds. These mesoporous carbon bodies enabled faster adsorption kinetics compared to a typical GAC (F400). ATC has therefore the potential to be applied in a treatment system aiming at specific charged compounds and shorter contact time.

- **To which degree can the novel adsorbent be regenerated electrochemically?**

OMP-loaded ATC could be electrochemically regenerated. Reverse adsorption could be achieved on neutral, positively and negatively charged compounds in multiple cycles of regeneration without significant decline. Among seven studied OMP, over 60% of the initial adsorption capacity for five OMP could be restored after five regeneration cycles. Under this fixed and unseparated cell configuration, electrodesorption was supposed to be the major mechanism responsible for regeneration. Permanent and partial loss of adsorption capacity was recorded, probably due to poor NOM desorption and change in surface chemistry. Certain OMP compounds could be fully degraded without residuals left in the solution, hinting at the possibility of successful regenerations without secondary treatment of desorbed OMP. ATC is therefore a promising material for performing in-situ regeneration.

- **How do the operating parameters (applied current, treatment time) affect the regeneration efficiency?**

The regeneration efficiency was generally not positively correlated with elevating applied current. Increasing cell voltage was not always beneficial to the electrochemical process. Prolonged treatment time improved RE, but the marginal benefit was uneconomical. ATC achieved comparable RE with relatively low energy input compared to other adsorbents in previously published studies. Changes in the cell configuration should be first considered to improve overall regeneration performance.

- **How does the electrochemical process affect the physical stability of the novel carbon?**

The electrochemical process mainly decreased the mesopore volume of ATC. A partial loss of micropores resulted in a permanent loss of adsorption capacity for OMP removal. Carbon bodies remained intact and in shape after cycles of the electrochemical process. Poor NOM regeneration was responsible and more concerning for the loss of adsorption capacity. Physical stability of this material was not the major concern for continuous regeneration.

- **To which degree can the PFAS-loaded novel adsorbent be regenerated electrochemically?**

Long-chain PFAS regeneration was achieved without a significant drop in RE over cycles of regeneration. ATC's mesoporous property is a probable contributor to long-chained PFAS desorption. Short-chain PFAS regeneration was unfavorable due to significant blockage of micropores. This material is therefore proven to be a potential for PFAS adsorption and regeneration. It is suggested to continue research on PFAS regeneration with cathodic regeneration. Enhanced electrostatic repulsion is especially beneficial for desorption of both NOM and anodic PFAS species.

6 LIMITATIONS AND FURTHER RECOMMENDATIONS

After the pre-test, it was decided to continue the adsorption and regeneration experiments only with ATC. The exclusion of FMC does not mean that it is not appropriate for drinking water or wastewater treatment. It is of great interest to conduct adsorption and especially electrochemical regeneration on FMC. Its iron contents are thought to be appropriate candidates for the electro-Fenton process. Convention Fenton approach requires addition and mixing of hydrogen peroxides and iron (McQuillan et al., 2018). Upon electrochemical process, external addition and handling of hydrogen peroxides can be avoided since they are generated during operation. Iron content in the material can take part in the Fenton process, which further reduces the operational costs. The Fenton process also assists decomposition of hydrogen peroxide (oxidizing agent limited to certain organic species (Siegrist et al., 2011)) into hydroxyl radicals (stronger oxidation agents) (McQuillan et al., 2018). Utilizing FMC in electrochemical regeneration not only increases the potential indirect oxidation rate but also eliminates additional iron catalyst dosage. With the promising regeneration results on ATC, it is advised to conduct further studies on another version of this novel material.

Titanium plates are employed as electrodes in this study. The electrodes materials play an important role in the electrochemical process and should be further investigated. Titanium is generally more expensive and difficult to obtain. Zhang et al., (2013) suggested other metal oxide electrodes such as RuO_2 and IrO_2 can be alternative materials, especially for industrial applications. Longer lifetimes and higher electro-catalytic activity enable them to be prevailing anode materials.

In the OMP regeneration experiment, a high initial dosage was utilized to exhaust adsorption sites on adsorbents. It is suspected that the adopted concentration was not high enough to fully saturate the material. As a result, differences in the effects of regeneration among OMP compounds were not significant. Compared to other previous studies, much higher dosages ($> 100 \text{ mg/L}$) were often used. It is therefore suggested to increase the initial concentration of each adsorption cycle.

In reality, contaminants concentrations are much lower than the dosage adopted in this study. Continuous flow in the reactor means that the adsorption process would encounter more NOM competition. In this sense, regeneration of NOM is of utmost importance to employ this material and method into industrial applications.

Experiments with varying applied current revealed that lower current could be applied. This was constrained by the DC power supply in this study. It is suggested that lower cell voltage can be tested in further studies to optimize the current efficiency. Slower rate of electrolysis of water is achieved by lowering cell voltage. The slower water splitting then creates fewer air bubbles which restrict mass transfer. The energy input, however, cannot be too low to maintain basic front formation and continuous generation of oxidizing species. The operating parameters can be optimized by striking a balance between energy and regeneration efficiency.

Due to material availability, only titanium plates were considered for the electrochemical cell. Direct oxidation on electrodes surfaces are one of the key oxidation pathways for contaminants degradation. In section 4.8, it is shown that limited OMP compounds were sensitive to direct oxidation in the bulk solution. Having other alternatives could investigate the interaction between various electrodes materials and different OMP compounds.

Only one cell configuration was built for this study. Different desorption and oxidation mechanisms are highly relevant to electrochemical cell configurations. It is realized that poor NOM regeneration resulted in permanent loss of adsorption capacity for both OMP and PFAS removal. Cathodic regeneration, which promotes electrodesorption and distorts adsorptive equilibrium, is highly recommended to be the next step to optimize the treatment.

Upon improvement of the regeneration process on this material, one may consider scaling-up as the further development towards industrial applications. Several factors should be examined beforehand. In reality, a large amount of exhausted adsorbents is regenerated during each regeneration batch. The thickness of the adsorbent bed may greatly influence the current efficiency. The mode of regeneration can be in circulation flow or in batch (as shown in this study). Configuration targeting NOM liberation could be essential as well.

BIBLIOGRAPHY

- Aktaş, Ö., &Çeçen, F. (2007). Bioregeneration of activated carbon: A review. *International Biodeterioration and Biodegradation*, 59(4), 257–272. <https://doi.org/10.1016/j.ibiod.2007.01.003>
- Álvarez, P. M., Beltrán, F. J., Gómez-Serrano, V., Jaramillo, J., &Rodríguez, E. M. (2004). Comparison between thermal and ozone regenerations of spent activated carbon exhausted with phenol. *Water Research*, 38(8), 2155–2165. <https://doi.org/10.1016/j.watres.2004.01.030>
- Appleman, T. D., Higgins, C. P., Quiñones, O., Vanderford, B. J., Kolstad, C., Zeigler-Holady, J. C., &Dickenson, E. R. V. (2014). Treatment of poly- and perfluoroalkyl substances in U.S. full-scale water treatment systems. *Water Research*, 51, 246–255. <https://doi.org/10.1016/j.watres.2013.10.067>
- Asghar, H. M. A., Roberts, E. P. L., Hussain, S. N., Campen, A. K., &Brown, N. W. (2012). Wastewater treatment by adsorption with electrochemical regeneration using graphite-based adsorbents. *Journal of Applied Electrochemistry*, 42(9), 797–807. <https://doi.org/10.1007/s10800-012-0439-8>
- Bain, E. J., Calo, J. M., Spitz-Steinberg, R., Kirchner, J., &Axén, J. (2010). Electrosorption/electrodesorption of arsenic on a granular activated carbon in the presence of other heavy metals. *Energy and Fuels*, 24(6), 3415–3421. <https://doi.org/10.1021/ef901542q>
- Bán, A., Schäfer, A., &Wendt, H. (1998). Fundamentals of electrosorption on activated carbon for wastewater treatment of industrial effluents. *Journal of Applied Electrochemistry*, 28(3), 227–236. <https://doi.org/10.1023/A:1003247229049>
- Barbosa, M. O., Moreira, N. F. F., Ribeiro, A. R., Pereira, M. F. R., &Silva, A. M. T. (2016). Occurrence and removal of organic micropollutants: An overview of the watch list of EU Decision 2015/495. *Water Research*, 94, 257–279. <https://doi.org/10.1016/j.watres.2016.02.047>
- Baresel, C., Harding, M., &Fang, J. (2019). Ultrafiltration/granulated active carbon-biofilter: Efficient removal of a broad range of micropollutants. *Applied Sciences (Switzerland)*, 9(4). <https://doi.org/10.3390/app9040710>
- Bentel, M. J., Yu, Y., Xu, L., Li, Z., Wong, B. M., Men, Y., &Liu, J. (2019). Defluorination of Per- and Polyfluoroalkyl Substances (PFASs) with Hydrated Electrons: Structural Dependence and Implications to PFAS Remediation and Management. *Environmental Science and Technology*, 53(7), 3718–3728. <https://doi.org/10.1021/acs.est.8b06648>
- Berenguer, R., Marco-Lozar, J. P., Quijada, C., Cazorla-Amorós, D., &Morallón, E. (2010). Electrochemical regeneration and porosity recovery of phenol-saturated granular activated carbon in an alkaline medium. *Carbon*, 48(10), 2734–2745. <https://doi.org/10.1016/j.carbon.2010.03.071>
- Blanchard, G., Maunaye, M., &Martin, G. (1984). Removal of heavy metals from waters by means of natural zeolites. *Water Research*, 18(12), 1501–1507. [https://doi.org/10.1016/0043-1354\(84\)90124-6](https://doi.org/10.1016/0043-1354(84)90124-6)
- Brandts, J., Wagemaker, L., Basf, P. B., Hoekstra, J., Jenneskens, L., &Uu, J. G. (2020). *Water purification with Fe on partly graphitized carbon bodies ■ Electrochemical oxidation of absorbed apolar pollutants Water purification with Fe on partly graphitized carbon.*
- Brown, N. W., Roberts, E. P. L., Chasiotis, A., Cherdron, T., &Sanghrajka, N. (2004). Atrazine removal using adsorption and electrochemical regeneration. *Water Research*, 38(13), 3067–3074. <https://doi.org/10.1016/j.watres.2004.04.043>
- Cantoni, B., Turolla, A., Wellmitz, J., Ruhl, A. S., &Antonelli, M. (2021). Perfluoroalkyl substances (PFAS) adsorption in drinking water by granular activated carbon: Influence of activated carbon and PFAS characteristics. *Science of the Total Environment*, 795, 148821. <https://doi.org/10.1016/j.scitotenv.2021.148821>

- Chen, H., Wang, X., Zhang, C., Sun, R., Han, J., Han, G., Yang, W., & He, X. (2017). Occurrence and inputs of perfluoroalkyl substances (PFASs) from rivers and drain outlets to the Bohai Sea, China. *Environmental Pollution*, 221, 234–243. <https://doi.org/10.1016/j.envpol.2016.11.070>
- Cordner, A., DeLa Rosa, V. Y., Schaidler, L. A., Rudel, R. A., Richter, L., & Brown, P. (2019). Guideline levels for PFOA and PFOS in drinking water: the role of scientific uncertainty, risk assessment decisions, and social factors. *Journal of Exposure Science and Environmental Epidemiology*, 29(2), 157–171. <https://doi.org/10.1038/s41370-018-0099-9>
- Dalahmeh, S., Tirgani, S., Komakech, A. J., Niwagaba, C. B., & Ahrens, L. (2018). Per- and polyfluoroalkyl substances (PFASs) in water, soil and plants in wetlands and agricultural areas in Kampala, Uganda. *Science of the Total Environment*, 631–632, 660–667. <https://doi.org/10.1016/j.scitotenv.2018.03.024>
- DeRidder, D. J., Verliefde, A. R. D., Heijman, S. G. J., Verberk, J. Q. J. C., Rietveld, L. C., Van DerAa, L. T. J., Amy, G. L., & VanDijk, J. C. (2011). Influence of natural organic matter on equilibrium adsorption of neutral and charged pharmaceuticals onto activated carbon. *Water Science and Technology*, 63(3), 416–423. <https://doi.org/10.2166/wst.2011.237>
- deRidder, D. J., Villacorte, L., Verliefde, A. R. D., Verberk, J. Q. J. C., Heijman, S. G. J., Amy, G. L., & vanDijk, J. C. (2010). Modeling equilibrium adsorption of organic micropollutants onto activated carbon. *Water Research*, 44(10), 3077–3086. <https://doi.org/10.1016/j.watres.2010.02.034>
- Delgado, L. F., Charles, P., Glucina, K., & Morlay, C. (2012). The removal of endocrine disrupting compounds, pharmaceutically activated compounds and cyanobacterial toxins during drinking water preparation using activated carbon-A review. *Science of the Total Environment*, 435–436, 509–525. <https://doi.org/10.1016/j.scitotenv.2012.07.046>
- Diamantopoulou, I., Skodras, G., & Sakellariopoulos, G. P. (2010). Sorption of mercury by activated carbon in the presence of flue gas components. *Fuel Processing Technology*, 91(2), 158–163. <https://doi.org/10.1016/j.fuproc.2009.09.005>
- ElGamal, M., Mousa, H. A., El-Naas, M. H., Zacharia, R., & Judd, S. (2018). Bio-regeneration of activated carbon: A comprehensive review. *Separation and Purification Technology*, 197(August 2017), 345–359. <https://doi.org/10.1016/j.seppur.2018.01.015>
- Elmoznino, J., Vlahos, P., & Whitney, M. (2018). Occurrence and partitioning behavior of perfluoroalkyl acids in wastewater effluent discharging into the Long Island Sound. *Environmental Pollution*, 243, 453–461. <https://doi.org/10.1016/j.envpol.2018.07.076>
- Eriksson, U., Haglund, P., & Kärrman, A. (2017). Contribution of precursor compounds to the release of per- and polyfluoroalkyl substances (PFASs) from waste water treatment plants (WWTPs). *Journal of Environmental Sciences (China)*, 61, 80–90. <https://doi.org/10.1016/j.jes.2017.05.004>
- Fenton, S. E., Ducatman, A., Boobis, A., DeWitt, J. C., Lau, C., Ng, C., Smith, J. S., & Roberts, S. M. (2021). Per- and Polyfluoroalkyl Substance Toxicity and Human Health Review: Current State of Knowledge and Strategies for Informing Future Research. *Environmental Toxicology and Chemistry*, 40(3), 606–630. <https://doi.org/10.1002/etc.4890>
- Ferrández-Gómez, B., Ruiz-Rosas, R., Beaumont, S., Cazorla-Amorós, D., & Morallón, E. (2021). Electrochemical regeneration of spent activated carbon from drinking water treatment plant at different scale reactors. *Chemosphere*, 264. <https://doi.org/10.1016/j.chemosphere.2020.128399>
- Foo, K. Y., & Hameed, B. H. (2009). A short review of activated carbon assisted electrosorption process: An overview, current stage and future prospects. *Journal of Hazardous Materials*, 170(2–3), 552–559. <https://doi.org/10.1016/j.jhazmat.2009.05.057>
- Gallen, C., Eaglesham, G., Drage, D., Nguyen, T. H., & Mueller, J. F. (2018). A mass estimate of perfluoroalkyl substance (PFAS) release from Australian wastewater treatment plants. *Chemosphere*, 208, 975–983. <https://doi.org/10.1016/j.chemosphere.2018.06.024>
- García-Otón, M., Montilla, F., Lillo-Ródenas, M. A., Morallón, E., & Vázquez, J. L. (2005). Electrochemical Regeneration of Activated Carbon Saturated with Toluene. *Journal of Applied Electrochemistry*, 35(3), 319–325. <https://doi.org/10.1007/s10800-004-7470-3>

- Gavrilescu, M., Demnerová, K., Aamand, J., Agathos, S., & Fava, F. (2015). Emerging pollutants in the environment: Present and future challenges in biomonitoring, ecological risks and bioremediation. *New Biotechnology*, 32(1), 147–156. <https://doi.org/10.1016/j.nbt.2014.01.001>
- Gogate, P. R., & Pandit, A. B. (2004). A review of imperative technologies for wastewater treatment I: Oxidation technologies at ambient conditions. *Advances in Environmental Research*, 8(3–4), 501–551. [https://doi.org/10.1016/S1093-0191\(03\)00032-7](https://doi.org/10.1016/S1093-0191(03)00032-7)
- Ho, Y. S., & McKay, G. (1998). Sorption of dye from aqueous solution by peat. *Chemical Engineering Journal*, 70(2), 115–124. [https://doi.org/10.1016/S1385-8947\(98\)00076-X](https://doi.org/10.1016/S1385-8947(98)00076-X)
- Hornig, G., Northcott, K., Snape, I., & Stevens, G. (2008). Assessment of sorbent materials for treatment of hydrocarbon contaminated ground water in cold regions. *Cold Regions Science and Technology*, 53(1), 83–91. <https://doi.org/10.1016/j.coldregions.2007.08.004>
- Houtz, E. F., Sutton, R., Park, J. S., & Sedlak, M. (2016). Poly- and perfluoroalkyl substances in wastewater: Significance of unknown precursors, manufacturing shifts, and likely AFFF impacts. *Water Research*, 95, 142–149. <https://doi.org/10.1016/j.watres.2016.02.055>
- Houtz, E., Wang, M., & Park, J. S. (2018). Identification and Fate of Aqueous Film Forming Foam Derived Per- and Polyfluoroalkyl Substances in a Wastewater Treatment Plant [Research-article]. *Environmental Science and Technology*, 52(22), 13212–13221. <https://doi.org/10.1021/acs.est.8b04028>
- Huang, C. C., & Su, Y. J. (2010). Removal of copper ions from wastewater by adsorption/electrosorption on modified activated carbon cloths. *Journal of Hazardous Materials*, 175(1–3), 477–483. <https://doi.org/10.1016/j.jhazmat.2009.10.030>
- Huang, H. H., Lu, M. C., Chen, J. N., & Lee, C. T. (2003). Catalytic decomposition of hydrogen peroxide and 4-chlorophenol in the presence of modified activated carbons. *Chemosphere*, 51(9), 935–943. [https://doi.org/10.1016/S0045-6535\(03\)00042-0](https://doi.org/10.1016/S0045-6535(03)00042-0)
- Karimi-Jashni, A., & Narbaitz, R. M. (2005). Electrochemical reactivation of granular activated carbon: pH dependence. *Journal of Environmental Engineering and Science*, 4(3), 187–194. <https://doi.org/10.1139/S04-055>
- Katsoyiannis, I. A., Canonica, S., & von Gunten, U. (2011). Efficiency and energy requirements for the transformation of organic micropollutants by ozone, O₃/H₂O₂ and UV/H₂O₂. *Water Research*, 45(13), 3811–3822. <https://doi.org/10.1016/j.watres.2011.04.038>
- Kim, M. K., Kim, T., Kim, T. K., Joo, S. W., & Zoh, K. D. (2020). Degradation mechanism of perfluorooctanoic acid (PFOA) during electrocoagulation using Fe electrode. *Separation and Purification Technology*, 247(April), 116911. <https://doi.org/10.1016/j.seppur.2020.116911>
- Leng, C. C., & Pinto, N. G. (1997). Effects of surface properties of activated carbons on adsorption behavior of selected aromatics. *Carbon*, 35(9), 1375–1385. [https://doi.org/10.1016/S0008-6223\(97\)00091-2](https://doi.org/10.1016/S0008-6223(97)00091-2)
- Li, F., Duan, J., Tian, S., Ji, H., Zhu, Y., Wei, Z., & Zhao, D. (2020). Short-chain per- and polyfluoroalkyl substances in aquatic systems: Occurrence, impacts and treatment. *Chemical Engineering Journal*, 380(June 2019), 122506. <https://doi.org/10.1016/j.cej.2019.122506>
- Li, Q., Snoeyink, V. L., Mariñas, B. J., & Campos, C. (2003). Elucidating competitive adsorption mechanisms of atrazine and NOM using model compounds. *Water Research*, 37(4), 773–784. [https://doi.org/10.1016/S0043-1354\(02\)00390-1](https://doi.org/10.1016/S0043-1354(02)00390-1)
- Lin, H., Niu, J., Ding, S., & Zhang, L. (2012). Electrochemical degradation of perfluorooctanoic acid (PFOA) by Ti/SnO₂-Sb, Ti/SnO₂-Sb/PbO₂ and Ti/SnO₂-Sb/MnO₂ anodes. *Water Research*, 46(7), 2281–2289. <https://doi.org/10.1016/j.watres.2012.01.053>
- Lindh, C. H., Rylander, L., Toft, G., Axmon, A., Rignell-Hydbom, A., Giwercman, A., Pedersen, H. S., Góalczyk, K., Ludwicki, J. K., Zvezday, V., Vermeulen, R., Lenters, V., Heederik, D., Bonde, J. P., & Jönsson, B. A. G. (2012). Blood serum concentrations of perfluorinated compounds in men from Greenlandic Inuit and European populations. *Chemosphere*, 88(11), 1269–1275. <https://doi.org/10.1016/j.chemosphere.2012.03.049>

- Lompe, K. M., Vo Duy, S., Peldszus, S., Sauvé, S., & Barbeau, B. (2018). Removal of micropollutants by fresh and colonized magnetic powdered activated carbon. *Journal of Hazardous Materials*, 360(March), 349–355. <https://doi.org/10.1016/j.jhazmat.2018.07.072>
- Lücking, F., Köser, H., Jank, M., & Ritter, A. (1998). Iron powder, graphite and activated carbon as catalysts for the oxidation of 4-chlorophenol with hydrogen peroxide in aqueous solution. *Water Research*, 32(9), 2607–2614. [https://doi.org/10.1016/S0043-1354\(98\)00016-5](https://doi.org/10.1016/S0043-1354(98)00016-5)
- Martin, R. J., & Ng, W. J. (1984). Chemical regeneration of exhausted activated carbon-I. *Water Research*, 18(1), 59–73. [https://doi.org/10.1016/0043-1354\(84\)90048-4](https://doi.org/10.1016/0043-1354(84)90048-4)
- Martínez-Huitle, C. A., Rodrigo, M. A., Sirés, I., & Scialdone, O. (2015). Single and Coupled Electrochemical Processes and Reactors for the Abatement of Organic Water Pollutants: A Critical Review. *Chemical Reviews*, 115(24), 13362–13407. <https://doi.org/10.1021/acs.chemrev.5b00361>
- Matamoros, V., & Bayona, J. M. (2006). Elimination of pharmaceuticals and personal care products in subsurface flow constructed wetlands. *Environmental Science and Technology*, 40(18), 5811–5816. <https://doi.org/10.1021/es0607741>
- Mattson, J. A., Mark, H. B., Malbin, M. D., Weber, W. J., & Crittenden, J. C. (1969). Surface chemistry of active carbon: Specific adsorption of phenols. *Journal of Colloid And Interface Science*, 31(1), 116–130. [https://doi.org/10.1016/0021-9797\(69\)90089-7](https://doi.org/10.1016/0021-9797(69)90089-7)
- McQuillan, R.V., Stevens, G. W., & Mumford, K. A. (2018). The electrochemical regeneration of granular activated carbons: A review. *Journal of Hazardous Materials*, 355(April), 34–49. <https://doi.org/10.1016/j.jhazmat.2018.04.079>
- Mehta, M. P., & Flora, J. R. V. (1997). Effects of electrochemical treatment of granular activated carbon on surface acid groups and the adsorptive capacity for phenol. *Water Research*, 31(9), 2171–2176. [https://doi.org/10.1016/S0043-1354\(97\)00057-2](https://doi.org/10.1016/S0043-1354(97)00057-2)
- Miller, C. M., & Valentine, R. L. (1995). Hydrogen peroxide decomposition and quinoline degradation in the presence of aquifer material. *Water Research*, 29(10), 2353–2359. [https://doi.org/10.1016/0043-1354\(95\)00059-T](https://doi.org/10.1016/0043-1354(95)00059-T)
- Mohammad-Khah, A., & Ansari, R. (2009). Activated charcoal: Preparation, characterization and applications: A review article. *International Journal of ChemTech Research*, 1(4), 859–864.
- Moreno-Castilla, C. (2004). Adsorption of organic molecules from aqueous solutions on carbon materials. *Carbon*, 42(1), 83–94. <https://doi.org/10.1016/j.carbon.2003.09.022>
- Mumford, K. A., Rayner, J. L., Snape, I., & Stevens, G. W. (2014). Hydraulic performance of a permeable reactive barrier at Casey Station, Antarctica. *Chemosphere*, 117(1), 223–231. <https://doi.org/10.1016/j.chemosphere.2014.06.091>
- Narbaitz, R. M., & Karimi-Jashni, A. (2009). Electrochemical regeneration of granular activated carbons loaded with phenol and natural organic matter. *Environmental Technology*, 30(1), 27–36. <https://doi.org/10.1080/09593330802422803>
- Narbaitz, Roberto M., & Cen, J. (1994). Electrochemical regeneration of granular activated carbon. *Water Research*, 28(8), 1771–1778. [https://doi.org/10.1016/0043-1354\(94\)90250-X](https://doi.org/10.1016/0043-1354(94)90250-X)
- Narbaitz, Roberto M., & Karimi-Jashni, A. (2012). Electrochemical reactivation of granular activated carbon: Impact of reactor configuration. *Chemical Engineering Journal*, 197, 414–423. <https://doi.org/10.1016/j.cej.2012.05.049>
- Narbaitz, Roberto M., & McEwen, J. (2012). Electrochemical regeneration of field spent GAC from two water treatment plants. *Water Research*, 46(15), 4852–4860. <https://doi.org/10.1016/j.watres.2012.05.046>
- Navalon, S., Dhakshinamoorthy, A., Alvaro, M., & Garcia, H. (2011). Heterogeneous Fenton catalysts based on activated carbon and related materials. *ChemSusChem*, 4(12), 1712–1730. <https://doi.org/10.1002/cssc.201100216>
- Neti, N. R., & Misra, R. (2012). Efficient degradation of Reactive Blue 4 in carbon bed electrochemical reactor. *Chemical Engineering Journal*, 184, 23–32. <https://doi.org/10.1016/j.cej.2011.12.014>
- Newcombe, G., & Drikas, M. (1997). Adsorption of NOM onto activated carbon: Electrostatic and non-electrostatic effects. *Carbon*, 35(9), 1239–1250. [https://doi.org/10.1016/S0008-6223\(97\)00078-X](https://doi.org/10.1016/S0008-6223(97)00078-X)

- Nidheesh, P.V., & Gandhimathi, R. (2012). Trends in electro-Fenton process for water and wastewater treatment: An overview. *Desalination*, 299, 1–15. <https://doi.org/10.1016/j.desal.2012.05.011>
- Oller, I., Malato, S., & Sánchez-Pérez, J. A. (2011). Combination of Advanced Oxidation Processes and biological treatments for wastewater decontamination-A review. *Science of the Total Environment*, 409(20), 4141–4166. <https://doi.org/10.1016/j.scitotenv.2010.08.061>
- Oriňáková, R., Wiemhöfer, H. D., Paulsdorf, J., Barinková, V., Bednáriková, A., & Smith, R. M. (2006). Impedance study of Ni-Co electro-deposition on Fe powder particles in fluidised bed systems. *Journal of Solid State Electrochemistry*, 10(7), 458–464. <https://doi.org/10.1007/s10008-005-0015-9>
- Pan, C. G., Liu, Y. S., & Ying, G. G. (2016). Perfluoroalkyl substances (PFASs) in wastewater treatment plants and drinking water treatment plants: Removal efficiency and exposure risk. *Water Research*, 106, 562–570. <https://doi.org/10.1016/j.watres.2016.10.045>
- Panaretakis, T., Shabalina, I. G., Grandér, D., Shoshan, M. C., & Depierre, J. W. (2001). Reactive oxygen species and mitochondria mediate the induction of apoptosis in human hepatoma HepG2 cells by the rodent peroxisome proliferator and hepatocarcinogen, perfluorooctanoic acid. *Toxicology and Applied Pharmacology*, 173(1), 56–64. <https://doi.org/10.1006/taap.2001.9159>
- Park, M., Wu, S., Lopez, I. J., Chang, J. Y., Karanfil, T., & Snyder, S. A. (2020). Adsorption of perfluoroalkyl substances (PFAS) in groundwater by granular activated carbons: Roles of hydrophobicity of PFAS and carbon characteristics. *Water Research*, 170. <https://doi.org/10.1016/j.watres.2019.115364>
- Pelekani, C., & Snoeyink, V. L. (1999). Competitive adsorption in natural water: Role of activated carbon pore size. *Water Research*, 33(5), 1209–1219. [https://doi.org/10.1016/S0043-1354\(98\)00329-7](https://doi.org/10.1016/S0043-1354(98)00329-7)
- Peng, B., Chen, L., Que, C., Yang, K., Deng, F., Deng, X., Shi, G., Xu, G., & Wu, M. (2016). Adsorption of Antibiotics on Graphene and Biochar in Aqueous Solutions Induced by π - π Interactions. *Scientific Reports*, 6(August), 1–10. <https://doi.org/10.1038/srep31920>
- Piazzoli, A., & Antonelli, M. (2018). Application of the Homogeneous Surface Diffusion Model for the prediction of the breakthrough in full-scale GAC filters fed on groundwater. *Process Safety and Environmental Protection*, 117, 286–295. <https://doi.org/10.1016/j.psep.2018.04.027>
- Rahman, M. F., Peldszus, S., & Anderson, W. B. (2014). Behaviour and fate of perfluoroalkyl and polyfluoroalkyl substances (PFASs) in drinking water treatment: A review. *Water Research*, 50, 318–340. <https://doi.org/10.1016/j.watres.2013.10.045>
- Rajeshwar, K., Ibanez, J. G., & Swain, G. M. (1994). Electrochemistry and the environment. *Journal of Applied Electrochemistry*, 24(11), 1077–1091. <https://doi.org/10.1007/BF00241305>
- Rajkumar, D., & Palanivelu, K. (2004). Electrochemical treatment of industrial wastewater. *Journal of Hazardous Materials*, 113(1–3), 123–129. <https://doi.org/10.1016/j.jhazmat.2004.05.039>
- Renner, R. (2001). Growing concern over perfluorinated chemicals. *Environmental Science and Technology*, 35(7). <https://doi.org/10.1021/es012317k>
- Salvador, F., Martín-Sánchez, N., Sánchez-Hernández, R., Sánchez-Montero, M. J., & Izquierdo, C. (2015). Regeneration of carbonaceous adsorbents. Part II: Chemical, Microbiological and Vacuum Regeneration. *Microporous and Mesoporous Materials*, 202(C), 277–296. <https://doi.org/10.1016/j.micromeso.2014.08.019>
- Savlak, O., & Belgin, K. (2014). Electrochemical Regeneration of Cr (VI) Saturated Granular and Powder Activated Carbon : Comparison of Regeneration Efficiency Belgin Karabacakoglu. *Industrial & Engineering Chemistry Research*, 53. <https://doi.org/10.1021/ie30111a011>
- Semmens, M. J., Norgaard, G. E., Hohenstein, G., & Staples, A. B. (1986). Influence of pH on the removal of organics by granular activated carbon. *Journal / American Water Works Association*, 78(5), 89–93. <https://doi.org/10.1002/j.1551-8833.1986.tb05749.x>
- Seo, S. H., Son, M. H., Shin, E. S., Choi, S. D., & Chang, Y. S. (2019). Matrix-specific distribution and compositional profiles of perfluoroalkyl substances (PFASs) in multimedia environments. *Journal of Hazardous Materials*, 364, 19–27. <https://doi.org/10.1016/j.jhazmat.2018.10.012>

- Sharma, S., Shetti, N. P., Basu, S., Nadagouda, M. N., & Aminabhavi, T. M. (2022). Remediation of per- and polyfluoroalkyls (PFAS) via electrochemical methods. *Chemical Engineering Journal*, 430(P2), 132895. <https://doi.org/10.1016/j.cej.2021.132895>
- Siegrist, R. L., Crimi, M., Simpkin, T. J., Brown, R. A., & Unger, M. (2011). *In situ chemical oxidation for groundwater remediation*.
- Sinha, H. K., & Dogra, S. K. (1989). Environmental effects on the absorption and fluorescence spectral characteristics of Benzimidazole-2-carboxylic Acid and its ester. In *Bulletin of the Chemical Society of Japan* (Vol. 62, Issue 8, pp. 2668–2675). <https://doi.org/10.1246/bcsj.62.2668>
- Srivastava, A., Gupta, B., Majumder, A., Gupta, A. K., & Nimbhorkar, S. K. (2021). A comprehensive review on the synthesis, performance, modifications, and regeneration of activated carbon for the adsorptive removal of various water pollutants. *Journal of Environmental Chemical Engineering*, 9(5), 106177. <https://doi.org/10.1016/j.jece.2021.106177>
- Sun, H., Liu, Z., Wang, Y., & Li, Y. (2013). Electrochemical in situ regeneration of granular activated carbon using a three-dimensional reactor. *Journal of Environmental Sciences (China)*, 25(S1), S77–S79. [https://doi.org/10.1016/S1001-0742\(14\)60630-6](https://doi.org/10.1016/S1001-0742(14)60630-6)
- Takagi, S., Adachi, F., Miyano, K., Koizumi, Y., Tanaka, H., Mimura, M., Watanabe, I., Tanabe, S., & Kannan, K. (2008). Perfluorooctanesulfonate and perfluorooctanoate in raw and treated tap water from Osaka, Japan. *Chemosphere*, 72(10), 1409–1412. <https://doi.org/10.1016/j.chemosphere.2008.05.034>
- Tijani, J. O., Fatoba, O. O., & Petrik, L. F. (2013). A review of pharmaceuticals and endocrine-disrupting compounds: Sources, effects, removal, and detections. *Water, Air, and Soil Pollution*, 224(11). <https://doi.org/10.1007/s11270-013-1770-3>
- Tran, H. N., You, S. J., Hosseini-Bandegharai, A., & Chao, H. P. (2017). Mistakes and inconsistencies regarding adsorption of contaminants from aqueous solutions: A critical review. *Water Research*, 120(May), 88–116. <https://doi.org/10.1016/j.watres.2017.04.014>
- Trautmann, A. M., Schell, H., Schmidt, K. R., Mangold, K. M., & Tiehm, A. (2015). Electrochemical degradation of perfluoroalkyl and polyfluoroalkyl substances (PFASs) in groundwater. *Water Science and Technology*, 71(10), 1569–1575. <https://doi.org/10.2166/wst.2015.143>
- VanVliet, B. M. (1991). Regeneration of activated carbon. *Journal of The South African Institute of Mining and Metallurgy*, 91(5), 159–167.
- Wang, L., & Balasubramanian, N. (2009). Electrochemical regeneration of granular activated carbon saturated with organic compounds. *Chemical Engineering Journal*, 155(3), 763–768. <https://doi.org/10.1016/j.cej.2009.09.020>
- Wang, Q., Zietzschmann, F., Hofman-Caris, R., Jiang, N., Schuster, J., Wang, Z., Yu, J., Yang, M., & Rietveld, L. C. (2022). Unraveling competition versus adsorbability of dissolved organic matter against organic micropollutants onto activated carbon. *Separation and Purification Technology*, 292(March), 120942. <https://doi.org/10.1016/j.seppur.2022.120942>
- Weng, C. H., & Hsu, M. C. (2008). Regeneration of granular activated carbon by an electrochemical process. *Separation and Purification Technology*, 64(2), 227–236. <https://doi.org/10.1016/j.seppur.2008.10.006>
- Westerhoff, P., Yoon, Y., Snyder, S., & Wert, E. (2005). Fate of endocrine-disruptor, pharmaceutical, and personal care product chemicals during simulated drinking water treatment processes. *Environmental Science and Technology*, 39(17), 6649–6663. <https://doi.org/10.1021/es0484799>
- Worch, E. (2012). 3 Adsorption equilibrium I: General aspects and single-solute adsorption. *Adsorption Technology in Water Treatment*, 41–76. <https://doi.org/10.1515/9783110240238.41>
- Wu, X., Yang, X., Wu, D., & Fu, R. (2008). Feasibility study of using carbon aerogel as particle electrodes for decoloration of RBRX dye solution in a three-dimensional electrode reactor. *Chemical Engineering Journal*, 138(1–3), 47–54. <https://doi.org/10.1016/j.cej.2007.05.027>

- Wu, Z., Cong, Y., Zhou, M., & Tan, T. (2005). P-Nitrophenol abatement by the combination of electrocatalysis and activated carbon. *Chemical Engineering Journal*, 106(1), 83–90. <https://doi.org/10.1016/j.cej.2004.10.009>
- Xu, L., Zhao, H., Shi, S., Zhang, G., & Ni, J. (2008). Electrolytic treatment of C.I. Acid Orange 7 in aqueous solution using a three-dimensional electrode reactor. *Dyes and Pigments*, 77(1), 158–164. <https://doi.org/10.1016/j.dyepig.2007.04.004>
- Yu, J., Lv, L., Lan, P., Zhang, S., Pan, B., & Zhang, W. (2012). Effect of effluent organic matter on the adsorption of perfluorinated compounds onto activated carbon. *Journal of Hazardous Materials*, 225–226, 99–106. <https://doi.org/10.1016/j.jhazmat.2012.04.073>
- Zanella, O., Bilibio, D., Priamo, W. L., Tessaro, I. C., & Féris, L. A. (2017). Electrochemical regeneration of phenol-saturated activated carbon—proposal of a reactor. *Environmental Technology (United Kingdom)*, 38(5), 549–557. <https://doi.org/10.1080/09593330.2016.1202327>
- Zhan, J., Wang, Y., Wang, H., Shen, W., Pan, X., Wang, J., & Yu, G. (2016). Electro-peroxone regeneration of phenol-saturated activated carbon fiber: The effects of irreversible adsorption and operational parameters. *Carbon*, 109, 321–330. <https://doi.org/10.1016/j.carbon.2016.08.034>
- Zhang, Chao, Jiang, Y., Li, Y., Hu, Z., Zhou, L., & Zhou, M. (2013). Three-dimensional electrochemical process for wastewater treatment: A general review. *Chemical Engineering Journal*, 228, 455–467. <https://doi.org/10.1016/j.cej.2013.05.033>
- Zhang, Chaojie, Yan, H., Li, F., & Zhou, Q. (2015). Occurrence and fate of perfluorinated acids in two wastewater treatment plants in Shanghai, China. *Environmental Science and Pollution Research*, 22(3), 1804–1811. <https://doi.org/10.1007/s11356-013-2044-8>
- Zhang, H. (2002). Regeneration of exhausted activated carbon by electrochemical method. *Chemical Engineering Journal*, 85(1), 81–85. [https://doi.org/10.1016/S1385-8947\(01\)00176-0](https://doi.org/10.1016/S1385-8947(01)00176-0)
- Zhou, M. H., & Lei, L. C. (2006). Electrochemical regeneration of activated carbon loaded with p-nitrophenol in a fluidized electrochemical reactor. *Electrochimica Acta*, 51(21), 4489–4496. <https://doi.org/10.1016/j.electacta.2005.12.028>
- Zhou, M., & Lei, L. (2006). The role of activated carbon on the removal of p-nitrophenol in an integrated three-phase electrochemical reactor. *Chemosphere*, 65(7), 1197–1203. <https://doi.org/10.1016/j.chemosphere.2006.03.054>
- Zhou, W., Meng, X., Gao, J., Zhao, H., Zhao, G., & Ma, J. (2021). Electrochemical regeneration of carbon-based adsorbents: a review of regeneration mechanisms, reactors, and future prospects. *Chemical Engineering Journal Advances*, 5(December 2020), 100083. <https://doi.org/10.1016/j.cej.2020.100083>
- Zhuo, Q., Deng, S., Yang, B., Huang, J., Wang, B., Zhang, T., & Yu, G. (2012). Degradation of perfluorinated compounds on a boron-doped diamond electrode. *Electrochimica Acta*, 77, 17–22. <https://doi.org/10.1016/j.electacta.2012.04.145>
- Zhuo, Q., Deng, S., Yang, B., Huang, J., & Yu, G. (2011). Efficient electrochemical oxidation of perfluorooctanoate using a Ti/SnO₂-Sb-Bi anode. *Environmental Science and Technology*, 45(7), 2973–2979. <https://doi.org/10.1021/es1024542>
- Zou, J., Peng, X., Li, M., Xiong, Y., Wang, B., Dong, F., & Wang, B. (2017). Electrochemical oxidation of COD from real textile wastewaters: Kinetic study and energy consumption. *Chemosphere*, 171, 332–338. <https://doi.org/10.1016/j.chemosphere.2016.12.065>

APPENDIX A – OMP PROPERTIES AND INITIAL SPIKED CONCENTRATION

Table A: 1 OMP properties and initial spiked concentration.

Group	Compound	Acronym	CAS no.	Application	MW (g/mol) ^a	Log K _{ow} ^b	Charge at pH 7 ^c	pK _s ^d	Minimal projection diameter (nm) ^e	Maximal projection diameter (nm) ^e	Initial spiked concentrations				
											Adsorption experiments (µg/L)			Regeneration experiments (mg/L) in tap water	
											Milli-Q water	Tap water	WWTP effluent	With regeneration	Without regeneration
Neutral	1H-Benzotriazole	BTA	95-14-7	Corrosion inhibitors	119.1	1.44	0	1.6; 8.6	3.66	4.12	8.41	1.47	9.39	-	-
	5-Methyl-1H-benzotriazole	TTA	136-85-6	Corrosion inhibitors	133.2	1.71	0	2.2; 8.8	4.05	4.43	5.72	0.47	5.80	-	-
	Carbamazepine	CBZ	298-46-4	Anticonvulsant	236.3	2.45	0	13.9	4.48	5.76	10.60	10.58	11.03	-	-
	Hydrochlorothiazide	HCT	58-93-5	Diuretic	297.7	-0.07	0	0.6; 14	4.13	5.67	8.64	13.90	14.41	-	-
	Caffeine	CAF	58-08-2	Stimulant	194.2	-0.07	0	14	4.44	5.03	9.60	9.01	6.50	4.80	4.83
	Theophylline	TPL	58-55-9	Stimulant	180.2	-0.02	0	3.5; 8.7	4.34	4.98	18.24	15.19	14.30	-	-
Positively charged	Metoprolol	MTL	37350-58-6	Beta blocker	267.4	1.88	+	9.7	4.39	10.07	9.47	10.44	12.45	-	-
	Propranolol	PPL	525-66-6	Beta blocker	259.3	3.48	+	9.4	4.66	7.41	7.34	9.94	12.03	-	-
	Sotalol	STL	3930-20-9	Beta blocker	272.4	0.24	+	8.2; 9.1	4.21	7.94	9.79	9.18	11.44	2.77	2.81
	Trimethoprim	TMP	738-70-5	Antibiotic	290.3	0.91	+	1.3; 7.2	4.97	6.95	8.60	8.46	8.86	-	-
	Metformin	MET	657-24-9	Anti-diabetic	129.2	-2.64	+	12.4	3.79	4.88	6.25	6.42	11.00	4.13	5.14
Negatively charged	Diclofenac	DFC	15307-86-5	Anti-inflammatory	296.2	4.51	-	4.1	3.79	4.88	8.99	8.82	9.79	-	-
	Ketoprofen	KET	22071-15-4	Anti-inflammatory	254.3	3.12	-	4.5	4.37	6.58	8.84	7.86	8.44	4.52	4.56
	Clofibric acid	CA	882-09-7	Herbicide	214.7	2.57	-	3.5	3.5	6.2	10.35	9.90	10.40	-	-
	Sulfadimethoxine	SDM	122-11-2	Antibiotic	310.3	1.63	-	2.0; 6.7	5.09	7.57	7.08	7.02	8.45	-	-
	Sulfamethoxazole	SMX	723-46-6	Antibiotic	253.3	0.89	-	1.8; 5.8	5.4	5.88	9.77	9.07	9.73	5.13	5.17
Zwitterion	Gabapentin	GBP	60142-96-3	Anticonvulsant	171.2	-1.1	+/-zwitterion	3.7; 10	4.14	4.99	8.29	8.01	9.03	4.74	4.86

^a MW: molecular weight (PubChem 2022).

^b Octanol-water partition coefficient (PubChem 2022).

^c Neutral (0), positive (+),negative (-).

^d (PubChem 2022).

^e Estimated values retrieved from SPARC (ARChem, <http://www.archemcalc.com/>).

APPENDIX B – CHEMICAL STRUCTURES OF OMP MOLECULES

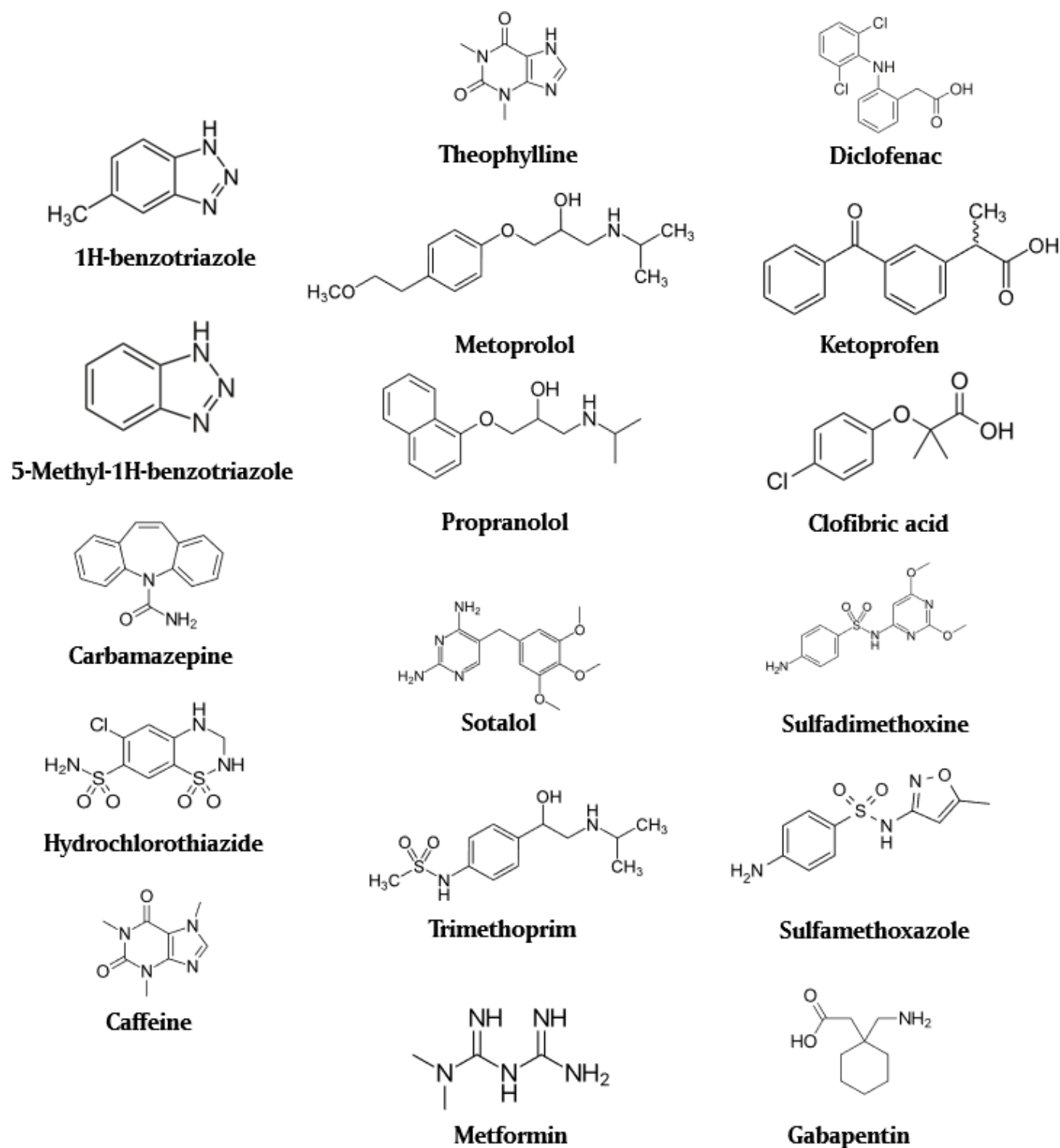


Fig. A: 1 Chemical structures of OMP molecules.

APPENDIX C – OMP ADSORPTION ISOTHERM PLOTS

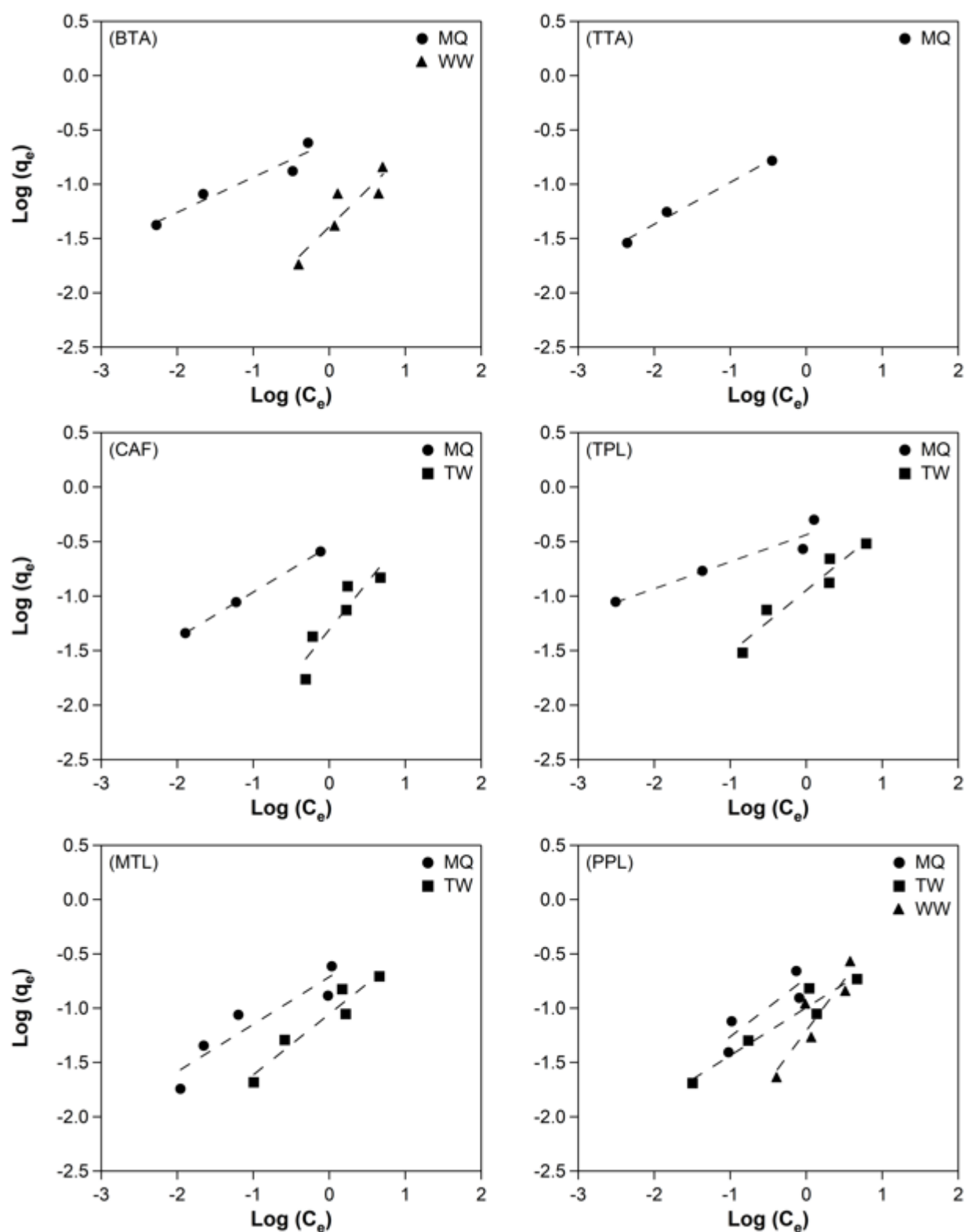


Fig. A: 2 OMP adsorption isotherm plots.

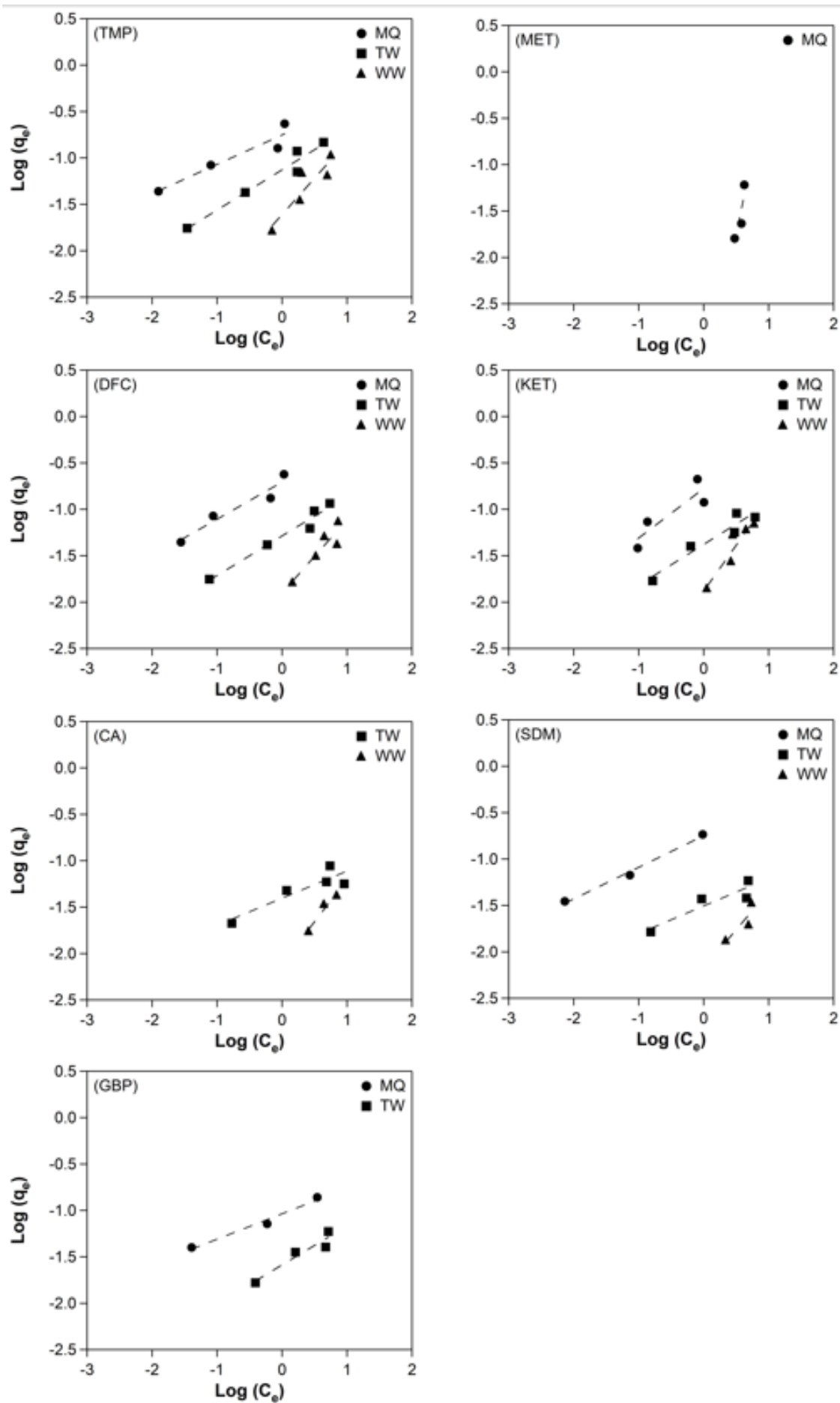


Fig. A: 3 OMP adsorption isotherm plots (cont.).

APPENDIX D – OMP ADSORPTION KINETIC PLOTS

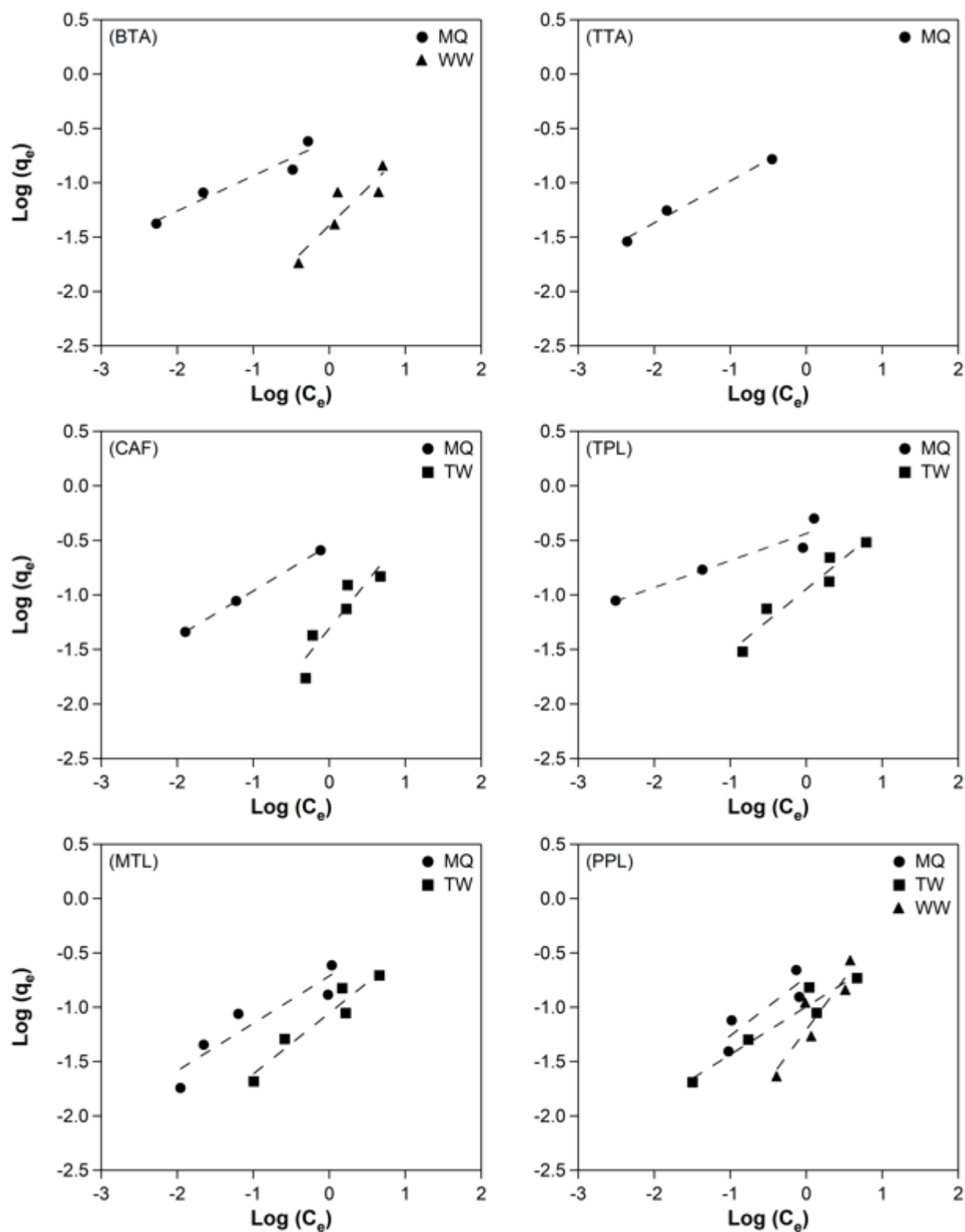


Fig. A: 4 OMP adsorption kinetic plots.

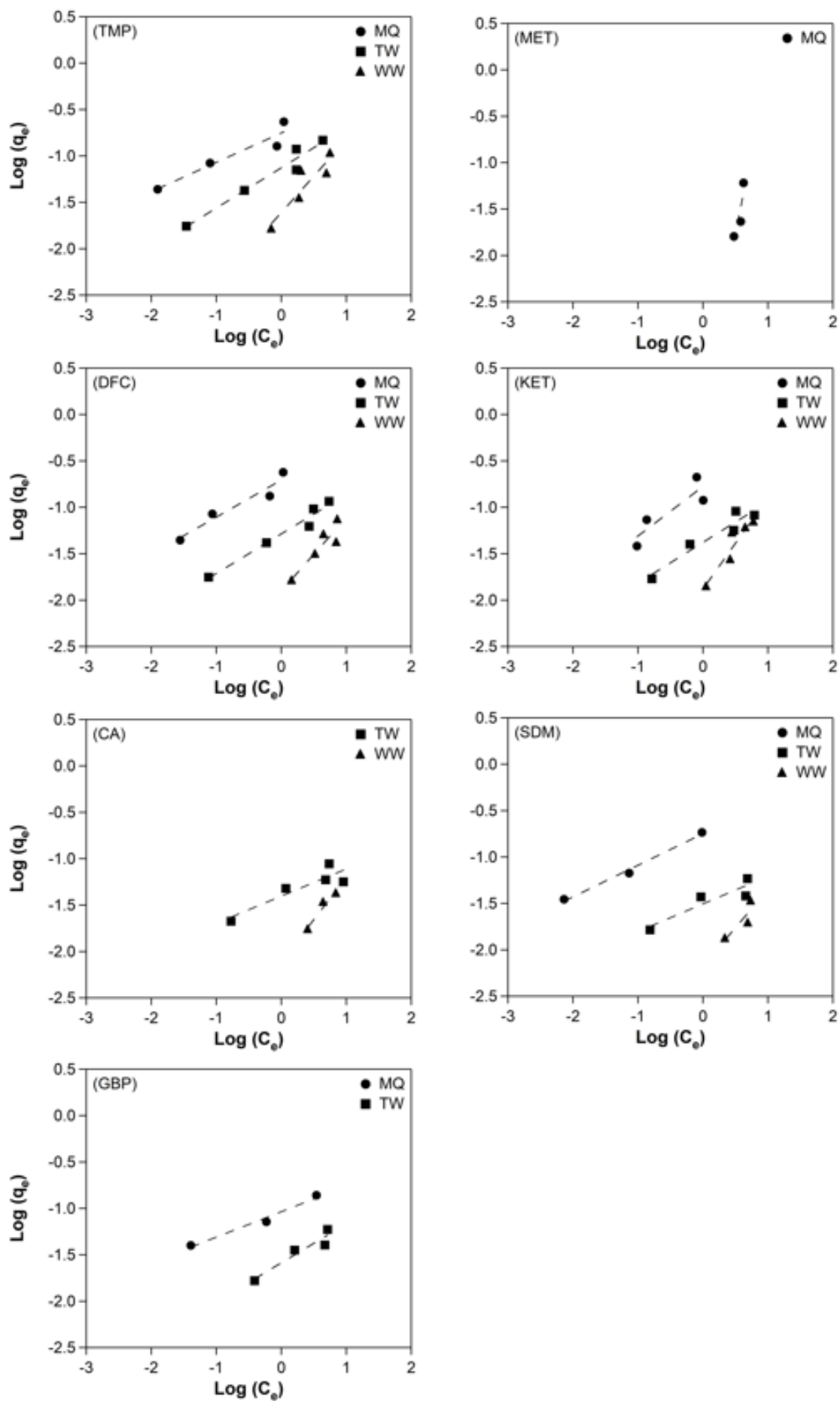


Fig. A: 5 OMP adsorption kinetic plots (cont.).

APPENDIX E - Protocol of making OMP stock solution

Protocol of making OMP stock solution

Version date: 06-May-2022

Author and other contributor:

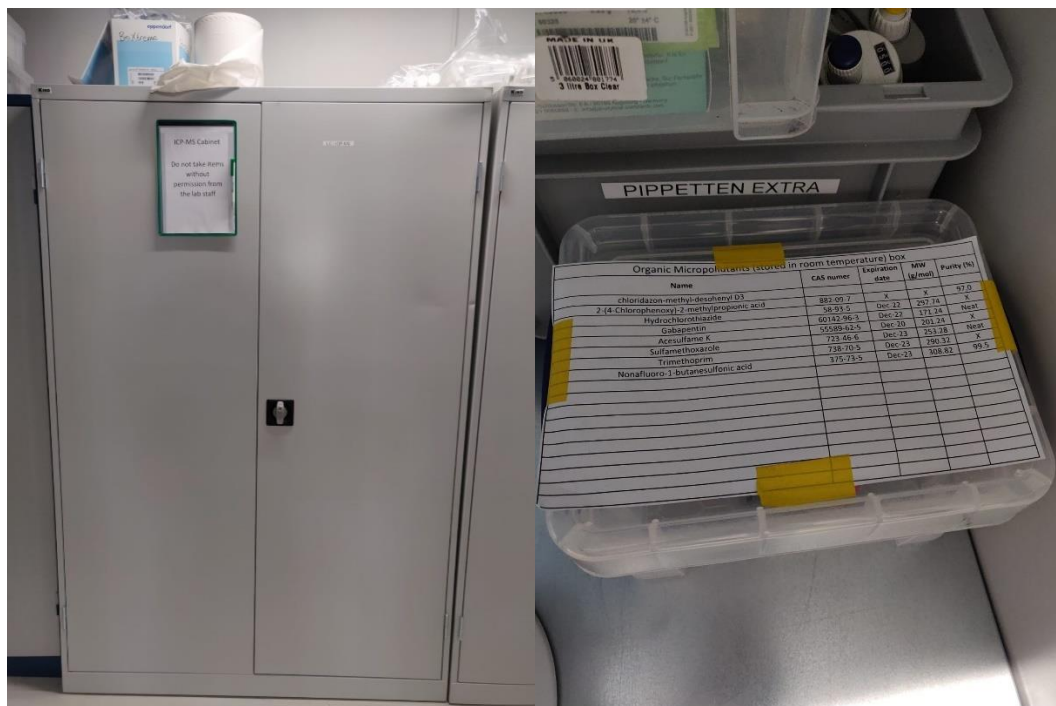
Connie Au, Nan Jiang, Kim Lompe

OMP storage location:

Most of the OMPs are stored in the boxes in the refrigerator outside blue lab. The refrigerator is labelled as “Discrete Analyzer Fridge”. The list of the OMPs that should be stored in the refrigerator can be found on top of the box.



Other OMPs which are suggested to be stored in the room temperature are stored in the box in the ICP-MS locker.



All OMPs are required to store in dark environment. The labels list each OMP's properties including the name of compound, expiry date, molecular weight, purity and CAS number. Solubility is not often specified on every bottles. It can be checked on PubChem.

Preparation before making stock solution:

1. Calculate actual weight of dosage to obtain target weight for each pollutant:

Please follow the following formula:

$$\text{actual weight} = \text{target weight} * \frac{\text{proportion}}{\text{purity}} * 100$$

$$\text{proportion} = \frac{\text{molecular weight of the designated pollutant}}{\text{actual analyte}}$$

Some of the powders do not contain only the pollutants. For instance, diclofenac sodium, sotalol hydrochloride, etc. Take diclofenac sodium as an example, you are targeting to weight 40 mg of diclofenac.




$$\text{proportion} = \frac{\text{MW of diclofenac sodium}}{\text{MW of diclofenac}} = \frac{318.13}{296.15} = 1.0742$$


With the purity of the compound (99.9)

$$\text{actual weight} = 40 * \frac{1.0742}{99.9} * 100 = 43.01 \text{ MG}$$

2. Rank the solubility of each compound from lowest to highest:

It is suggested to start dosing the compound with low solubility. Solubility can be found on the powder bottles or Pubchem.

Materials		
Items	Properties / preparation	Quantity
Stock solution bottle	<ul style="list-style-type: none"> Size of the bottle depends on the volume of stock solution. It is suggested that the volume of the bottle is not much larger than the volume of the stock solution. Otherwise it is easy to have residual compound on the wall of the bottle. The bottle should be clean and TOC-free before use. Use washing up liquid to clean the inner surface (including the bottle cap). Wash out the washing up liquid until no bubbles is visible. Rinse it with ultrapure water 3 times. Combust the glass ware at 550°C for at least 4 hours. The oven is located at the corner of green lab. It is suggested to use bottles with large cap to facilitate powder dosage. 	No. of stock solution 
Volumetric flask	For measuring ultrapure water.	
Analytic balance	Use the balance located in the yellow lab to weigh the powder. It is the most precise balance in the water lab. The minimum weight can be measured is 0.01 mg. However it is suggested to always weigh the powder over 1 mg to avoid errors due to balance. <div style="display: flex; align-items: center;">   </div>	

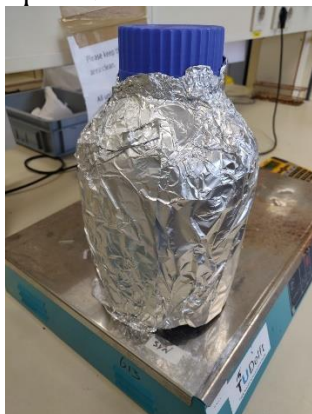
Foldable weighing tray			No. of OMP types
Plastic spatula			No. of OMP types

Procedures:

1. Make a list OMP selected for the stock solution.
2. Calculate the actual weight of dosage for each compound.
3. Rank them according to the solubility.
4. Prepare all the materials and collect the desired OMP powders.
5. Fill a volumetric flask with ultrapure water. Keep the water in the flask at this stage.
6. Use the analytical balance in the Yellow Lab.
7. Start with the OMP with the lowest solubility.
8. Use the spatula to add the desired weight of powder to the plastic weighing tray. Adjust to desired mass is dosed and note down the mass. (Tip: by tapping onto your spatula you can carefully dose the amount of powder to fall on your tray.)
9. Gently drop the powder down into the bottle.
10. Rinse the weighing tray with water from the volumetric flask to ensure no residual powder is left.
11. Repeat step 8 to 11 until all the compounds are added.
12. Ensure that no residual powder is left on the inner surface. Rinse with the remaining ultrapure water and shake the bottle gently. (Tip: Check the bottleneck!)
13. Fill the bottle with ultrapure water until desired volume is reached. Perform this always with volumetric flask.
14. Put in one magnetic stirring bar.



15. Close the cap firmly.
16. Label the bottle with your name/project name, compounds, concentration.
17. Wrap the bottle with aluminium foil to keep the solution in dark.



18. Mix the solution well with magnetic stirrer until most of the powders is dissolved. Empirically, it takes 3 – 14 days.
19. Store in refrigerator before use.

Disposal of unused stock solution or used OMP working solutions:

OMP solution are not allowed to be flushed down the drain. Always dispose them into the jerry can (category III: Non halogen organic waste in solution) which can be found in the fume hood. When these jerry cans are full swap them with an empty jerry can with the same label from the cabinet in the waste area.

After proper liquid disposal, place the glass ware beside the washing machine in the yellow lab. They will be washed by lab technicians.

Always ask the lab staff if you are unsure or have any questions.

Remarks:

It is normal that some of the compounds deviate from the target concentration. For example, the target concentration is 10 ug/L. The measured concentration could be in the range of 8-11 ug/L. Degradation could also take place after long periods of storage.

Before using the solution, have it stirred and wait until the solution reaches room temperature.

[illegible]

Phase 3 Loading and re-adsorption experiment										Experiment ID	Carbon ID	Water matrix	Material type	OMP loading mg OMP / g GAC	GAC dose g	actual GAC dose g	Volume mL	OMP conc mg/L	OMP mg	ultrapure mL	time points h	LCMS # samples
<p>Timeline: begins on 30/3</p> <p>OMP loading to saturate carbon for regeneration experiment</p> <p>Identical OMP concentration in all cases.</p> <p>Glassware volume reduced to 200 mL for acceleration</p> <p>Only tap water is used as background soltion.</p> <p>500x dilution</p> <p>Regeneration efficiency calculated by percentage of restored loading</p>										cycle 0	C01	tap water	Acid wash	5	0.2	0.2	200	5	1	10	0, 24, 48, 120	4
										cycle 1	C02	tap water	Acid wash	5	0.2	0.2	200	5	1	10	0, 24, 48, 120	4
										cycle 2	C03	tap water	Acid wash	5	0.2	0.2	200	5	1	10	0, 24, 48, 120	4
										cycle 3	C04	tap water	Acid wash	5	0.2	0.2	200	5	1	10	0, 24, 48, 120	4
										cycle 4	C05	tap water	Acid wash	5	0.2	0.2	200	5	1	10	0, 24, 48, 120	4
										cycle 5	C06	tap water	Acid wash	5	0.2	0.2	200	5	1	10	0, 24, 48, 120	4
<p>Carbon ID legend:</p> <p>C01 - C06: same batches of carbon undergoing 6 cycles of adsorption with 5 cycles of regeneration in between</p> <p>C07 - C12: same batches of carbon undergoing 6 cycles of adsorption</p> <p>C20 - C23: 4 batches of carbon undergoing 2 cycles of adsorption and 1 cycle of regeneration with varying current</p> <p>C24 - C27: same 4 batches of carbon (C20 - C23) for re-adsorption</p> <p>C30 - C32: 4 batches of carbon undergoing 2 cycles of adsorption and 1 cycle of regeneration with varying regeneration time</p> <p>C33 - C35: same 4 batches of carbon (C30 - C32) for re-adsorption</p> <p>Experiment ID legend:</p> <p>RA: regeneration experiment with varying current</p> <p>Number: applied current (mA)</p> <p>RT: regeneration experiment with varying regeneration time</p> <p>Number: treatment time (h)</p>										No regeneration	C07	tap water	Acid wash	5	0.2	0.2	200	5	1	10	0, 24, 48, 120	4
										No regeneration	C08	tap water	Acid wash	5	0.2	0.2	200	5	1	10	0, 24, 48, 120	4
										No regeneration	C09	tap water	Acid wash	5	0.2	0.2	200	5	1	10	0, 24, 48, 120	4
										No regeneration	C10	tap water	Acid wash	5	0.2	0.2	200	5	1	10	0, 24, 48, 120	4
										No regeneration	C11	tap water	Acid wash	5	0.2	0.2	200	5	1	10	0, 24, 48, 120	4
										No regeneration	C12	tap water	Acid wash	5	0.2	0.2	200	5	1	10	0, 24, 48, 120	4
										Current batch												
										RA10	C20	tap water	Acid wash	5	0.2	0.2	200	5	1	10	0,24,48,96,168	5
										RA30	C21	tap water	Acid wash	5	0.2	0.2	200	5	1	10	0,24,48,96,168	5
										RA60	C22	tap water	Acid wash	5	0.2	0.2	200	5	1	10	0,24,48,96,168	5
										RA80	C23	tap water	Acid wash	5	0.2	0.2	200	5	1	10	0,24,48,96,168	5
										Re-current batch												
										RA10	C24	tap water	Acid wash	5	0.2	0.2	200	5	1	10	0,24,48,96,168	5
										RA30	C25	tap water	Acid wash	5	0.2	0.2	200	5	1	10	0,24,48,96,168	5
										RA60	C26	tap water	Acid wash	5	0.2	0.2	200	5	1	10	0,24,48,96,168	5
										RA80	C27	tap water	Acid wash	5	0.2	0.2	200	5	1	10	0,24,48,96,168	5
										Time batch												
										RT0.5	C30	tap water	Acid wash	5	0.2	0.2	200	5	1	10	0,24,48,161	4
										RT2	C31	tap water	Acid wash	5	0.2	0.2	200	5	1	10	0,24,48,161	4
										RT5	C32	tap water	Acid wash	5	0.2	0.2	200	5	1	10	0,24,48,161	4
										Re-time batch												
										RT0.5	C33	tap water	Acid wash	5	0.2	0.2	200	5	1	10	0,24,48,161	4
										RT2	C34	tap water	Acid wash	5	0.2	0.2	200	5	1	10	0,24,48,161	4
										RT5	C35	tap water	Acid wash	5	0.2	0.2	200	5	1	10	0,24,48,161	4
										total												112

Phase 4 Regeneration experiment

Place the content in phase 3 to the electrochemical cell and regenerate

Timeline: begins on 5/4

To what extent can the OMP-loaded material be regenerated electrochemically?

How do operating parameters affect the regeneration efficiency?

Experiment ID legend:

R1-R5: 5 cycles of regeneration

RA: regeneration experiment with varying current

Number: applied current (mA)

RT: regeneration experiment with varying regeneration time

Number: treatment time (h)



Experiment	Experiment	Carbon ID	Electrolyte	applied current mA	treatment time h	Electrolyte volume mL	time points min	LCMS # samples
cycle 1	R1	C01	tap water	30	3	250		
cycle 2	R2	C02	tap water	30	3	250	30,60,90,120,150,180	6
cycle 3	R3	C03	tap water	30	3	250	10,20,30,60,90,120,150,180	8
cycle 4	R4	C04	tap water	30	3	250	10,20,30,60,90,120,150,180	8
cycle 5	R5	C05	tap water	30	3	250	10,20,30,60,90,120,150,180	8
vaious current	RA10	C20	tap water	10	1	250		-
	RA30	C21	tap water	30	1	250		-
	RA60	C22	tap water	60	1	250		-
	RA100	C23	tap water	80	1	250		-
various time	RT0.5	C30	tap water	60	0.5	250		-
	RT2	C31	tap water	60	2	250		-
	RT5	C32	tap water	60	5	250		-
total								30

Phase 5 PFAS regeneration experiment

Timeline: begins on 3/6

Can long-chain and short-chain PFAS adsorp on this material?

To what extent can the PFAS-loaded material be regenerated electrochemically?

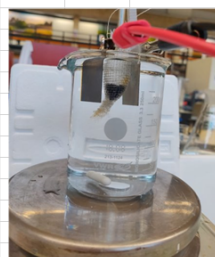
How does the chain length affect the regeneration efficiency?

Identical regeneration condition with OMP regeneration

Carbon ID legend:

PF: PFAS loading

Number: same batch of carbon undergoing 4 cycles of adsorption and 3 cycles of regeneration



Experiment	Carbon ID	Water matrix	Material type	PFAS loading mg PFAS / g	GAC dose mg	actual GAC dose g	Volume mL	PFAS conc mg/L	PFAS mg	ultrapure mL	time points h	# samples
PFAS loading	PF1	tap water	Acid wash	25	200	0.2	50	100	5	5	10 0, 87	2
	PF2	tap water	Acid wash	25	200	0.2	50	100	5	5	10 0, 72	2
	PF3	tap water	Acid wash	25	200	0.2	50	100	5	5	10 0, 72	2
	PF4	tap water	Acid wash	25	200	0.2	50	100	5	5	10 0, 72	2
Experiment	Experieme	Carbon ID	Electrolyte		applied current mA	treatment time h	Electrolyte volume mL				time points min	# samples
PFAS regeneration	PFA	PF1	tap water		30	3	250				180	1
	PFB	PF2	tap water		30	3	250					
	PFC	PF3	tap water		30	3	250				180	1
							</					